ROLE OF LIPOCALIN 2
IN KAINATE-INDUCED NEURODEGENERATION

CHIA WAN JIE

B.Sc. (Life Sci.) (Hons.), NUS

A THESIS SUBMITTED FOR THE DEGREE OF DOCTOR OF PHILOSOPHY

NUS GRADUATE SCHOOL FOR

INTEGRATIVE SCIENCES AND ENGINEERING

NATIONAL UNIVERSITY OF SINGAPORE

2011

ACKNOWLEDGEMENTS

I would like to extend my utmost gratitude to my supervisor and mentor, Associate Professor Gavin Stewart Dawe for his patience, advice and guidance throughout my PhD candidature. It was a great pleasure to work alongside him, and the many stimulating discussions with him have left me admiring his passion and dedication in research. This work would not be possible without his deep insights and optimism, which provided me a well-rounded postgraduate training.

My sincere gratitude to my Thesis Advisory Committee members, Associate Professor Ong Wei Yi and Dr. He Beiping, for their precious time and input. Special thanks go to Prof. Ong Wei Yi who suggested the topic of my study, giving me a head start and assistance with the first manuscript.

I am also indebted to my fellow colleagues in the laboratory, especially to Dr. Francis Tan for providing me with moral support, stimulating input for my project and for sharing his technical expertise in primary neuronal culture and confocal microscopy; and also to Dr. Alice Lim for her advice on *in vivo* studies and statistical analysis. My thanks also go out to my other lab members for sharing invaluable technical experiences and helpful discussions on my project, and more importantly, making the laboratory a pleasant environment to work in.

Last but not least, I am indebted to my family whose unfaltering support throughout these years has kept me on the track to complete this thesis. Without their love and understanding, this thesis would not be possible.

TABLE OF CONTENTS

SUMMARY

Lipocalin 2 (LCN2) is a member of the lipocalin family, which has diverse roles in infections, iron homeostasis, apoptosis, tumourigenesis, inflammation, renal physiology and pathology. Yet, little is known about the functions of LCN2 in the central nervous system (CNS). In view of recent studies that showed an association of LCN2 with apoptosis via LCN2R, the present study investigates the role of LCN2 in kainate (KA)-induced neurodegeneration. Intracerebroventricular injection of KA in rats induces neuronal loss in the hippocampal formation. Therefore, the KA model was used as a neurodegeneration model to elucidate the role of LCN2 in neurodegeneration in the hippocampus.

Despite microarray studies reporting substantial upregulation of LCN2 mRNA expression after some forms of brain insults, the expression and localisation of LCN2 had not been characterised physiologically. Thus, LCN2's tissue distribution and expression were analysed in the normal rat brain. High LCN2 expression in the olfactory bulb, cerebellum and brainstem suggested that these brain regions may be potential routes of entry for microorganisms since LCN2 is known as a bacteriostatic agent. After KA injury, LCN2 was highly upregulated and expressed in the astrocytes in the lesioned hippocampal region.

Since the interaction of LCN2 with its receptor (LCN2R) has been suggested to have an effect on apoptosis via Bim, a pro-apoptotic protein, it was important to examine LCN2R's cellular localisation. LCN2R was expressed in the hippocampal pyramidal neurons physiologically. After KA injury, LCN2R neuronal expression was reduced, but upregulated in the activated microglia. Coincidentally, Bim was also upregulated in activated microglia after KA treatment, but these microglia were not apoptotic. Only at 1 day post-KA injection, selective neurons with high Bim

expression were apoptotic. However, it is unclear if the upregulation of Bim was an effect of the interaction between LCN2 and LCN2R.

The effect of LCN2 on Bim-mediated apoptosis in neurons was further examined when primary hippocampal neurons were treated with recombinant LCN2 (rLCN2, apo-LCN2), and rLCN2:iron:enterochelin (holo-LCN2) to mimic the substantial LCN2 release after KA injury. Both treatments interacted with the LCN2R expressed on the neurons and were internalised into the neuronal cell bodies. Apo-LCN2 had no effect on apoptosis, while upregulation of Bim and decreased cell survival were detected in holo-LCN2-treated neurons, indicating the pro-apoptotic effect of holo-LCN2. It is possible that holo-LCN2 may import iron into the neurons, where it increases intracellular free iron to promote ROS production, thus increasing their vulnerability to oxidative stress and apoptosis.

The present study addressed the expression and localisation of LCN2 and its receptor, LCN2R, in the hippocampus after KA injury and their association with Bim-mediated apoptosis. Besides Bim, the apoptotic role of LCN2 was also dependent on its iron status as only iron-loaded LCN2 produced a pro-apoptotic effect. This pro-apoptotic effect of iron-loaded LCN2 may account for a select population of cell demise in KA-induced neurodegeneration. Elucidation of the role of LCN2 in the KA-induced neurodegeneration model could serve as a stepping stone to understand the role of LCN2 in other neurodegenerative diseases as interventions can be targeted at the interaction between LCN2 and LCN2R to retard neurodegeneration in general.

LIST OF TABLES

LIST OF FIGURES

LIST OF ILLUSTRATIONS

LIST OF ABBREVIATIONS

AD	Alzheimer's Disease
AMPA	α-amino-3-hydroxyl-5-methyl-4-isoxazole-propionate
Apo-LCN2	Iron-lacking LCN2
bp	Base pair
BS	Brainstem
BSA	Bovine serum albumin
CA	Cornu Ammonis
$CaCl_2$	Calcium chloride
CB	Cerebellum
CNPase	2', 3'-cyclic nucleotide 3'-phosphodiesterase
CNS	Central nervous system
DAB	3,3-diaminobenzidine tetrahydrochloride
DAPI	4',6-diamidino-2-phenylindole
DG	Dentate gyrus
DMEM	Dulbecco’s modified Eagle’s medium
DNA	Deoxyribonucleic acid
Ent	Enterochelin (enterobactin)
et al.	et alia (and others)
FCX	Frontal cortex
Fe	Iron
GFAP	Glial fibrillary acidic protein
HC	Hippocampus
Holo-LCN2	Iron-loaded LCN2
HT	Hypothalamus
Icv	Intracerebroventricular

IgG	Immunoglobulin G
Ip	Intraperitoneal
KA	Kainate (kainic acid)
KA1d	1 day post-KA injection
KA2wk	2 weeks post-KA injection
KA3d	3 days post-KA injection
LCN1	Lipocalin 1
LCN2	Lipocalin 2
LCN2R	Lipocalin 2 receptor
MAP2	Microtubule associated protein
mRNA	Messenger RNA
MTS	3-(4,5-dimethylthiazol-2-yl)-5-(3-carboxymethoxyphenyl)-2-(4-sulfophenyl)-2H-tetrazolium, inner salt
NMDA	N-methyl-D-aspartate
Olf	Olfactory bulb
PBS	Phosphate-buffered saline
PCR	Polymerase chain reaction
PD	Parkinson's Disease
ROS	Reactive oxygen species
RT-PCR	Reverse transcription polymerase chain reaction
SCX	Somatosensory cortex
SEM	Standard error of mean
SPSS	Statistic package for social sciences
Str	Striatum
TBS	Tris buffered saline
TBS-T	Tris buffered saline containing tween-20
TH	Thalamus

CHAPTER 1

INTRODUCTION

1. Neurodegeneration

Neurodegeneration refers to any pathological condition that primarily affects the neurons. Neurodegenerative diseases represent a group of neurological disorders with heterogeneous clinical and pathological expressions, such as Alzheimer's disease (AD), Parkinson's disease (PD), Huntington's disease (HD) and amyotrophic lateral sclerosis (ALS), effecting specific subsets of neurons in various functional anatomic systems (Calne et al., 1992; Przedborski et al., 2003).

1.1 Causes of neurodegeneration

Different neurodegenerative disorders have their own risk factors specific to the disease. However, the common risk factors for developing degenerative disorders are: increasing age, genetics and environmental factors (Jellinger, 2003, 2009, 2010; Przedborski et al., 2003). As many of these diseases have late-onset, it suggests the involvement of neurons gradually losing their function with age. Some neurodegenerative diseases have clear familial occurrence, which suggests a genetic basis. For instance, in HD, the disease runs as an autosomal dominant trait among the affected families (Przedborski et al., 2003). Even for PD, AD and ALS, about 10% of all cases are familial with specific genetic defect(s) that are identifiable and inheritable (Cho, 2010; Przedborski et al., 2003). From genetic linkage studies and molecular work, some genetic alterations were observed, such as mutations in the amyloid precursor protein (APP), presenilin 1 and 2 genes to alter amino acid β-amyloid (Aβ) peptide production in AD (Elder et al., 2010; Schaeffer et al., 2011); mutations of α-synuclein gene in PD (Beal, 2001; Shimohama et al., 2003); and mutations in SOD1 in ALS (Gruzman et al., 2007). However, most neurodegenerative diseases are sporadic, which can be a result of environmental and genetic risks

combined together. Genetically determined components that confer further susceptibility to an environmental factor could initiate neurodegenerative processes (Calne et al., 1992), as some neurodegenerative conditions arise in geographic or temporal clusters due to exposure to toxic compounds (Przedborski et al., 2003).

1.2. Models of many neurodegenerative disorders

To understand more about the basis of the pathophysiology in neurodegenerative diseases, many models have been used. For instance, for AD: transgenic mouse models with APP, presenilin or Tau mutations or Aβ-induced neurodegeneration (Elder et al., 2010; Schaeffer et al., 2011); and for PD: *in vivo* neurotoxin models of 1-methyl-4-phenyl-1,2,3,6-tetrahydropyridine (MPTP), 6-hydroxydopamine (6-OHDA) and rotenone and transgenic animals of Drosophila and murine α-synuclein overexpression (Beal, 2001; Shimohama et al., 2003). However, these models are designed to exhibit hallmarks of the actual clinical or pathological condition of the disease, not models of neurodegeneration in general. Although many hypotheses were discussed to explain neuronal death in neurodegeneration, it is known that excitotoxicity is an underlying cause of neuronal damage in cerebral ischaemia, epilepsy, PD, and AD (Doble, 1999; Meldrum, 2000; Wang et al., 2005). Therefore, to investigate the role of lipocalin 2 (LCN2) in neurodegeneration in general, the administration of excitotoxins (such as excitatory amino acids) will serve as a better tool in the present study as they can produce neuronal damage with some degree of specificity (i.e., receptor type, ion channel type).

1.3. Excitotoxin models for neurodegeneration

In many neurodegenerative diseases, neurodegeneration of the hippocampus is of particular concern as it affects learning and memory (Price, 1986). Excitotoxins that are often used for hippocampal lesioning studies include, ibotenic acid (IBO), *N*-methyl-D-aspartate (NMDA), kainate (KA) and quisqualate (Jarrard, 2002). IBO was not used in this study as it results in nonspecific patterns of cell loss of the hippocampus (dentate gyrus, hilar cells, CA1-CA3 pyramidal neurons) in the rat (Jarrard, 2002; Kohler et al., 1979). The high density of NMDA receptors on the CA1 pyramidal neurons may account for the selectivity of NMDA-induced lesions for CA1 (Greenamyre et al., 1985). In both IBO and NMDA lesioning models, no secondary damage was observed outside the hippocampus (Jarrard, 2002; Kohler et al., 1979). In contrast, KA results in selective cell loss at CA3, hilar cells and CA1 region and produces secondary damage in extrahippocampal structures (Patel et al., 1986). KA-induced excitotoxic neurodegeneration is often accompanied with excess calcium influx, inflammation, glia activation, oxidative stress (due to generation of reactive oxygen species (ROS) and reactive nitrogen species (RNS)), apoptotic and necrotic cell death (Wang et al., 2005; Zheng et al., 2011). These characteristics are similar to the pathological conditions in most neurodegenerative diseases. Therefore, KA-induced neurodegeneration was applied as a model of neurodegeneration in the present study.

2. Kainate-induced neurodegeneration

2.1. Kainate (KA)

Kainate, or kainic acid (KA) (2-carboxy-4-(1-methylethenyl)-3-pyrrolidineacetic acid), an acidic pyrolidine isolated from the seaweed *Digenea simplex* (Coyle, 1987), is an analogue of the excitatory amino acid L-glutamate. Glutamate, the major excitatory amino acid transmitter in the CNS, exerts its action by binding to glutamate receptors (GluRs). GluRs include the ionotropic receptors (iGluRs) and metabotropic receptors (mGluRs). In response to synaptically released glutamate, iGluRs generally provide rapid postsynaptic depolarisations and play major roles in neural transmission, synaptic plasticity, and learning and memory. There are three major subtypes of iGluRs: *N*-methyl-D-aspartate (NMDA), α-amino-3-hydroxyl-5-methyl-4-isoxazole-propionate (AMPA), and kainate (KA) receptors (Bloss and Hunter, 2010; Meldrum, 2000). KA is a non-degradable analogue of glutamate and is 30 times more potent in neurotoxicity than glutamate (Bleakman and Lodge, 1998).

2.2. Receptors that bind KA

KA is a potent agonist at AMPA and kainate classes of glutamate receptors in the CNS (Berger et al., 1986; Bleakman and Lodge, 1998). Both AMPARs and KARs, often collectively referred as non-NMDA receptors can bind KA, but KARs have about 1000-fold higher affinity for KA (Bloss and Hunter, 2010; Herb et al., 1992).

2.3. KA-induced excitotoxicity

KA is often used to induce excitotoxicity: stimulation of the non-NMDA receptors can result in rapid increase of free intracellular calcium (Ca^{2+}). Ca^{2+}

overload can damage the neurons in various ways, such as activation of Ca^{2+}-dependent enzymes (e.g. phospholipase A2, C, protein kinase C, endonucleases) and generation of ROS. With excessive Ca^{2+} and ROS, mitochondrial membrane potential collapses and results in the opening of mitochondrial permeability transition pores, releasing cytochrome-c and apoptotic-inducing factor (AIF), leading to activation of caspases and apoptosis (Wang et al., 2005). Overload of Ca^{2+} can also directly cause mitochondrial swelling and damage, reduction in ATP, increase in ROS, oxidising proteins, lipids and DNA, resulting in necrosis (Wang et al., 2005). Notably, KA-induced neuronal cell death bears hallmarks of both necrosis and apoptosis (Filipkowski et al., 1994; Kaminska et al., 1994; Pollard et al., 1994a; 1994b).

2.4. KA on the hippocampus

2.4.1. Select vulnerability in the hippocampus to KA

KA administration to rodents has been often used as an animal model to study mechanisms of neurodegenerative pathways. The hippocampus is especially sensitive to the excitatory and neurotoxic insult of KA (Suzuki et al., 1995) and is most affected by KA compared to other structures in the brain (Ben-Ari et al., 1981).

KA can be administered into the rodents to induce neuronal loss in select regions of the brain, depending on the method of administration - systemic or intracerebral injections of KA. Systemic administration includes subcutaneous, intraperitoneal or intravenous administrations of KA which cause neuronal death in the CA4, CA3 and CA1 subfields, but to a lesser extent in the CA2 subfield (Sperk et al., 1983; Sperk, 1994). Since very little (a few percent) of the systematically injected KA can reach the receptors in the brain (Berger et al., 1986; Nadler et al., 1980b), the

low bioavailability contributes to the variation in the response to KA (Sperk, 1994). Intracerebral injections have included intra-amygdala, intra-hippocampal and intracerebroventricular injections of KA (Sperk, 1994). Pyramidal cells of the CA3 and CA4 regions were most sensitive to intra-hippocampal injection of KA (Kohler et al., 1979), while intra-amygdala KA injection results in pronounced cell death within CA3 subfields (Ben-Ari et al., 1980; Pollard et al., 1994b). In contrast, intracerebroventricular (icv) administration of KA causes greatest cellular damage in the CA3 subfield ipsilateral to the injection, and lesser damage to the CA1 subfield (Nadler et al., 1978; 1980a; Schwob et al., 1980). It also produces more consistent hippocampal lesions compared to systemic KA injections (Ong et al., 1996; 1999). Across all routes of administration, the dentate gyrus (DG) and the CA2 are usually unaffected by the KA-induced excitotoxicity (Sperk, 1994).

The selective vulnerability of neurons to KA is largely contributed by the heterogeneous distribution of low and high affinity KA binding sites in the brain. Within the hippocampus, the highest density of high affinity KA receptors is around the mossy fibre terminals in the CA3 region of the hippocampus (Malva et al., 1998; Patel et al., 1986), while high densities of NMDA and AMPA receptors were detected at the basal and apical dendrites of the CA1 pyramidal neurons (Greenamyre et al., 1985). This suggests why CA3 pyramidal neurons are most vulnerable to KA-induced excitotoxicity.

In the present study, icv injection of KA was performed in order to study KA-induced neurodegeneration on the hippocampus as it produces consistent hippocampal lesions (Ong et al., 1999) and an orderly hierarchy of degeneration, which can mimic the pathology in neurodegenerative diseases (McGeer and McGeer, 1982). Intrahippocampal injection may be too invasive as it can cause physical injury to the hippocampus. The additional tissue injury at the lesioned site may induce

unnecessary upregulation of LCN2, confounding the effects of physical injury with KA-induced neuronal injury. On the other hand, icv KA injection permits exposure of hippocampal cells over the broad anterior-posterior surface of the hippocampus bordering on the lateral ventricles (McGeer and McGeer, 1982). Therefore, the effect observed would be a consequence of KA, the excitotoxin, rather than physical injury. Unilateral injection was performed at the right lateral ventricle so that neurodegeneration could be observed at the ipsilateral site of injection, while saline-injected animals served as control.

2.4.2. Glial activation

KA-induced neurodegeneration is accompanied with reactive gliosis - the response of endogenous glial cells reacting to the signals from the injured neurons (Streit et al., 1999). Activation of astrocytes and microglia (Jorgensen et al., 1993; Mitchell et al., 1993; Wang et al., 2005) and increases in expression of inflammatory cytokines were observed in lesioned areas (Ravizza et al., 2005; Rizzi et al., 2003).

After icv injection of KA, upregulation of activated microglia peaked at one month and declined thereafter (Jorgensen et al., 1993; Mitchell et al., 1993). Normally, microglia exist as ramified microglia (resting microglia), with small (5-10μm) oval cell bodies, with nuclei filling most of the soma, and numerous processes radiating from the soma. During neuronal injury, microglia become activated, with enlarged cell bodies and shorter, stouter processes, which appear to be spherical, rod-shaped and pleomorphic or amoeboid-like, unlike the ramified morphology. Finally, the activated microglial cells become phagocytic microglia (Streit et al., 1999; Streit, 2000).

In response to KA injury, astrocytes are activated and undergo reactive astrocytosis. Reactive astrocytes are characterised by their large cytoplasmic mass (hypertrophy), long, thick processes and increased expression of glial fibrillary acidic protein (GFAP) (Bendotti et al., 2000). Hence, GFAP is a well-known marker for reactive astrocytosis (Ding et al., 2000). Upregulation of GFAP was observed in the CA3 and CA1 subfields of the lesioned hippocampus as early as one day after KA administration and peaked at one month after the injection (Jorgensen et al., 1993; Mitchell et al., 1993).

2.4.3. Other models of KA-induced injury

Due to its wide-ranging effects on the hippocampus and extrahippocampal tissue, neuronal damage induced by KA also results in repeated temporal lobe seizures (Ben-Ari et al., 1984; Ben-Ari, 1985; Gruenthal et al., 1986; Sater and Nadler, 1988), cerebral ischaemia-reperfusion (Dykens et al., 1987) and production of oxidative stress (Candelario-Jalil et al., 2001). Therefore, besides being a model of neurodegeneration, KA has also been widely used as a model for ischaemic damage, temporal lobe epilepsy and oxidative damage (Benavides et al., 1990; Gluck et al., 2000; Groticke et al., 2008; Ratte and Lacaille, 2006).

3. Lipocalin 2 (LCN2)

3.1. Lipocalin family

Lipocalin 2 (LCN2) is a member of the lipocalin protein family, which is a large group of small extracellular proteins. These proteins have a large degree of diversity at the sequence level, but they have a highly conserved three-dimensional structure that is comprised of a single eight-stranded continuously hydrogen-bonded antiparallel beta-barrel, enclosing an internal ligand-binding site (Flower, 1996). They are characterised by a range of different molecular-recognition properties: 1) The ability to bind a range of small hydrophobic molecules, 2) binding to specific cell-surface receptors and 3) the formation of complexes with soluble macromolecules. They have a variety of different functions, including retinol transport, cryptic colouration, olfaction, pheromone transport, enzymatic synthesis of prostaglandins, regulation of immune responses, and mediation of cell homeostasis (Flower et al., 1993; Flower, 1994, 1996).

Most lipocalins share three characteristic conserved sequence motifs, corresponding to the three main structurally conserved regions of the lipocalin fold and are known as kernel lipocalins, such as the retinol binding protein (RBP), apolipoprotein D (apoD), prostaglandin D synthase (PGDS) and LCN2 (Flower et al., 1991). The more divergent family members, the outlier lipocalins, share two or less of the three motifs and are more diverse, such as the odorant-binding protein (OBP), von Ebner's-gland protein and α_1-acid glycoproteins (Flower et al., 1993).

3.2. History of Lipocalin 2

LCN2, is a 25kDa protein, also known as 24p3 (murine orthologue), neutrophil gelatinase-associated lipocalin (NGAL, human orthologue), α-2-

microglobulin-related protein (rat orthologue), 24-kDa superinducible protein (SIP24), uterocalin and siderocalin. The cDNA of the rat orthologue was fortuitously isolated during screening of a cDNA library for other purposes and GeneBank revealed the protein to be related to rat α-2-microglobulin. Hence it was named “α-2-microglobulin-related protein” (Chan et al., 1988).

Mouse 24p3 protein, the product of the single gene, 24p3, was first noted due to its increase in mRNA expression in cultured mouse kidney cells infected by SV40 and polyoma virus (Hraba-Renevey et al., 1989). Following that, from motif matching, high global homology, especially to rat α-2-microglobulin-related protein, and its consistency with the size and pattern of cysteine residues with other family members, mouse 24p3 was identified as a member of the lipocalin family (Flower et al., 1991). Isolation of a protein named “SIP24” secreted from Balb/c 3T3 mouse fibroblasts stimulated with fibroblast growth factor (FGF) and cycloheximide, an inhibitor of protein synthesis, which was shown later to be identical to mouse 24p3 (Davis et al., 1991; Liu and Nilsen-Hamilton, 1995). “SIP24” was then known as “superinducible protein”, due to the enhanced synthesis by cells and “24” due to its molecular weight estimated from SDS-PAGE (Davis et al., 1991; Hamilton et al., 1985; Nilsen-Hamilton et al., 1982).

In 1993, the human orthologue of LCN2 was identified as a protein of unknown function associated with 92kDa gelatinase/MMP9 in human neutrophils. Through immunoblotting and immunoprecipitation, a 135kDa form of gelatinase was found to be a complex of the 92kDa gelatinase and an “unknown” 25kDa protein. Sequence homology revealed a high degree of similarity with rat α-2-microglobulin-related protein and mouse 24p3 protein, suggesting the 25kDa “unknown” protein to be the human orthologue of 24p3, hence it was named “neutrophil gelatinase-associated lipocalin (NGAL)” (Kjeldsen et al., 1993). NGAL could exist as a

monomer, homodimer or as a heterodimer with gelatinase and was stored in specific granules within the neutrophils (Kjeldsen et al., 1994).

Among all three orthologues of LCN2, on the amino acid level, rat α-2-microglobulin-related protein and mouse 24p3 protein are 80% identical, while NGAL is 63.5% identical to α-2-microglobulin-related protein, and 62% identical to 24p3 (Kjeldsen et al., 1993; 2000). The high degree of identity at the cDNA level further validates that rat α-2-microglobulin-related protein and mouse 24p3 protein are homologues of NGAL (Bundgaard et al., 1994).

With the characterisation and identification of this novel lipocalin member, lipocalin 2 (LCN2), many studies were performed to understand its distribution and expression in normal and pathological cells and tissues, in order to elucidate its biological function.

Two decades from the first time LCN2 was isolated, LCN2 has now been shown to have diverse roles in infections, iron transport, inflammation, apoptosis, tumourigenesis, renal physiology, hematopoiesis and reproductive biology. In this thesis, only a few aspects that are relevant to the possible roles and functions of LCN2 in KA-induced excitotoxicity will be covered in detail. Due to the immense body of work done on different orthologues of LCN2 and various aspects of its functions, LCN2 has been named differently. In this thesis, since rat animal models were used, the rat orthologue of lipocalin 2 will be addressed as “LCN2”. In addition, lipocalin 2 in general, which includes orthologues from all species, will be referred as “LCN2”.

3.3. Ligands of LCN2

LCN2, like most lipocalins, was thought to bind ligands and interact with specific cell-surface receptors to modulate cellular processes. Hence, by X-ray crystallography, atomic absorption and X-ray fluorescence analysis, mouse and human orthologues of LCN2 were reported to bind specifically and with high affinity to bacterial catecholate-type ferric siderophores (Coles et al., 1999; Goetz et al., 2000; Goetz et al., 2002). It was the structure of NGAL (human orthologue of LCN2) that led to the inference of its ligand. Similar to other lipocalins of the lipocalin family, LCN2 has an eight-stranded anti-parallel β barrel, enclosing a ligand binding site (calyx), with short 3_{10}-helix at the N-terminus and α-helix at the C-terminus. Unlike most lipocalin calyces, which have distinct hydrophobic linings, the calyx of LCN2 is lined with polar and positively-charged residues and is shallower and broader than most lipocalin calyces (Coles et al., 1999; Goetz et al., 2000).

When NGAL (human orthologue of LCN2) was expressed in bacteria, it was co-purified with a red chromophore, which was tightly associated but not covalently bound with the purified NGAL. The heavy atom of the chromophore was identified as iron by atomic absorption and X-ray fluorescence spectroscopy (Goetz et al., 2002). Binding and analytical studies then identified the red chromophore as ferric enterochelin (Fe:Ent) with a net charge of -3 (Raymond et al., 2003). Complex structural analyses reveal that LCN2 binds Fe:Ent by intercalating the positively charged side chains of the three protein residues (Arg 81, Lys 125 and Lys 134) between the three catecholate rings of Fe:Ent, creating a novel hybrid of ionic and cation-π interactions (Clifton et al., 2009; Goetz et al., 2002). Despite the additional stabilising van der Waals and hydrogen bonds, the Fe:Ent does not fill all of the calyx sub-pockets completely (Goetz et al., 2002). This suggests that the LCN2 calyx may be optimised for other ligands (Coles et al., 1999; Goetz et al., 2000; 2002). An

interesting point to note was NGAL:iron:enterochelin was in a 1:1:1 stoichiometry (Goetz et al., 2002).

Enterochelin (Ent, enterobactin) is a siderophore of many enteric bacteria. Siderophores are low molecular weight (500-1500Da) compounds produced by bacteria, fungi graminaceous plants with high affinity for iron (Fe^{3+}) to scavenge iron from the environment. Siderophores can be categorised into three board classes based on the chemistry of chelation: hydroxamates, phenolates/catecholates or α-hydroxycarboxylates (Braun and Killmann, 1999; Hider and Kong, 2010). However, qualitative binding assays reveal that LCN2 binds with catecholate-type ferric siderophores (e.g. parabactin and cepabactin), but not hydroxamate-type ferric siderophores (e.g. aerobactin, ferrichrome, and desferrioxamine B) (Goetz et al., 2002). Before the elucidation of mammalian siderophores in 2010, ferric enterochelin was often used as a surrogate to investigate LCN2's role on iron delivery in mammalian cells.

Hence with the ability to scavenge iron from bacteria, LCN2 was later studied to be a bacteriostatic agent in bacterial infection which will be discussed later in *Section 3.5.1*.

3.4. Receptors of LCN2

Like other lipocalin family members, LCN2 has a receptor binding patch, suggesting it has receptors (Flower, 1996). Two cell surface receptors of different molecular structure have been identified: 1) Megalin, a multi-ligand receptor and 2) 24p3R, receptor for 24p3, the murine orthologue of LCN2 (Devireddy et al., 2005; Hvidberg et al., 2005).

3.4.1. Megalin

Megalin, also known as gp330 or low density lipoprotein-related protein 2 (LRP2), is a multi-ligand, endocytic receptor with significant physiological functions. The name “megalin” was suggested due to its large size of 600kDa (Saito et al., 1994). Megalin is a 4,600-amino acid transmembrane protein with a large amino-terminal extracellular domain, a single transmembrane domain and a short carboxy-terminal cytoplasmic tail (Saito et al., 1994). The protein belongs to the low-density lipoprotein receptor (LDLR) family. Other mammalian receptors include the LDL receptor, the very-low-density lipoprotein (VLDL) receptor, the LDLR-related protein and the apolipoprotein E receptor 2 (ApoER2) (Gliemann, 1998).

Megalin is expressed in many absorptive epithelia facing transcellular fluids, such as the small intestine, epididymis, thyroid cells, epithelium of the eye and the choroid plexus (Kounnas et al., 1994; Zheng et al., 1994). It is also localised in the apical endocytic pathway of the renal proximal tubule and in the glomeruli (Kerjaschki and Farquhar, 1982, 1983). Its endocytic scavenger receptor function in the kidney proximal-tubule epithelium (Kerjaschki and Farquhar, 1983; Kerjaschki et al., 1984) where low molecular weight proteins are reabsorbed into the tubules from the glomerular filtrate, has been widely discussed. Being a promiscuous receptor, it interacts with lactoferrin (Willnow et al., 1992) and has a large number of ligands, including other lipocalins, such as vitamin-binding proteins (vitamin D- and retinol-binding proteins) (Nykjaer et al., 1999), apolipoproteins (apoB, apoE and apoH), and other low molecular weight peptides and hormones (insulin, epidermal growth factor, prolactin and lysozyme) (Christensen and Birn, 2001, 2002).

Megalin-deficient mice showed defective tubular reabsorption and increased urinary excretion of low molecular weight proteins including LCN2 (Leheste et al., 1999), which suggests that megalin is required for re-uptake of LCN2. With surface

plasmon resonance, megalin was reported as a cellular receptor for NGAL and binds with it with high affinity, mediating its cellular uptake (Hvidberg et al., 2005).

3.4.2. 24p3R (murine orthologue)

A receptor for 24p3 (murine orthologue of LCN2), 24p3R, was first discovered in leukocytic cell lines as a cell surface receptor mediating the apoptotic effect of 24p3 (Devireddy et al., 2001; Devireddy et al., 2005). It is a highly conserved protein also known as brain type organic cation transporter (BOCT), belonging to the organic cation transporter family (OCT, SLC22) made up of ATP-independent facilitative transporters that are responsible for the uptake, reabsorption and excretion of drugs, nutrients and metabolites. OCTs are characterised by 12 putative transmembrane domains (TMDs), a large extracellular loop with multiple glycosylation sites between TMDs 6 and 7 and intracellular N and C-terminal (Koepsell et al., 1998). 24p3R, also known as SLC22A17, BOCT1, shares sequence similarity with the other BOCT proteins from TM2 to TM12. 24p3R has a shorter N-terminus than other members and is without a comparable TM1 domain, indicating that the N-terminus is extracellular (Bennett et al., 2011).

Northern blot results reveal *24p3R* expression to be highest in the brain and kidney, intermediate expression in the liver, low expression in the heart, stomach and testis, and absent in the muscles (Bennett et al., 2011). The tissue expression of 24p3R suggests its importance in the brain and kidney, where LCN2 has also been expressed (Chia et al., 2011; Yang et al., 2002b). Among brain and brain-derived cells, the choroid plexus had the highest expression of *24p3R*, followed by primary neurons, whole brain, NG108 neuroblastoma, C6 astroglioma and the primary astrocytes had the lowest expression (Bennett et al., 2011). Therefore, 24p3R may

be involved in functions in the brain and blood brain barrier as LCN2 was shown to be upregulated at the choroid plexus after peripheral inflammation (Marques et al., 2008). 24p3R protein expression was also widely expressed in heart, lung, liver, kidney, stomach, small intestine, testis, uterus, ovary and placenta tissues from mice (Devireddy et al., 2005). Since in this thesis, *in vivo* studies were performed in the rat animal model, 24p3R will be referred as “LCN2R”.

3.5. Roles of LCN2 in various aspects

Since the isolation of LCN2 in 1988, many studies were done on different orthologues of LCN2. Therefore, due to diverse roles of LCN2, this thesis will focus on a few aspects in which LCN2 plays a major role, such as in renal physiology, kidney injuries, tumourigenesis, and aspects of LCN2 that are relevant to its possible role in KA-induced neurodegeneration, such as its role in bacterial infections, iron transport and apoptosis will be covered in detail.

3.5.1. Infections and innate immunity

LCN2 is rapidly upregulated in many models of infection, including infections involving *Escherichia coli*, *Klebsiella pneumonia* (Fischbach et al., 2006; Flo et al., 2004; Wu et al., 2010), *Chlamydia pneumonia* (Rodriguez et al., 2007), *Salmonella typhimurium* (Godinez et al., 2008; Nairz et al., 2007; Raffatellu et al., 2009), and Mycobacteria (Halaas et al., 2010; Martineau et al., 2007; Saiga et al., 2008), which indicates an important function of LCN2 as a bacteriostatic agent (Li and Chan, 2011). As mentioned earlier, due to its ability to bind bacterial catecholate-type ferric siderophore with specificity and affinity, it can interfere with iron acquisition by bacteria.

Under aerobic conditions, iron is primarily in the ferric (Fe^{3+}) oxidation state and forms insoluble complexes readily. Although iron is essential for cell survival, levels of free iron (Fe^{2+}) must be kept in check as it can be potentially toxic, either by catalysing the generation of free radicals, or by promoting the growth of bacteria. Therefore, in the human body, the majority of iron is sequestered by iron-binding proteins. Most iron is bound by haemoglobulin; transferrin transports iron between cells and is usually 30-40% saturated in the serum; ferritin sequesters free iron

intracellularly (Harrison and Arosio, 1996; Ponka et al., 1998); and lactoferrin is released from neutrophils at sites of inflammation with a bacteriostatic effect (Ellison, 1994; Jurado, 1997).

As bacteria require iron for growth, they release bacterial siderophore proteins, such as enterochelin (enterobactin, Ent) that bind ferric iron with an extraordinary high affinity, which is greater than that of the above mentioned mammalian iron-binding proteins (Barasch and Mori, 2004; Flo et al., 2004; Goetz et al., 2002). Bacteria express receptors for the bacterial siderophore to facilitate iron uptake. In response to bacterial infection, Toll-like receptors on immune cells

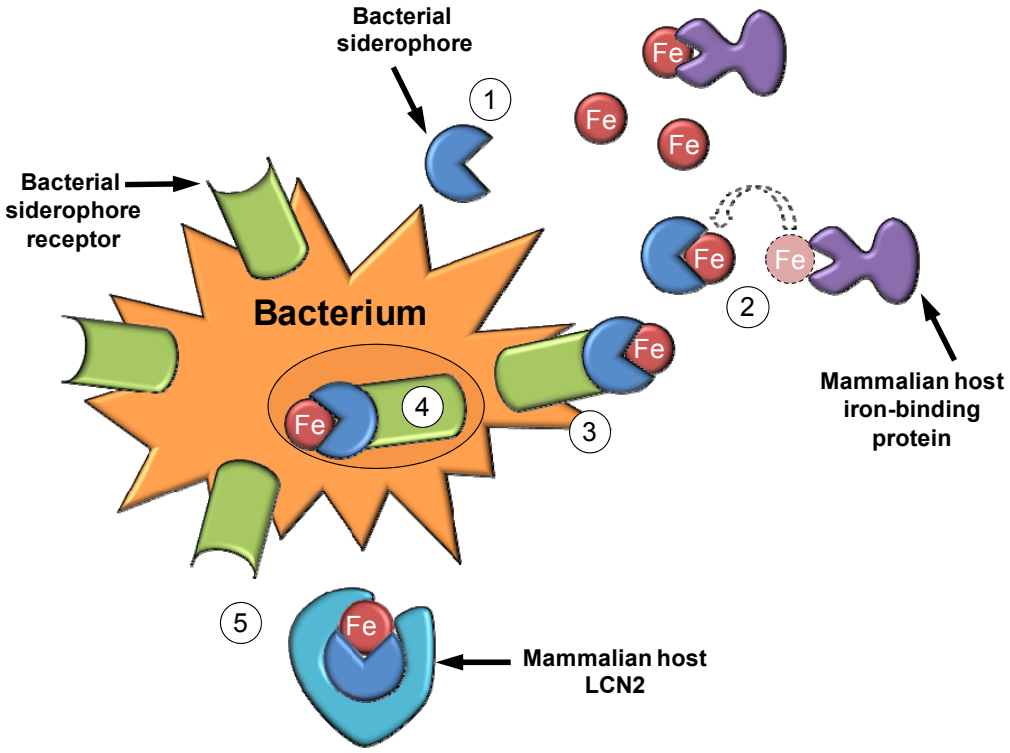

Fig. 1.1. Schematic diagram of the function of LCN2 in bacterial infection. (1) Bacteria (orange) release bacterial siderophore (blue). (2) Bacterial siderophore binds iron (red) with higher affinity than competing iron-binding proteins expressed by the mammalian host (purple) e.g. transferrin. (3) Bacteria express siderophore receptors (green) to bind the iron-bacterial siderophore complex. (4) The iron is subsequently internalised into the bacterium. (5) Mammalian host LCN2 (light blue) binds to the iron-bacterial siderophore complex with similar affinity to the bacterial siderophore receptor, thus preventing bacteria from capturing iron from mammalian hosts. Not drawn to scale.

stimulate the transcription, translation and secretion of LCN2 by the host. Secreted LCN2 then binds the bacterial siderophore-iron complex, forms a tricomplex, to be taken into the host cells. Since LCN2 binds siderophore with similar affinity to the siderophore receptor of the bacteria, it competes with bacteria for the siderophore-iron complex and inhibits bacterial growth (Flo et al., 2004; Goetz et al., 2002) (Fig. 1.1).

LCN2 is thus an important component of innate immunity against bacterial infection, and LCN2-deficient mice showed increased susceptibility to bacterial infection due to failure of iron sequestration by LCN2 (Berger et al., 2006; Flo et al., 2004). It is also interesting to note that another lipocalin, LCN1, also known as tear lipocalin, is able to bind a broader spectrum of siderophores, exhibiting anti-microbial activity, though the nature of the mechanism has yet to be elucidated (Fluckinger et al., 2004).

3.5.2. Inflammation

Other than LCN2's involvement in bacterial infection, marked increases in the local and systemic expression of LCN2 have been reported in various inflammatory conditions in affected tissues of the respiratory, gastro-enteric, and renal structures (Alpizar-Alpizar et al., 2009; Dittrich et al., 2010; Grigoryev et al., 2008).

In 1995, LCN2 was identified as an acute phase protein due to the rapid elevation of its mRNA and protein expression in mouse serum and liver during the acute phase response induced by turpentine injection (Liu and Nilsen-Hamilton, 1995). This further emphasised its role in inflammation as acute phase proteins are defined as proteins with at least 25% change in plasma concentration at the beginning of the inflammatory process (Ceciliani et al., 2002; Gabay and Kushner,

1999; Morley and Kushner, 1982). An example of an acute phase protein is C-reactive protein (CRP), which was detected in the plasma of patients during the acute phase of pneumococcal infection (Tillett and Francis, 1930).

Similarly, LCN2 has been reported as a choroid plexus acute phase protein in peripheral inflammation induced by systemic lipopolysaccharide (LPS) (Marques et al., 2008). LCN2 was also upregulated in inflammatory salivary tissues (Woo et al., 2007), livers in acute and chronic experimental liver injury (Borkham-Kamphorst et al., 2011) and lung tissues with airway inflammation (Dittrich et al., 2010). Authors had also suggested a protective role for LCN2 in allergic airway disease, as blocking of LCN2 increased inflammation and reduced apoptosis (Dittrich et al., 2010). The upregulation of LCN2 after inflammation indicates its possible involvement in inflammation, as the purpose of acute phase proteins is to restore homeostasis as soon as possible.

LCN2 has also been associated with obesity (Wang et al., 2007; Yan et al., 2007) and its related metabolic conditions, such as insulin-resistance (Wang et al., 2007; Yan et al., 2007) and hyperglycemia (Wang et al., 2007) due to their increasingly recognition as inflammatory conditions. As LCN2 was highly expressed in the adipose tissues *in vivo* and *in vitro*, it is also known as an adipokine (Yan et al., 2007; Zhang et al., 2008). As an adipokine, LCN2 has been reported to have an anti-inflammatory effect by inducing PPARγ expression, antagonising TNFα effects in adipocytes and suppressing LPS stimulation on cytokine expression in macrophages (Zhang et al., 2008).

3.5.3. Tumourigenesis and other biological processes

3.5.3.1. Cancer and tumourigenesis

Other than inflammation, LCN2 has recently been widely studied in tumourigenesis. LCN2 was elevated in several human cancers, including leukaemia (Kaneta et al., 2003; Villalva et al., 2008) and breast (Bauer et al., 2008; Fernandez et al., 2005), gastric (Kubben et al., 2007), colorectal (Conrotto et al., 2008; Madoz-Gurpide et al., 2006), ovarian (Lim et al., 2007; Santin et al., 2004) and pancreatic (Furutani et al., 1998; Han et al., 2002) cancers, suggesting its involvement in cancer.

Matrix metallopeptidase-9 (MMP-9) complexes with LCN2 were found in about 90% of the urine samples of breast cancer patients, which were absent from healthy women, indicating the use of LCN2/MMP9 as potential biomarker for diagnosis (Fernandez et al., 2005). Furthermore, elevated LCN2 strongly correlated with a poor prognosis in human primary breast cancer (Bauer et al., 2008). LCN2 was suggested to promote cell metastasis, as it induced epithelial to mesenchymal transition (EMT) via the estrogen receptor α/Slug axis, and increased migration and invasion. The formation of complexes of LCN2 with MMP9 protected the latter from degradation, resulting in promotion of breast tumourigenesis (Yang et al., 2009). The upregulation or presence of LCN2/MMP9 complex has also been observed in cerebral tumours (Smith et al., 2008), gastric carcinoma tissue (Kubben et al., 2007), and biopsy samples of oesophageal squamous cell carcinoma (ESCC) (Zhang et al., 2007).

On the other hand, LCN2 levels were observed in benign and well-differentiated ovarian and pancreatic carcinomas respectively, but were absent in high-grade carcinomas (Lim et al., 2007; Tong et al., 2008). Hence, LCN2 may have dual roles in promoting tumourigenesis and inhibiting the transition of neoplasias (cancerous tissues) towards more advanced grades of malignancy (Bolignano et al., 2010b). *In vitro*, after induction of EMT by EGF in ovarian carcinoma models, LCN2

levels were reduced and LCN2 overexpression in colon carcinoma, pancreatic carcinoma, and mouse mammary mesenchymal tumour cell lines resulted in reduction of adhesion, invasion and angiogenesis (Gupta et al., 2001; Hanai et al., 2005; Li and Chan, 2011; Tong et al., 2008), possibly suggesting an anti-angiogenesis or anti-metastatic function of LCN2.

In view of the conflicting studies on LCN2, the actual role of LCN2 in tumourigenesis remains to be elucidated, and LCN2 appears to have different effects on different type or grades of carcinoma, which could be either anti- or pro-tumourigenic.

3.5.3.2. Other biological processes

Other than its role in tumourigenesis, LCN2 has been implicated in other biological processes in the body. LCN2 may be involved in kidney development and differentiation as it promotes differentiation and structural organisation of renal epithelial cells (Yang et al., 2002a; 2002b). LCN2 has also been shown to be involved in the pathophysiological process of chronic renal disease, such as polycystic kidney disease and glomerulonephritis (Bolignano et al., 2008). Due to its high elevation in the serum and urine in renal injuries, and correlation with severity of renal impairment, LCN2 has been suggested as a biomarker or real-time indicator for detection of various renal injuries (Bolignano et al., 2008; Schmidt-Ott et al., 2006; 2007; Yang et al., 2003).

Other than in renal pathophysiology, LCN2 can also play a protective role in thermal dysregulation, where LCN2 is induced in the liver, heart and kidney *in vivo* with cold and heat stress. *In vitro* data have revealed that ectopic expression of LCN2 can protect cells against cold stress, while exogenous LCN2 administration

can enhance the toxicity of heat stress (Roudkenar et al., 2009). LCN2 is also involved in hematopoiesis as LCN2 suppresses red blood cell production in an autocrine manner and the growth of erythroid and monocyte/macrophage lineages *in vitro* (Bolignano et al., 2010a; 2005; Miharada et al., 2008). In addition, LCN2 is involved in reproductive biology (Chu et al., 2000; Elangovan et al., 2004; Lee et al., 2003; 2005).

3.5.4. Iron transport

Since LCN2 sequesters iron from bacterial cells during infection, many studies asked if it could traffic iron (with the help of a cofactor/mammalian siderophore) in or out of cells physiologically. In 2002, in the same journal that identified ferric enterochelin as a ligand of NGAL (human orthologue of LCN2) (Goetz et al., 2002), NGAL/24p3 (human and mouse orthologues of LCN2) was reported to deliver radioactive iron (^{59}Fe) to the cytoplasm of kidney cell lines (Yang et al., 2002b). NGAL/24p3 delivered iron into the cells via receptor-mediated endocytosis independent of the transferrin iron delivery pathway as the addition of transferrin did not block the entry of labelled NGAL/24p3 into the cells. Secondly, NGAL/24p3 and transferrin did not colocalise, as transferrin had a perinuclear staining while NGAL/24p3 was localised throughout the cytoplasm and close to the periphery of transferrin's localisation (Yang et al., 2002b). Instead, NGAL/24p3 colocalised with DMT1 iron transporters, which were found in late endosomes (Tabuchi et al., 2000).

Similar to lactoferrin, LCN2 trafficked iron to late endosomes and released iron at low pH (Abergel et al., 2008; Birgens et al., 1988; Nicholson et al., 1997). Late endosomes are more acidic than the early recycling vesicles and the low pH allows the conversion of ferric-catecholate to ferric salicylate, a substrate for reduction by

NADH or NADPH coupled ferrireductase (Ward et al., 1999). Hence, the bound ferric state (Fe^{3+}) is reduced to ferrous state (Fe^{2+}) and released (Abergel et al., 2008; Ward et al., 1999). In addition, the strong acidification degrades the siderophore (Abergel et al., 2008), but not LCN2 which can be recycled after iron release (Yang et al., 2002b). In other words, low pH in the late endosomes can result in the release of iron and degradation of the siderophore, and LCN2 has been postulated to be exported out of the cell for recycling.

Iron-loaded LCN2 increased cytoplasmic iron and regulated iron-responsive genes (by enhancing translation or promoting degradation of the mRNA), such as upregulation of ferritin and downregulation of transferrin receptor 1 (Yang et al., 2002b), and decreased levels of iron-regulatory protein IRP2 and conversion of IRP1 to cytosolic aconitase (Devireddy et al., 2010).

The biological function of LCN2 transporting iron was demonstrated by LCN2:Enterochelin (Ent) delivery of ^{55}Fe to the kidney proximal tubule *in vivo*. LCN2:Fe:Ent protected the kidney from ischaemic-reperfusion injury (ATN) in mice while iron-free LCN2 could only partially protect it (Mori et al., 2005), indicating Fe:Ent as the main component in holo-LCN2's protective effect. Holo-LCN2 also induced heme oxygenase-1 (HO-1), an important regulator of proximal tubule viability and for recovery from ATN (Mori et al., 2005).

This indicates that the iron-trafficking function of LCN2 may be protective as it can also protect kidneys from ATN by regulating other protective factors (Mishra et al., 2004; Mori et al., 2005). The protective effect of iron-loaded LCN2 was also observed in 24p3R-expressing HeLa cells, in which iron-loaded LCN2 increased intracellular iron and inhibited apoptosis (Devireddy et al., 2005).

3.5.5. Apoptosis

Besides the protective effect of LCN2 observed in iron delivery, LCN2 has been implicated in many pro- and anti-apoptotic functions, depending on the tissues, cell lines, pathological or physiological conditions.

24p3 (murine orthologue of LCN2) has been reported to be pro-apoptotic as the conditioned medium from interleukin-3 (IL-3) deprived FL5.12 cells (mouse pro-B lymphocytic cell line) contained 24p3, which induced apoptosis in naive FL5.12 cells with IL-3 present (Devireddy et al., 2001). In the same cell line, LCN2 mRNA and protein expression was upregulated in MK886-induced apoptosis. When the cells were stably transfected with antisense cDNA of 24p3, apoptosis was reduced, suggesting that 24p3 was pro-apoptotic (Tong et al., 2003). Overexpression of 24p3 increased the proportion of apoptotic epithelial cells by 3- to 4-fold in mammary epithelial cells (Bong et al., 2004). *In vitro*, LCN2 overexpression and LCN2 treatment increased the sensitivity of microglia, astrocytes and neurons to cytotoxic stimuli, which was abolished with the knockdown of LCN2 (Lee et al., 2007; 2009; 2011). The pro-apoptotic characteristic of LCN2 was further supported by its upregulation in 13-*cis*-retinoic acid-induced apoptosis in human sebaceous gland cells and the silencing of LCN2 inhibited apoptosis (Nelson et al., 2008).

On the other hand, LCN2 was also shown to be anti-apoptotic. Excessive amounts of purified recombinant LCN2 were not toxic to human lung adenocarcinoma A549 and Jurkat cells and LCN2 overexpressing cells had no abnormalities. Silencing of LCN2 enhanced the pro-apoptotic activity of celecoxib-related compounds, indicating the anti-apoptotic function of LCN2 (Tong et al., 2005). Although LCN2 is greatly upregulated in post-ischaemic kidneys, intravenous administration of LCN2 in mice before, during and after ischaemia, ameliorated the histopathological damage and apoptotic effects (Mishra et al., 2004)

Recently, LCN2's role in apoptosis has been associated with its ability to transport iron. LCN2 knockdown resulted in decreased iron content in human anaplastic thyroid carcinoma cells (FRO), which induced apoptosis under serum deprivation, but was abolished with the addition of iron or iron-loaded LCN2. The presence of LCN2 in FRO cells served as a pro-survival factor by binding and transporting iron in the cells (Iannetti et al., 2008). As discussed in the previous *Section 3.5.4*, endocytic delivery of LCN2:Fe:siderophore complex protects the kidney from ischaemia-reperfusion injury by upregulating HO-1, a protective enzyme, mitigating cell death (Mori et al., 2005). These are in agreement with the model proposed by Devireddy et al. (2005); holo-LCN2 (iron-loaded) has been suggested to inhibit apoptosis, while apo-LCN2 (iron-lacking) promotes apoptosis.

Until now, it is not clear if LCN2 is pro- or anti-apoptotic, as its functions vary from cell line to cell line and from *in vitro* to *in vivo* conditions. The varied roles of LCN2 in apoptosis could also be attributed to the differences in the orthologues of LCN2 (Kehrer, 2010; Klausen et al., 2005). For instance, 24p3 (mouse orthologue) was implicated in apoptosis of myeloid cells, but not NGAL (human orthologue) and NGAL was not an acute phase protein unlike 24p3 (Klausen et al., 2005). Furthermore, as opposed to murine and rat orthologues of LCN2, NGAL has an additional cysteine so NGAL can undergo homodimerisation and is able to heterodimerise with gelatinase unlike the rodent orthologues of LCN2 (Kjeldsen et al., 2000). Despite the diverging literature, it is clear that LCN2's involvement in iron transport and apoptosis are associated.

Despite the roles postulated for LCN2 in the periphery as mentioned in the previous sections, LCN2-deficient mice produced by two independent groups raised in specific pathogen-free facilities showed no defects in apoptosis, iron metabolism, kidney development and reproduction, arguing against an obligatory role for LCN2 in

these biological processes (Berger et al., 2006; Flo et al., 2004). It is possible that there are compensatory mechanisms that can substitute LCN2 in these processes, which may obscure LCN2's potential biological roles as discussed by many.

Most of the work reviewed in this thesis is not exhaustive of the roles and functions of LCN2, as the lipocalin has diverse roles. To help understand the role of LCN2 in KA-induced neurodegeneration, it would be most relevant to study LCN2's role in brain-derived cells *(Section 3.6)*. With the increase in iron and apoptosis in neurodegeneration, the association of LCN2 with apoptosis and iron transport will also be covered in greater details in the following section *(Section 3.7)*.

3.6. Role of LCN2 in brain-derived cells

Despite diverse studies in the periphery, little is known about LCN2 in the CNS. Lee, Suk and colleagues (2007, 2009, and 2011) are the first group to establish the pro-apoptotic effect of LCN2 in brain-derived cells - microglial, astrocytic, neuronal and glioblastoma cells (Lee et al., 2007; 2009; 2011; Zheng et al., 2009). These *in vitro* studies will be very useful for postulating LCN2's role in the brain.

Stable expression of LCN2 and treatment of LCN2 protein increased the sensitivity of primary microglia and BV-2 murine microglial cell lines to nitric oxide (NO)-induced apoptosis, which was abolished with the knockdown of LCN2. Furthermore, LCN2 treatment induced deramification of microglia to form the amoeboid morphology (Lee et al., 2007).

Similar to their previous study in 2007, Lee and colleagues showed that LCN2 sensitised primary astrocytes to cell death, which was negated with the silencing of LCN2. LCN2 also induced phenotypic change of astrocytes (reactive astrocytosis) through the Rho-ROCK (Rho kinase)-GFAP pathway (Lee et al., 2009).

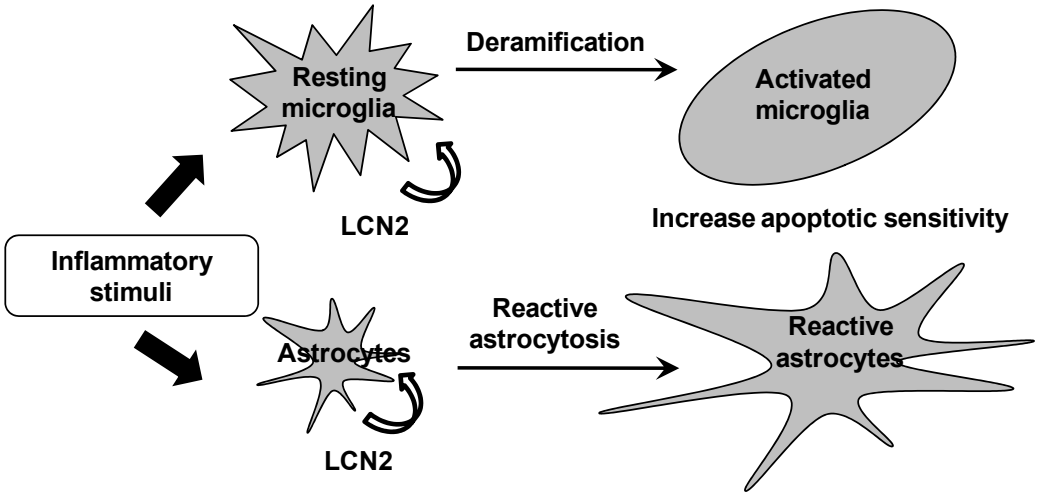

Fig. 1.2. Schematic diagram of LCN2's role in apoptosis and morphological changes in astrocytes and microglia *in vitro*. LCN2 is induced by inflammatory stimuli and acts on the receptors to induce pro-apoptotic effects and morphological changes on these cells in an autocrine manner. Apo-LCN2 has a pro-apoptotic effect on cells. Diagram adapted from Lee et al. (2007). Not drawn to scale.

Since LCN2 was induced in primary microglia, BV-2 microglial cells, primary astrocytes and C6 glioma cells upon inflammatory stimuli, the presence of 24p3R mRNA on these cells suggests that LCN2 acts in an autocrine manner to induce cell death sensitisation and morphological changes (Lee et al., 2007; 2009) (Fig. 1.2). Furthermore, LCN2 induced cell death sensitisation effects on B35 rat neuroblastoma and mice primary cortical neurons, and accelerated neuronal mobility and process extension, suggesting that LCN2 could regulate neuronal cell death, migration and morphology (Lee et al., 2011).

Interestingly, cell death sensitisation effects of LCN2 on C6 glioma and B35 neuroblastoma was abolished with the addition of iron:siderophore complex, a phenomenon which was similarly observed in the BV-2 microglial cells. Furthermore, LCN2-treated C6 glioma and B35 neuroblastoma cells had upregulated Bim expression, but upon Bim knockdown, the cell death sensitisation effect of LCN2 was abolished. The evidence strongly suggests the involvement of iron and Bim in the cell death sensitising effect of LCN2 in the astrocytic and neuronal cells. Despite this, the pro-apoptotic effect of LCN2 on BV-2 microglia was not Bim-mediated, suggesting that LCN2 may have other ways of inducing apoptosis (Lee et al., 2007; 2009; 2011)

The pro-apoptotic effect of LCN2 was also observed in human glioblastoma cells (U87MG, U373MG and T98G cells), as the addition of LCN2 significantly increased the sensitivity of the cells to anti-cancer drugs in a dose-dependent manner (Zheng et al., 2009).

Results from the brain-derived cells show that LCN2 is likely to be pro-apoptotic and could either sensitise cells to cytotoxic stimuli or directly cause cell death at a high concentration (50 μg/ml) (in glioblastoma cells). Also, the presence of iron appears to affect the cell death sensitising effects of LCN2. Discrepancies in the involvement of Bim in the LCN2-induced cell sensitisation between the microglia, and

the neurons and astrocytes *in vitro*, serve as a cautionary signal not to assume the same mechanism for different cell types when examining LCN2-mediated apoptosis *in vivo*. The pro-apoptotic effect of LCN2 and the anti-apoptotic effect of LCN2 with the iron:siderophore is consistent with the model proposed by Devireddy et al. (2005), which will be discussed in detail in the following *Section 3.7.*

3.7. Association between LCN2, LCN2R and apoptosis

Recently, an association between LCN2, iron transport and apoptosis was made with the isolation of a cell surface receptor for 24p3 (murine orthologue of LCN2), i.e., 24p3R (Devireddy et al., 2005). 24p3R expressing-HeLa cells could bind and internalise both iron-free 24p3 (apo-24p3) and iron-loaded 24p3 (holo-24p3). Holo-24p3 increased intracellular iron, and did not induce apoptosis. In contrast, apo-24p3 treatment decreased intracellular iron and upregulated the pro-apoptotic protein, Bim. Bim shRNA reduced apo-24p3-induced apoptosis, indicating that the apoptosis was, at least in part, Bim-mediated.

Devireddy and colleagues' observations led to a proposed model expanded upon by Richardson (2005) in an influential review in *Cell.* The effects of LCN2 in iron uptake or apoptosis was dependent on its iron status. Holo-24p3 transports iron into cells via endosomes and releases iron at low pH (Abergel et al., 2008; Yang et al., 2002b). This increases intracellular iron and inhibits apoptosis. In contrast, internalised apo-24p3 binds to intracellular iron-siderophore complex to form holo-24p3, to be exported from the cell. Depletion of intracellular iron induces the expression of Bim, which leads to apoptosis (Devireddy et al., 2005; Richardson, 2005). This model postulates the presence of endogenous intracellular mammalian siderophore(s) (Devireddy et al., 2005) (Fig. 1.3).

This proposed mechanism led to a search for endogenous mammalian siderophores. Finally in June 2010, the same group, Devireddy, Green, and colleagues (2010), isolated the iron-binding moiety of the mammalian siderophore 2,5-dihydroxybenzoic acid (2,5-DHBA), similar to 2,3-DHBA, the iron-binding moiety of the bacterial enterochelin (Raymond et al., 2003). The murine enzyme responsible for the synthesis of 2,5-DHBA was identified as BDH2, the murine homologue of bacterial EntA, catalysing the synthesis of 2,3-DHBA (Liu et al., 1989). The human

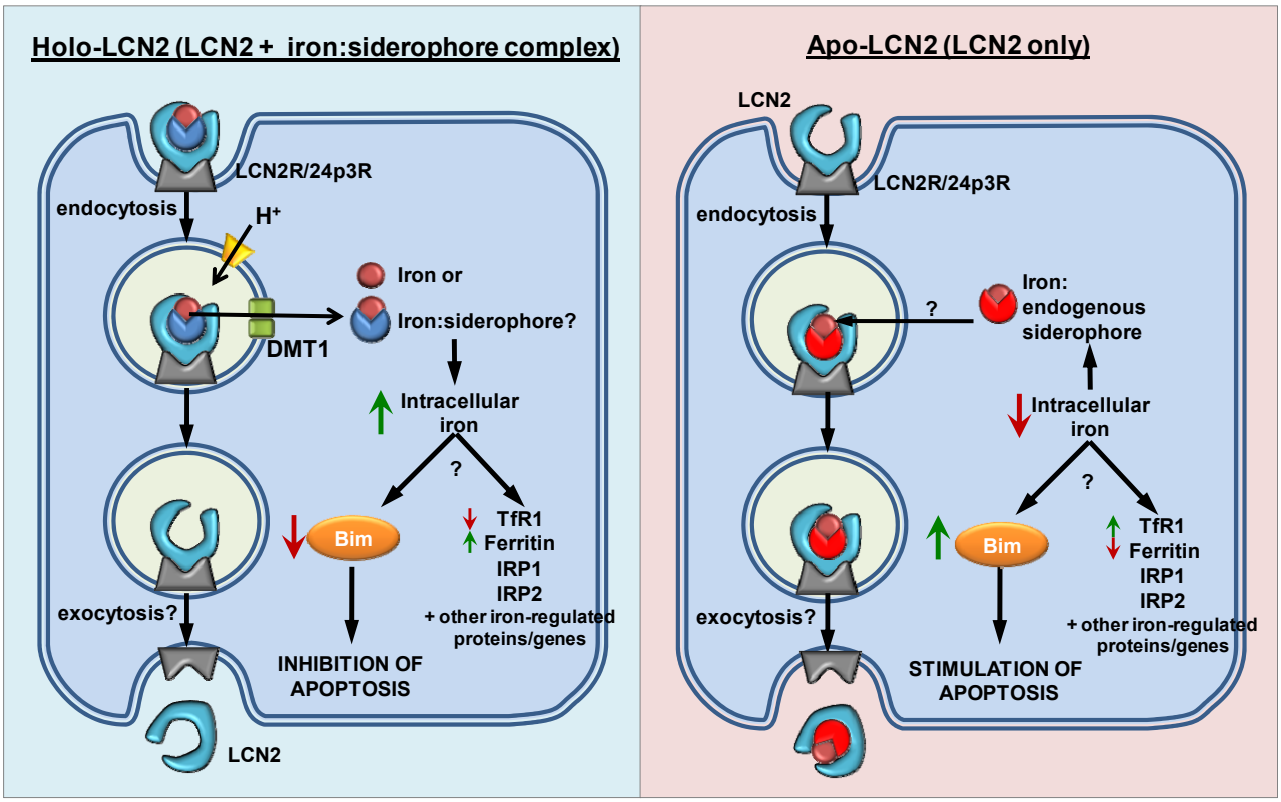

Fig. 1.3. Schematic diagram of the hypothesised association between LCN2, iron transport and apoptosis, mediated by LCN2R, in mammalian cells. In holo-LCN2 (left panel), LCN2 forms a tricomplex with iron:siderophore to bind to the receptor, LCN2R. Internalisation of holo-LCN2 is mediated by LCN2R, and transports iron into the cell. This leads to an increase in intracellular iron, which reduces Bim expression and inhibits apoptosis. A concomitant reduction in transferrin receptor 1 (TfR1) expression and rise in ferritin expression also occurs. In the absence of iron:siderophore complex (right panel), LCN2 alone is internalised and reduces the intracellular iron stores, triggering an increase in Bim expression and stimulating apoptosis. This is facilitated by novel mammalian siderophores which form complexes with intracellular iron to bind apo-LCN2 to form holo-LCN2 to be exported via exocytosis, thus transporting iron out of the cell. Intracellular iron levels can also induce changes in iron-regulated proteins/genes such as iron regulatory protein 1 and 2. Diagrams adapted from Richardson (2005). Not drawn to scale.

homologue of BDH2 was identified as a short-chain dehydrogenase/reductase family member originally called DHRS6 and now known as BDH2 (Guo et al., 2006).

Previously, they postulated that the internalisation of apo-24p3 led to cellular iron efflux via an intracellular mammalian siderophore (Devireddy et al., 2005). Interestingly, in BDH2 knockdown (KD) cells, no ^{55}Fe was detected in the

extracellular medium upon apo-24p3 treatment. BDH2 KD cells had increased cytoplasmic iron levels (as indicated by colourimetric, fluorescence assays, iron-regulated (ferritin and transferrin receptor 1) and iron-regulatory proteins (IRP1 and IRP2)), ROS production and sensitivity to oxidative stress-induced apoptosis. Therefore, the knockdown effects of BDH2 were consistent with their previous hypothesis because, with the depletion of intracellular siderophores, intracellular iron levels are elevated without iron efflux, which in turn increase ROS production, enhancing the sensitivity of cells to oxidative stress (Devireddy et al., 2010). In contrast, in BDH2 KD cells, mitochondria iron stores were depleted and zebrafish embryos failed to synthesise heme, indicating the requirement of BDH2 in mitochondrial iron homeostasis as well (Devireddy et al., 2010).

Likewise in June 2010, another group led by Bao, Strong, Barash and colleagues (2010) identified catechols as ligands of LCN2 from mouse and human urine samples with kidney injuries or disease. LCN2 and catechol:Fe^{3+} were injected into mice separately, but the complex was found in many organs, the kidney, lung and liver, while unbound catechols were rapidly cleared. This indicates LCN2 was able to bind catechol:Fe^{3+} *in vivo*, delivering iron to the kidney. LCN2 was reported to bind catechols with poor affinity, but the presence of Fe^{3+} increases the binding affinity by a 100-fold. As proposed by Goetz et al. (2002), the LCN2:catechol:iron was internalised via receptor-mediated endocytosis and trafficked into late endosomes, in which the LCN2:catechol:iron complex releases iron upon acidification at pH 6.0. *In vivo*, autoradiography revealed that LCN2:catechol:iron complex delivered iron to the proximal tubules of the kidney, and after glomerular filtration of the tricomplex, iron transported by endocytosis at the apical membrane was suggested to be mediated by the LCN2 receptors (24p3R or megalin) (Bao et al., 2010).

The proposed mechanism of apo- and holo-LCN2's effects on iron transport and apoptosis, together with the elucidation of the novel endogenous mammalian siderophores, leads to the question of whether LCN2 has similar roles in the CNS and if mammalian siderophres are present. *In vitro*, apo-24p3 induced Bim-mediated apoptosis in primary astrocytes and neurons, which was abolished by the addition of iron:siderophore (Lee et al., 2009; 2011) supporting Devirddy et al. (2005)'s proposed mechanism. However, the same cannot be assumed *in vivo*, and the role of LCN2 in neurodegeneration, specifically KA-induced neurodegeneration, remains to be identified.

4. Hypothesis and Aim

LCN2 has been widely studied in the periphery, and with the mounting evidence of roles of LCN2 in the periphery, little is known about it in the CNS. Therefore, this thesis aims to bridge this gap of knowledge. The studies most relevant to the CNS involved the expression of LCN2 in brain-derived cells - primary astrocytes and microglia upon inflammatory stimuli. Lee, Suk and colleagues (2007, 2009) suggest LCN2 acts in an autocrine manner to mediate apoptosis by inducing cell death sensitisation and morphological changes of microglia and astrocytes. Pro-apoptotic effects of LCN2 in the primary astrocytes and C6 glioma cells were mediated by Bim and iron. This supports the proposed mechanism by Devireddy et al. (2005), which showed that iron-lacking LCN2 mediated by its receptor, LCN2R, decreased intracellular iron levels, and induced upregulation of Bim to trigger apoptosis. Although many studies have reported LCN2's involvement in apoptosis and LCN2 as an iron trafficking protein, this proposed mechanism helps to associate LCN2, iron transport and apoptosis via LCN2R.

Apoptosis and iron are both associated with neurodegeneration, as apoptosis is a major cause of neuronal death and excess iron is a feature of many neurodegenerative diseases as iron levels increase in brain regions that are affected by Alzheimer's and Parkinson's disease (Zecca et al., 2004). In consideration of LCN2's possible role in apoptosis in neurodegeneration, it can be hypothesised that LCN2 has a role in KA-induced neurodegeneration. Intracerebroventricular injection of KA in rats induces neuronal loss in select regions of the brain, in particular the hippocampal formation via excitotoxicity-mediated cell death (Nadler et al., 1978). Since damage to the hippocampus is a main concern in neurodegeneration as it affects memory and learning, the neuronal injury model adopted in this thesis is

targeted at the hippocampus. Three main areas will be discussed, namely 1) LCN2, 2) its receptor, LCN2R, and 3) the possible effects due to their interaction.

Although LCN2 has been detected *in vitro*, its expression is still unclear in the intact hippocampus. Therefore, to ascertain if LCN2 is present in the CNS, the first part of the thesis aims to analyse LCN2's distribution and cellular localisation in the normal rat brain and its expression and localisation changes after KA-induced neurodegeneration. Next, since LCN2 is reported to bind to its receptor LCN2R (Devireddy et al., 2005), it is crucial to elucidate LCN2R's cellular localisation before and after KA injury as it can give an indication of the role of LCN2. For instance, the presence of LCN2R in primary astrocytes and microglia indicates that LCN2 may act in an autocrine manner to sensitise the cells to self-regulatory apoptosis (Lee et al., 2007; 2009).

Since LCN2 has been reported to induce Bim-mediated apoptosis (Devireddy et al., 2005; Lee et al., 2009; 2011), the expression and cellular localisation of Bim after KA injury will be examined in the third chapter. Lastly, the findings from LCN2, LCN2R and Bim after KA-induced neurodegeneration will be analysed so as to postulate a possible mechanism for LCN2's role in apoptosis in the neurons during KA-induced neurodegeneration.

Elucidation of the role of LCN2 in the KA-induced neurodegeneration model will serve as a stepping stone for others to study LCN2 in other neurodegenerative diseases. Interventions can also be targeted at the interaction between LCN2 and LCN2R to ameliorate neurodegeneration.

CHAPTER 2

DISTRIBUTION AND EXPRESSION OF LCN2

IN NORMAL AND KA-LESIONED BRAIN

2.1. INTRODUCTION

Although LCN2 has been reported in a wide variety of tissues, especially in the kidney and tumourigenic tissues, little is known about its distribution, expression and cellular localisation in the CNS. Through several microarray analysis studies of various types of brain insults or injuries, LCN2 was detected in the CNS: Genome-wide expression profiling showed LCN2 to be upregulated in mouse brain tissues after focal cerebral ischaemia (MacManus et al., 2004) and, closer to the scope of the present study, *LCN2* gene expression was reported as the second highest upregulated gene in the cerebral cortex and hippocampus 24 hours post-intracerebroventricular lipopolysaccharide (LPS) injection in mice (Bonow et al., 2009). In the choroid plexus, high LCN2 mRNA and protein expression and localisation of LCN2 at the choroid epithelial were observed after peripheral administration of LPS in mice (Marques et al., 2008).

Despite reports on significant increases in expression of LCN2 after some forms of brain insult, no reports characterised LCN2's expression and localisation in the normal brain. LCN2 was expressed in primary astrocytes and microglia upon inflammatory stimuli (Lee et al., 2007; Lee et al., 2009). Hence it would be intriguing to find out if the same could be observed *in vivo*. This gap of knowledge will be addressed in this chapter with the detection of LCN2 mRNA and protein expression in various parts of the brain of normal rats and characterisation of the cellular localisation of LCN2. Further analysis will be done in the KA-induced neurodegeneration model to detect changes in LCN2 expression and cellular localisation.

In this KA-induced neurodegeneration model, the changes in LCN2 and related proteins in the hippocampus will be the main focus since the hippocampus is extremely vulnerable to numerous stressors, including excitotoxicity and oxidative

stress (Jellinger, 2009, 2010). With an important role in memory and learning, it is also the primary region of concern in many neurodegenerative diseases. For instance, for Alzheimer's disease, the hippocampus is often one of the earliest and most severely involved areas, as it is particularly vulnerable to oxidative damage (Reed et al., 2009).

KA is used in this thesis as a neurotoxin to induce excitotoxicity and neurodegeneration in CA3 and CA1 pyramidal neurons in the hippocampus. Intracerebroventricular (icv) injection of KA was chosen as the route of administration as it would not cause direct mechanical injury to the hippocampus, which might induce LCN2 expression unnecessarily (for explanation on the choice of neurotoxin and route of administration, refer to *Introduction*, *Sections 1.3* and *2.4.1).* KA was injected unilaterally into the right ventricle so that more pronounced effects of neurodegeneration can be observed at the ipsilateral site of injection, while saline-injected animals served as control.

To examine the role of LCN2 in the progression of acute to chronic neurodegeneration, timepoints 1 day, 3 days and 2 weeks post-KA injection were investigated. 1 day post-KA injection (abbreviated as KA1d) will illustrate the acute changes in the hippocampus; while at 3 days post-KA injection (abbreviated as KA3d), neuronal death is more prominent; and, since activation of glia was most significant at 2 weeks post-KA injection (abbreviated as KA2wk), this timepoint will help elucidate changes in gliosis after neurodegeneration (McGeer and McGeer, 1982; Nadler et al., 1978; 1980a).

This chapter aims to bridge the gap of knowledge between the vast literature of LCN2 in the periphery and in the CNS by examining the distribution and expression of LCN2 in normal and KA-lesioned brains.

2.2. MATERIALS AND METHODS

2.2.1. Animals and kainate (KA) injections

Male Wistar rats weighing approximately 200 g each were anaesthetised by intraperitoneal injection of ketamine (75 mg/kg) and xylazine (10 mg/kg). KA (1.2 µl of 1 mg/ml) was stereotaxically injected into the right lateral ventricle (coordinates: 1.0 mm caudal to bregma, 1.5 mm lateral to the midline, 4.5 mm from the surface of the cortex) using a microlitre syringe (5 µl Hamilton syringe, Model no.: 88000, 24 gauge needle, outer diameter of needle: 0.57 mm, inner diameter of needle: 0.31 mm). Experimental control rats were injected with 1.2 µl of normal saline instead of KA. All procedures involving animals were approved by the Institutional Animal Care and Use Committee, National University of Singapore (NUS).

2.2.2. Real-time RT-PCR

A total of 24 animals were used, four KA-injected animals versus four saline-injected control animals were sacrificed at 1 day, 3 days and 2 weeks after injection. Three animals were also sacrificed to study the tissue distribution of LCN2 in the normal brain. Tissues were freshly dissected from the brain and immersed into RNAlater (Ambicon, CA, USA), flash frozen and kept at -80°C until analysis. Total RNA was isolated using TRIzol reagent (Invitrogen, CA, USA) according to the manufacturer's protocol, and RNeasy Mini Kit (Qiagen Inc., CA, USA) was used to purify the RNA. The samples were reverse transcribed using High-Capacity cDNA Reverse Transcription Kits (Applied Biosystems, CA, USA). The reaction conditions were 25°C for 10 min, 37°C for 120 min and 85°C for 5 min. Real-time RT-PCR amplification was carried out using the 7500 Real-time RT-PCR system (Applied Biosystems, CA, USA) with Taq-Man Universal PCR Master Mix (Applied

Biosystems, CA, USA) and gene-specific primers and probes according to manufacturer's protocols (Assay ID: LCN2 (Rn00590612_m1); apoD (Rn00562832_m1); Rbp4 (Rn01451318_m1); LCN5 (Rn00577120_m1); PGDS (Rn00564605_m1)). β-actin (Part no: 4352340E) was used as an internal control. All primers and probes were synthesised by Applied Biosystems. The PCR conditions were: an initial incubation of 50°C for 2 min and 95°C for 10 min followed by 40 cycles of 95°C for 15 s and 60°C for 1 min. All reactions were carried out in triplicates. The threshold cycle, CT, which correlates inversely with the levels of target mRNA, was measured as the number of cycles at which the reporter fluorescence emission exceeds the preset threshold level. The amplified transcripts were quantified using the comparative CT method (Livak and Schmittgen, 2001), with the formula for relative fold change = $2^{-\Delta\Delta CT}$. The mean was calculated, and possible significant differences were analysed using Student's t-test. $p < 0.05$ was considered significant. RT-PCR was conducted on rat hippocampal tissues using specific primers to LCN2 transcript (Applied Biosystems, Assay ID: Rn00590612_m1). DNA gel electrophoresis was performed to separate the PCR products in a 1.5% agarose gel. The DNA bands were stained with ethidium bromide and visualised under UV irradiation.

2.2.3. Western blotting

Three KA-injected rats and three saline-injected control animals were sacrificed at 1 day, 3 days and 2 weeks after injection. Three normal rats were also sacrificed to analyse LCN2 protein levels in the untreated rat brain. The rats were anaesthetised by intraperitoneal injection of ketamine and xylazine and decapitated. The tissues were quickly removed and homogenised in cold lysis buffer containing Tris–HCl, pH 7.4, 10 mM EDTA, 150 mM NaCl, 0.5% Triton X-100 with protease

inhibitor cocktail (Roche Diagnostics, Indianapolis, IN, USA) and placed on the shaker for 1 hr at 4°C. After centrifugation at 12,000g for 30 min, the supernatant was collected, and protein concentration was determined using the BCA protein assay kit (Pierce Biotechnology, Rockford, IL, USA). Prior to gel electrophoresis, the protein lysates were denatured by heating the sample in the presence of SDS and DTT for 10 min at 95-100°C.

Total protein (60 µg) was resolved in 12% SDS-polyacrylamide gel under reducing conditions and electro-transferred to a nitrocellulose membrane (Biorad, CA, USA). Non-specific binding sites on the membrane were blocked by incubation with 5% non-fat milk for 1 hr. The membrane was then incubated overnight with polyclonal goat anti-LCN2 antibody at 1:200 (AF3508, R&D systems, Minneapolis, MN, USA). Specificity of the LCN2 antibody was verified by pre-incubating 10 µg/ml (10x) and 20 µg/ml (20x) of recombinant rat LCN2 (R&D systems, Minneapolis, MN, USA) with 1 µg/ml of LCN2 antibody overnight. After washing with 0.1% Tween-20 in TBS, the membrane was incubated with horseradish peroxidase-conjugated mouse anti-goat immunoglobulin lgG (1:10,000; Thermo Fisher Scientific, Rockford, IL, USA) for 1 hr at room temperature. The protein was visualised with SuperSignal West Pico chemiluminescent substrate (Thermo Fisher Scientific, Rockford, IL, USA) according to the manufacturer's instructions. Blots were treated with stripping buffer (Restore Western Blot Stripping Buffer, Thermo Fisher Scientific, Rockford, IL, USA) at room temperature for 10 min before reprobing of membrane with antibody to β-actin (Sigma, St. Louis, MO, USA). Exposed films were scanned with at least 300 dpi and the mean optical density of the protein bands of LCN2 was analysed by densitometry using lmageJ (NIH, Maryland, USA), and normalised to β-actin. The mean was calculated, and possible significant differences were analysed using Student's t-test. $p < 0.05$ was considered significant.

2.2.4. Immunohistochemistry

Three KA-injected rats and three saline-injected rats were sacrificed at 2 weeks. Rats were deeply anaesthetised and perfused through the left ventricle with 4% paraformaldehyde in 0.1 M phosphate buffer (pH 7.4). The brains were removed and blocks containing the hippocampus sectioned in the coronal plane at 100 µm thickness using a vibrating microtome. One set of free-floating sections was mounted on gelatinised slides and stained with cresyl fast violet (Nissl stain). Another set was washed for 3 hr in phosphate buffered saline (PBS; pH 7.4) to remove traces of fixative, quenched with 0.3% H_2O_2 and blocked with 5% rabbit serum in PBS-0.3% Triton X-100 and incubated overnight with polyclonal goat anti-LCN2 antibody at 1:50 (AF3508, R&D systems, Minneapolis, MN, USA). This was followed by washing and incubation for 1 hr in a 1:200 dilution of biotinylated rabbit anti-goat IgG (Vector, Burlingame, CA, USA), and reaction with an avidin-biotinylated horseradish peroxidase complex (Vector, Burlingame, CA, USA). The reaction was visualised by treatment in 0.05% 3,3-diaminobenzidine tetrahydrochloride (DAB) solution in Tris buffer containing 0.05% hydrogen peroxide for 1.5 min. Sections were mounted on gelatin-coated slides and counterstained with methyl green before coverslipping.

2.2.5. Double immunofluorescence labelling

A total of 24 animals were used, four KA-injected animals versus four saline-injected control animals each were sacrificed at 1 day, 3 days and 2 weeks after injection to study the effect of KA lesions. Three untreated rats were used to study the cellular localisation of LCN2 in the normal brain. The rats were anaesthetised by intraperitoneal injection of anaesthetic comprising ketamine and xylazine and transcardially perfused with Ringer solution, followed by 4% paraformaldehyde in

0.1M phosphate buffer (pH 7.4). The brains were dissected out, and blocks containing the KA- or saline-treated hippocampus were sectioned coronally at 20 μm using a freezing microtome. Some sections were stained with cresyl fast violet (Nissl stain) to visualise the hippocampal lesions. Sections from the olfactory bulb to the brainstem were collected for the three normal brains for detection of LCN2. Sections were soaked in phosphate buffered saline (PBS) for 30 min to remove traces of sucrose and permeabilised with PBS-0.3% Triton X-100 for 10 min. They were then blocked with 5% donkey serum in PBS-0.3% Triton X-100 for 1 hr, followed by incubation with goat polyclonal antibody to LCN2 at 1:200 (AF3508, R&D systems, MN, USA), rabbit polyclonal antibody to glial fibrillary acidic protein (GFAP, 1:1000, DakoCytomation, Glostrup, Denmark), or mouse monoclonal antibody to OX-42 (1:200, Chemicon, Temecula, CA, USA) overnight at 4°C. Specificity of the LCN2 antibody was verified by pre-incubating 20 μg/ml (20x) of recombinant rat LCN2 (R&D systems, Minneapolis, MN, USA) with 1 μg/ml of LCN2 antibody overnight. The sections were washed in PBS, and incubated for 1 hr at room temperature in 1:200 dilution of donkey anti-goat IgG (H+L) Alexa Fluor 555 and donkey anti-rabbit or donkey anti-mouse IgG (H+L) Alexa Fluor 488 (Invitrogen, CA, USA). The sections were then washed and mounted with ProLong® Gold antifade reagent with DAPI (Invitrogen, Carlsbad, CA, USA) and captured using a fluorescence microscope (Olympus BX51; Olympus Corporation, Tokyo, Japan) and a laser scanning confocal microscope (LSM 510, Carl Zeiss Göttingen, Germany). Colocalisation was established by analysing the overlap between the different labels by orthogonal reconstruction throughout the entire *z*-stack (LSM 510, Carl Zeiss Göttingen, Germany).

2.3. RESULTS

2.3.1. Expression of LCN2 in the normal brain

2.3.1.1. Tissue distribution of LCN2 mRNA levels in normal rat brain

Little is known about the distribution of LCN2 in the normal brain *in vivo*, thus the mRNA expression of LCN2 was detected with real-time RT-PCR analysis in different parts of the untreated rat brain, including the olfactory bulb, striatum, hippocampus, frontal cortex, somatosensory cortex, thalamus, hypothalamus, cerebellum and brainstem. The values are presented as fold difference relative to the lowest level among the different brain regions, i.e. the hippocampus. Highest levels of LCN2 mRNA was found in the olfactory bulb (7-fold relative to the hippocampus), followed by the brainstem, cerebellum, thalamus and hypothalamus (3- to 4-fold relative to the hippocampus). Low levels of LCN2 mRNA were detected in the striatum, frontal cortex and somatosensory cortex. The hippocampus has the lowest level of LCN2 mRNA. Both the left and right sides of the brain revealed a similar trend in the distribution of LCN2 mRNA expression (analysed by Student's t-test, not significant) (Fig. 2.1).

2.3.1.2. Tissue distribution of LCN2 protein levels in normal rat brain

With the knowledge that LCN2 mRNA is present in the brain, western blot analysis was performed to confirm the presence of LCN2 protein in the brain. A single band at approximately 25kDa in homogenates from different regions of the right side of normal rat brain was detected (Fig. 2.2A), consistent with the expected molecular weight of LCN2 (Kjeldsen et al., 1993; 2000).The highest level of LCN2 protein was found in the olfactory bulb, followed by the brainstem and the cerebellum

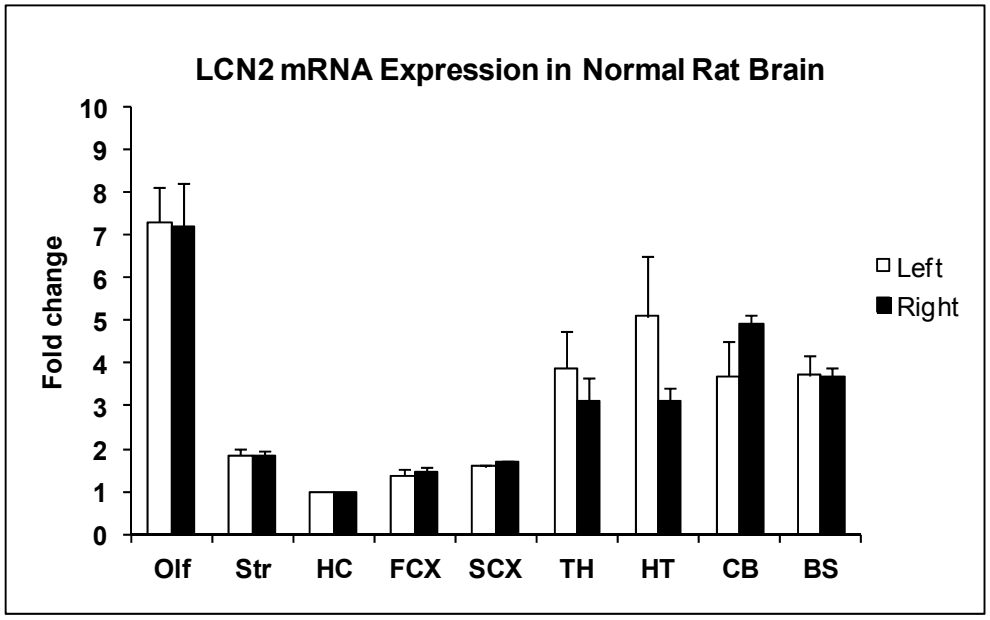

Fig. 2.1. Distribution of LCN2 mRNA expression in normal rat brain. Real-time RT-PCR analysis on all parts of the normal brains, both left and right sides. Olf: Olfactory bulb, Str: Striatum, HC: Hippocampus, FCX: Frontal cortex, SCX: Somatosensory cortex, TH: Thalamus, HT: Hypothalamus, CB: Cerebellum, BS: Brainstem. Olfactory bulb has the highest LCN2 mRNA levels, followed by the brainstem, cerebellum, hypothalamus and thalamus. Hippocampus has the lowest LCN2 mRNA expression. All data have been normalised for levels of β-actin mRNA expression within the same sample and was expressed relative to hippocampal LCN2 mRNA expression levels. Data are expressed as mean ± SEM, *n* = 3.

(Fig. 2.2B). Low LCN2 protein expression was observed in other parts of the brain, such as the striatum, frontal and somatosensory cortex. Among all the parts of the brain analysed, the hippocampus had the lowest level of LCN2 protein expression (Fig. 2.2B) consistent with the mRNA expression detected in Figure 2.1. The discrepancy between the mRNA levels and protein levels of LCN2 in the frontal cortex may be due to higher translational efficiency in this region.

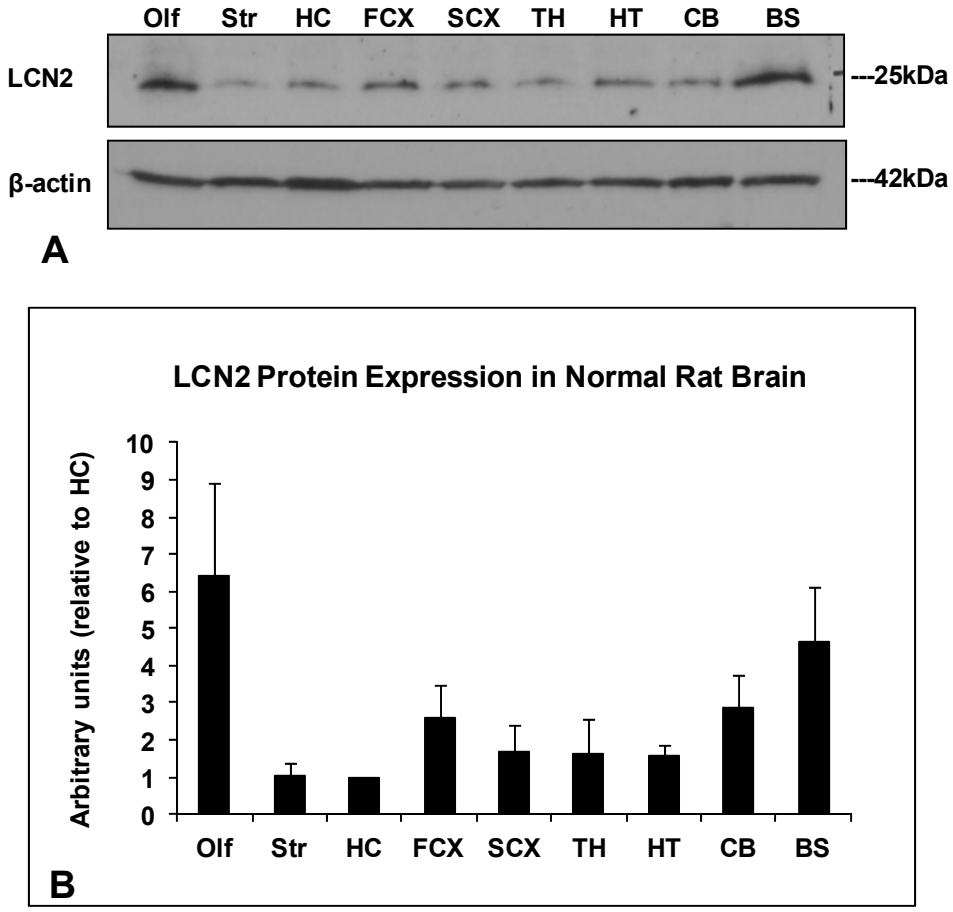

Fig. 2.2. Distribution of LCN2 protein expression in normal rat brain. (A) Western blot analysis of various parts of the right side of normal rat brain. Olf: Olfactory bulb, Str: Striatum, HC: Hippocampus, FCX: Frontal cortex, SCX: Somatosensory cortex, TH: Thalamus, HT: Hypothalamus, CB: Cerebellum, BS: Brainstem. The antibody to LCN2 detected a single band between 20 to 25kDa. (B) Densitometric analysis of LCN2 protein expression of various parts of the right side of the brain from three normal animals, normalised to β-actin, and again normalised to the hippocampus of each individual animal, as the hippocampus has the lowest protein expression. The olfactory bulb has the highest LCN2 protein expression, followed by the brainstem and cerebellum. Data are expressed as mean ± SEM, *n* = 3.

2.3.1.3. Immunoreactivity of LCN2 in normal rat brain

Understanding the distribution of LCN2 mRNA and protein levels in different regions of the normal rat brain, LCN2 immunostaining was performed on three brain structures with high LCN2 expression: the olfactory bulb, brainstem and cerebellum. LCN2 labelling was observed in the glomerular layer of the olfactory bulb (Fig. 2.3A) and in the lateral olfactory tract of the olfactory bulb. Immunoreactivity was also

detected in the cerebellar cortex (Fig. 2.3D) and different parts of the brainstem including the spinal trigeminal tract, ventral spinocerebellar tract, and the pyramidal tract (Fig. 2.3G). The LCN2 immunopositive cells in the olfactory bulb, cerebellum and brainstem were double-labelled with GFAP (Fig. 2.3B, E and H) indicating that they were astrocytes (Fig. 2.3C, F and I).

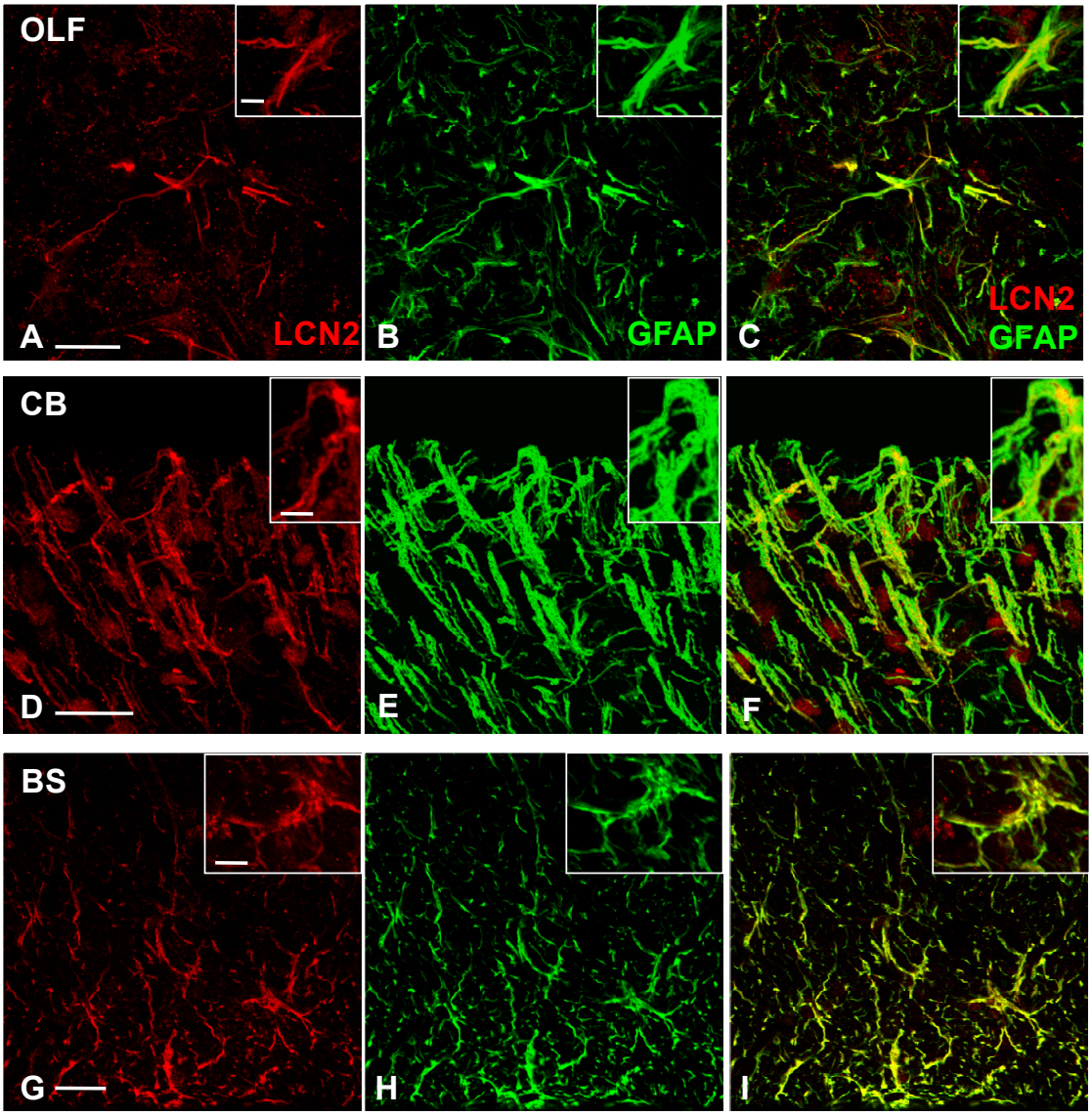

Fig. 2.3. Confocal micrographs of LCN2-positive cells in various parts of the normal rat brain. LCN2-positive cells at the (A) olfactory bulb, (D) cerebellum and (G) brainstem colocalised with the (B, E and H) GFAP-positive cells. (C, F and I) LCN2 colocalised with GFAP in the olfactory bulb (OLF), cerebellum (CB) and brainstem (BS). Scale=20 µm. Scale in insert=5 µm.

2.3.1.4. LCN2 mRNA and protein expression in the hippocampus

RT-PCR of the total RNA from normal hippocampus amplified a 88bp PCR product indicating that LCN2 mRNA was present in the normal hippocampus (Fig. 2.4A). Western blot analysis of the right hippocampi of three normal rats indicated faint protein bands around 25kDa (Fig. 2.4B). This weak expression of LCN2 corresponds with the previous data that LCN2 mRNA and protein expression in the hippocampus was the lowest among the other brain parts.

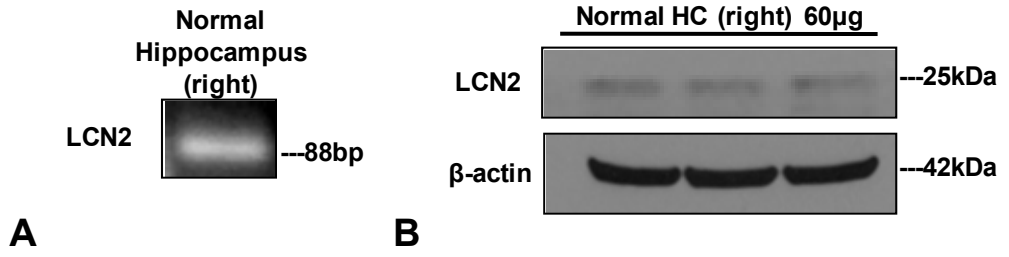

Fig. 2.4. LCN2 mRNA and protein expression in the right hippocampus of normal rat brain. (A) RT-PCR was conducted on the cDNA of the right hippocampus from a normal rat with specific primers to LCN2 transcript. (B) 60 µg of right hippocampus lysate from three individual normal animals were loaded for western blot analysis and probed with anti-LCN2.

2.3.2. Expression of LCN2 in Kainate-lesioned brain

2.3.2.1. Changes in LCN2 mRNA and protein expression in the rat hippocampus after LPS and KA treatment

As a preliminary study, icv injection of lipopolysaccharide (LPS) was performed on the animals. In LPS-treated animals, LCN2 mRNA in the right hippocampus was 20.8-fold ($p < 0.01$) relative to the saline controls (Fig. 2.5A). Denser bands were observed for LPS-treated right hippocampi relative to the saline injected-controls (Fig. 2.5B, top panel), indicating a 19.8 ($p < 0.01$) times increase in LCN2 protein levels by densitometric analysis (Fig. 2.5B, bottom panel).

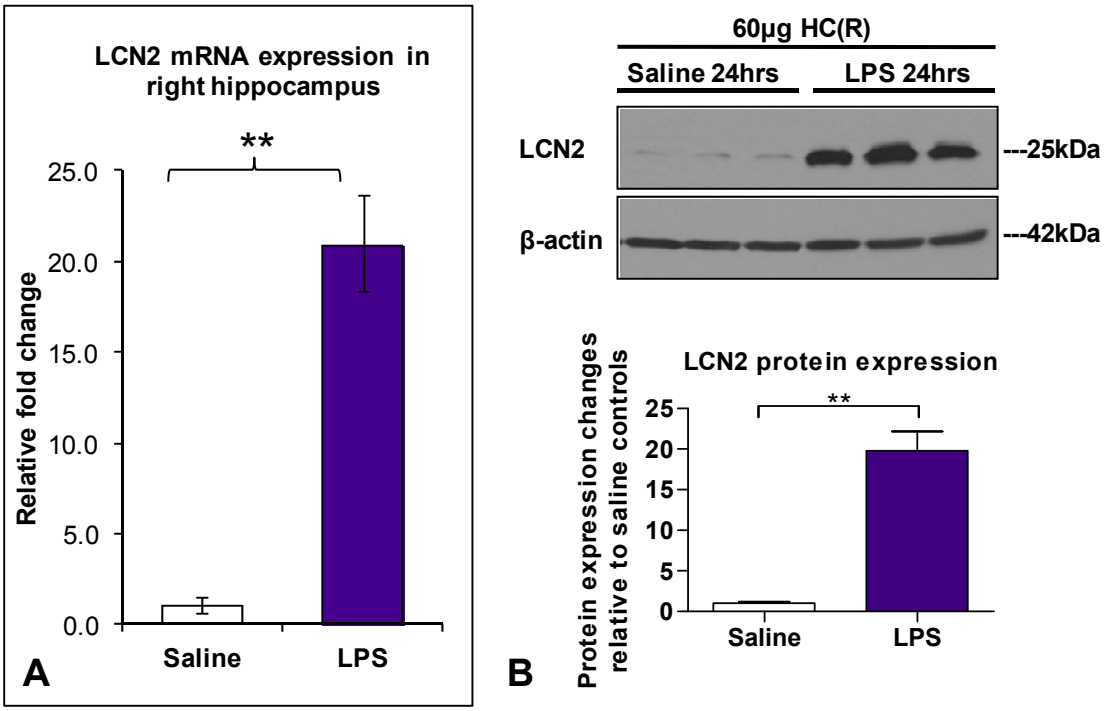

Fig. 2.5. LCN2 mRNA and protein upregulated after LPS treatment. (A) Real-time RT-PCR analysis on LCN2 mRNA expression changes of the right hippocampus 24 hours after icv LPS and saline administration. LCN2 mRNA levels increase significantly after LPS treatment. Data are expressed as mean ± SEM, n = 4 per treatment group. (B) Western blot analysis of LCN2 expression in LPS vs. saline injected animals (top panel) and densitometric analysis of western blot (bottom panel). LCN2 protein increased after LPS treatment. Data are expressed as mean ± SEM, n = 3 per treatment group. Analysed by Student's t-test, asterisks indicate significant difference (*p < 0.05, **p < 0.01, ***p < 0.001).

Kainate was administered via icv injection to induce neural injury. To understand the expression of LCN2 in acute and chronic conditions of neural injury- such as in kainate injury, three different timepoints were performed.

At 1 day, 3 days and 2 weeks post-KA injection, LCN2 mRNA expression was 5.6- (p < 0.01), 8.6- (p < 0.001) and 14.2- (p < 0.01) fold relative to their saline-injected controls, respectively (Fig. 2.6). Only the right hippocampus was studied because the unilateral icv injection was done at the right ventricle. A consistent increase in LCN2 mRNA expression was detected at all timepoints.

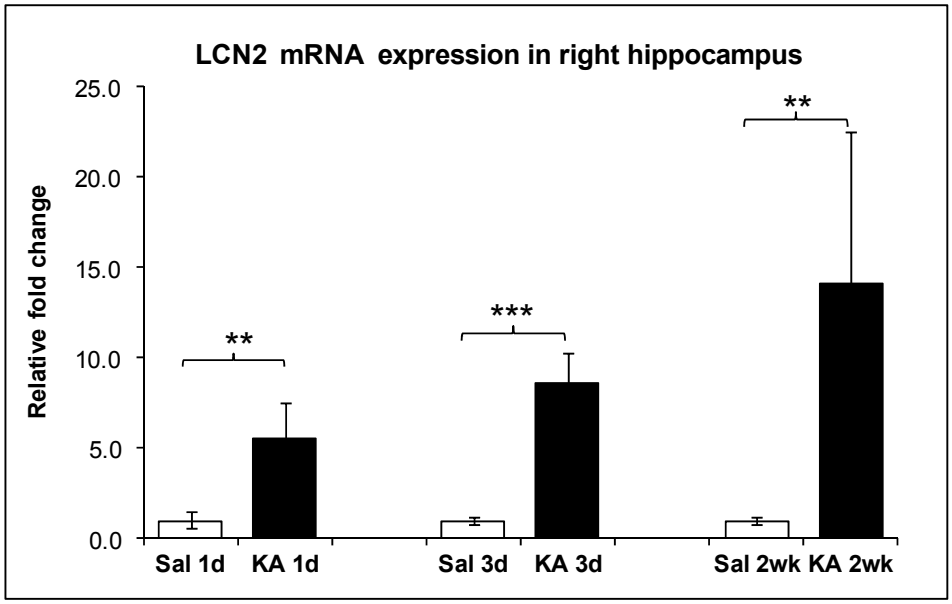

Fig. 2.6. LCN2 mRNA expression upregulated after KA injury. Real-time RT-PCR analysis on LCN2 mRNA expression changes of the right hippocampus at 1 day, 3 days and 2 weeks post-KA injection. LCN2 mRNA levels were increased in all timepoints. Data are expressed as mean ± SEM, $n = 4$ per treatment group. Analysed by Student's t-test, asterisks indicate significant difference (*$p < 0.05$, **$p < 0.01$, ***$p < 0.001$).

The increase of LCN2 in KA-treated animals at 1 day, 3 days and 2 weeks post-KA treatment was further validated by western blot analysis (Fig. 2.7). 3 days (Fig. 2.7B) and 2 weeks (Fig. 2.7C) post-KA injection hippocampi samples had greater band intensities than 1 day post-KA injection samples (Fig. 2.7A). From densitometric analysis, LCN2 protein levels were significantly upregulated at all three timepoints; 1 day, 3 days and 2 weeks post-KA injection samples had 2.7 ($p < 0.01$), 13.2 ($p < 0.001$) and 31.2 ($p < 0.01$) times increase in LCN2 protein respectively in comparison to their corresponding saline-injected controls (Fig. 2.7E).

This trend corresponded with the upregulation of LCN2 mRNA expression observed earlier. Therefore, the 2 weeks post-KA injection samples had the highest upregulation of LCN2 mRNA and protein expression compared to its saline controls, followed by 3 days post-KA injection samples, and lastly, the 1 day post-KA injection samples with the smallest upregulation in LCN2.

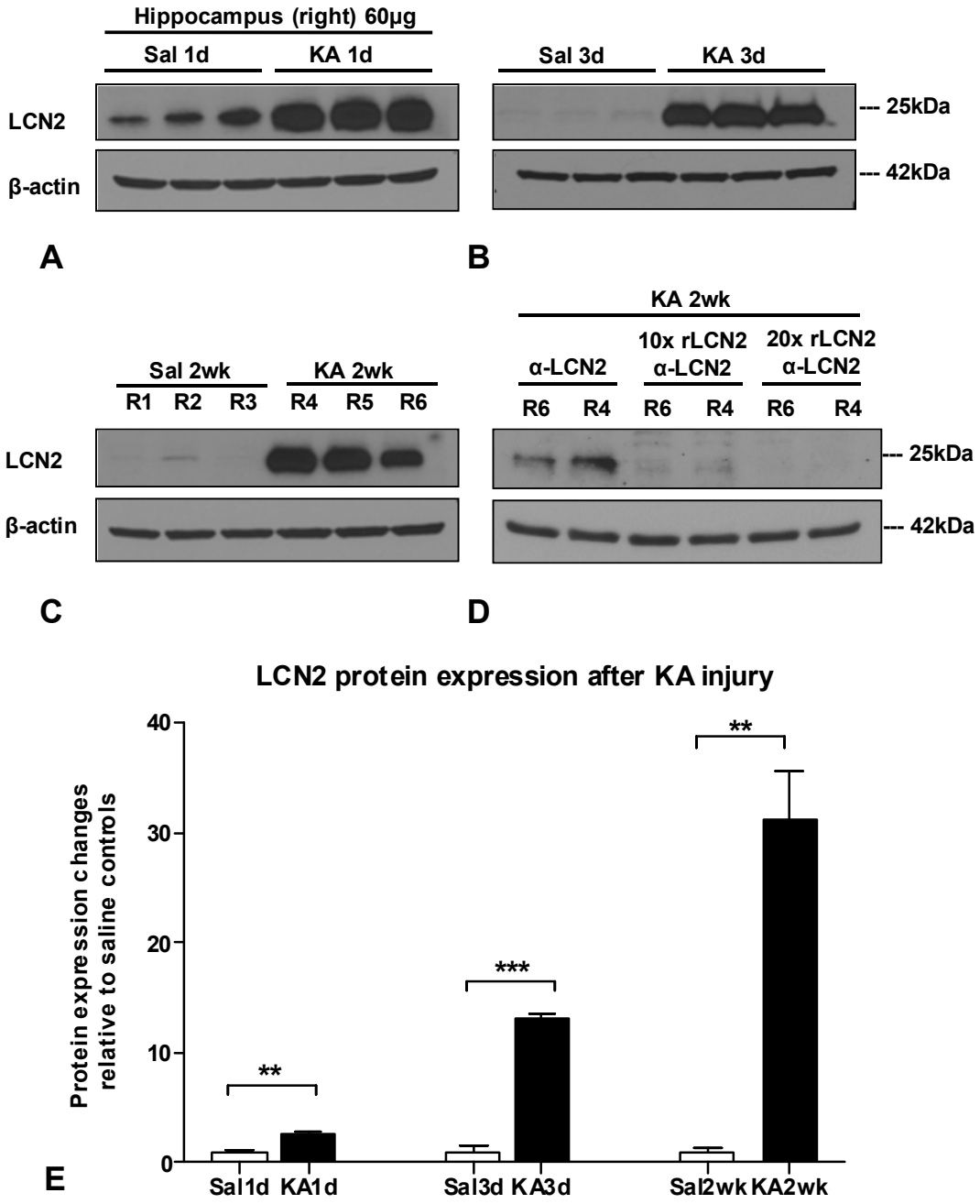

Fig. 2.7. LCN2 protein expression upregulated after KA injury. Western blot analysis of LCN2 in the right hippocampus at (A) 1 day, (B) 3 days and (C) 2 weeks post-KA injection, *n* = 3 per treatment group. (D) 2 weeks post-KA treatment hippocampi lysates, R6 and R4 were used for control experiments. First two lanes on the left: incubated with LCN2 antibody at 1 µg/ml, produced specific bands for LCN2. Next two lanes: LCN2 antibody pre-incubated with 10 µg/ml of blocking peptide, resulted in reduced intensity of the bands. Last two lanes: LCN2 antibody pre-incubated with 20 µg/ml of rLCN2, resulted in the absence of the LCN2 band, indicating specificity of the LCN2 antibody. (E) Densitometric analysis of LCN2 protein expression in KA-treated vs. saline-injected controls. Values are normalised with the saline-injected controls at the respective timepoints. Analysed by Student's t-test, asterisks indicate significant difference (*$p < 0.05$, **$p < 0.01$, ***$p < 0.001$). Data are expressed as mean ± SEM , *n* = 3 per treatment group.

Control experiments were performed with the antigen, recombinant LCN2 protein, as the blocking solution. Western blots incubated with the LCN2 antibody produced a single band at 25kDa. Blots incubated with 10 µg/ml antigen-absorbed LCN2 antibody, showed reduced intensity of the band at 25kDa; and blots incubated with 20 µg/ml antigen-absorbed LCN2 antibody showed absence of bands, indicating the specificity of the LCN2 antibody (Fig. 2.7D).

2.3.2.2. Changes in LCN2 immunoreactivity in the rat hippocampus after KA injury

Nissl staining was performed to observe the extent of neuronal damage at the 1 day, 3 days and 2 weeks post-KA injection. Hippocampal lesions were observed from the Nissl-stained sections at CA3 region at 1 day post-KA injection (Fig. 2.8B); and at CA1 and CA3 regions at 3 days (Fig. 2.8D) and 2 weeks post-KA injection (Fig. 2.8F). All saline-injected control sections showed absence of lesions (Fig. 2.8A, C and E).

LCN2 immunostaining was done to investigate the distribution and localisation of LCN2 in the lesioned hippocampus. At 3 days post-KA injection, LCN2 expression was regulated in the lesioned CA1 region (Fig. 2.8G). At 2 weeks post-KA injection, higher LCN2 immunoreactivity was observed in both the lesioned CA1 and CA3 regions (Fig. 2.8H) compared to 3 days post-KA injection sections. This correlated with the high LCN2 mRNA and protein levels at 2 weeks post-KA injection. The localisation of LCN2 in the hippocampal lesioned areas suggested that they may be expressed in glia, and not neuronal cells.

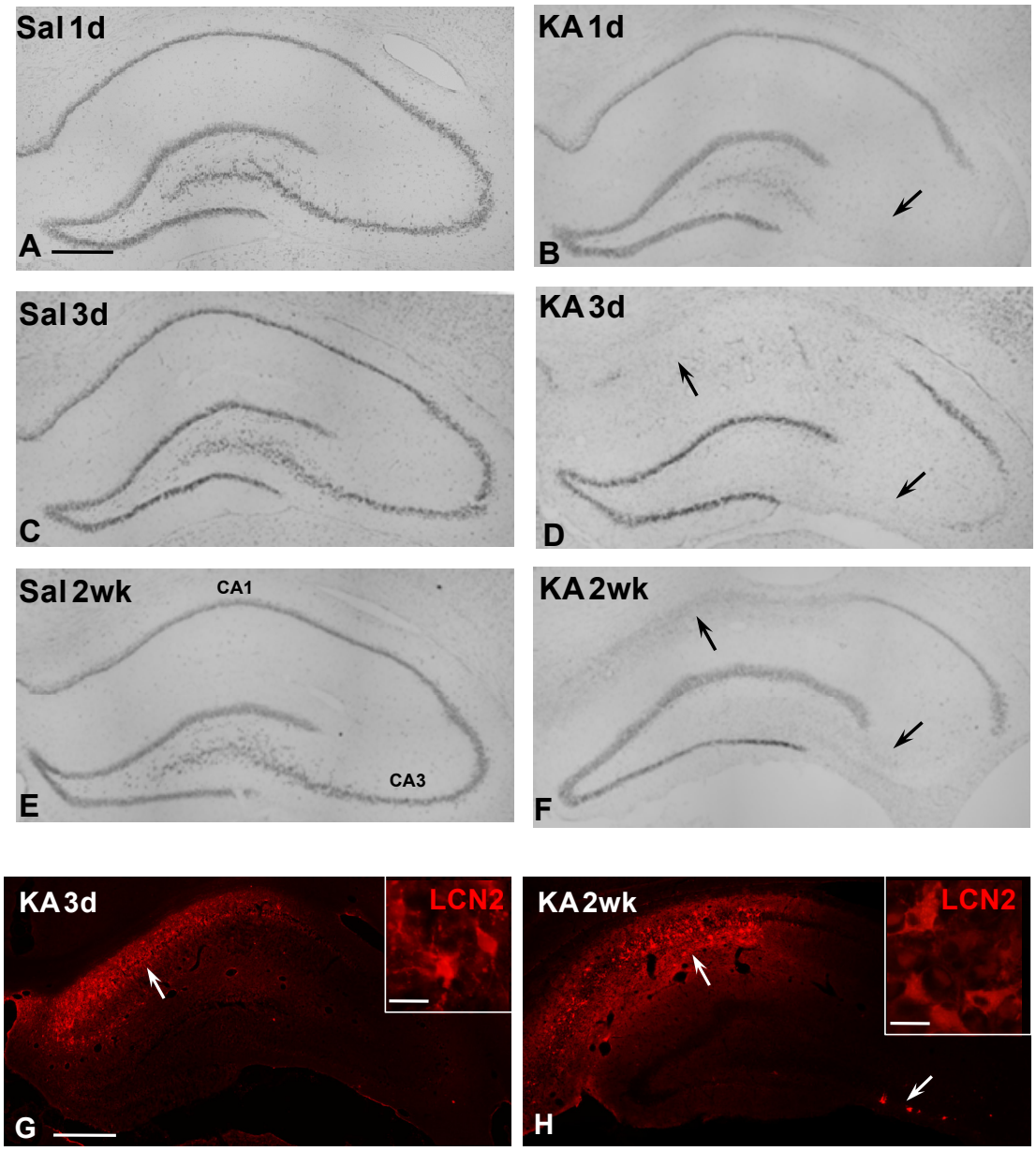

Fig. 2.8. LCN2 upregulation in hippocampal lesioned areas after KA injury. Light micrographs of Nissl-stained sections of the right hippocampus at 1 day, 3 days and 2 weeks post-KA/saline injection. Intact hippocampi were observed from (A) 1 day, (C) 3 days and (E) 2 weeks post-saline injection controls. In (B) 1 day post-KA injection animals, lesions are observed in the CA3 region, while in both (D) 3 days and (F) 2 weeks post-KA injection animals, lesions are observed in the CA1 and CA3 regions (indicated by black arrows). Scale=500 μm. (G, H) Fluorescence micrographs of LCN2 (red) upregulation in the hippocampal lesioned regions (indicated by white arrows). Scale=500 μm. At higher magnification shown in the inserts, LCN2 positive cells have glial-like morphology. Scale in insert=20 μm.

Immunoperoxidase staining was performed to confirm the LCN2 immunoreactivity at 2 weeks post-KA injection. No obvious immunoperoxidase staining was detected at the CA3 hippocampal region of saline-injected control animals (Fig 2.9A, C), consistent with a low level of LCN2 mRNA and protein in the normal hippocampus. In contrast, intense staining was observed in glial-like cells in the lesioned CA3 region of the 2 weeks post-KA injection sections (Fig. 2.9B, D). The labelled cells had large cell bodies and thick processes characteristic of astrocytes. Immunofluorescence also showed LCN2 upregulation in cells with characteristics of astrocytes (Fig. 2.9E). Sections incubated with the rLCN2-absorbed antibody showed absence of staining (Fig. 2.9F), indicating the specificity of the antibody.

Since at 2 weeks post-KA injection, the right hippocampus had high LCN2 mRNA and protein expression, double immunolabelling was performed to determine the identity of the immunopositive LCN2 cells. As LCN2 was upregulated in the lesioned areas of the hippocampus, LCN2 may be localised in glial cells, as reactive gliosis (activation of astrocytes and microglia) was often observed after KA injury. The reactive astrocytes were characterised by hypertrophic processes and increased expression of GFAP (a marker for astrocytes), while activated microglia were characterised by amoeboid morphology. The majority of the GFAP positive cells were double-labelled with LCN2 (Fig. 2.10A) and *z*-series reconstruction of cells showed the colocalisation of LCN2 with GFAP-positive cells (Fig. 2.10B). This indicates that LCN2 is expressed in the astrocytes. At higher magnification, LCN2 staining comprises of intense dots, which could represent vesicles or other intracellular organelles or inclusions (Fig. 2.10C). LCN2 did not colocalise with OX-42, a marker for microglia (Fig. 2.10D).

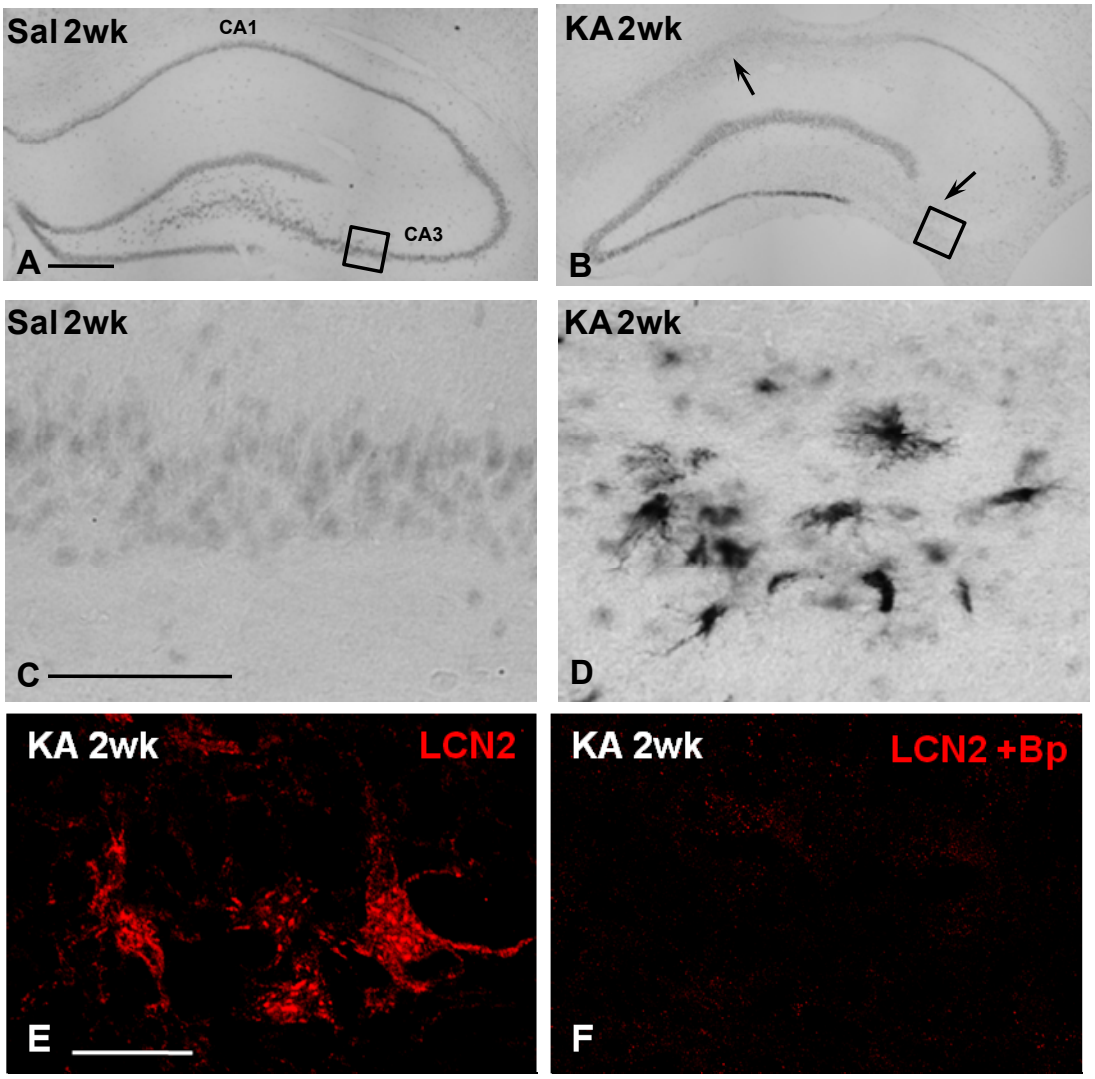

Fig. 2.9. Micrographs of LCN2 staining at 2 weeks post-KA injection. (A,B) Light micrographs of Nissl stained sections at 2 weeks post-KA (KA 2wk) and post-saline (Sal 2wk) injections (identical to Fig. 2.8E and 2.8F). Scale=500 µm. (C-D) Light micrographs of immunoperoxidase staining of the CA3 region of the right hippocampus as indicated by the square boxes in (A) and (B) at (C) 2 weeks post-saline and (D) 2 weeks post-KA injection. LCN2 was upregulated in CA3 region of the KA-treated animals. Scale=100 µm. (E) Confocal micrographs of CA1 field of the right hippocampus at 2 weeks post-KA injection indicating upregulation of LCN2-positive cells. (F) LCN2 antibody was pre-incubated with 20 µg/ml rLCN2 (Bp) for blocking study. LCN2 positive staining (red) was blocked, indicating specificity of the antibody. Scale=20 µm.

With the knowledge that LCN2 was expressed in the astrocytes of 2 weeks post-KA injection samples, double immunolabelling of LCN2 and GFAP was performed at other timepoints to examine the changes in LCN2 immunoreactivity in the lesioned hippocampus from 1 day to 3 days to 2 weeks post-KA injury.

In saline-injected control sections, negligible LCN2 staining was detected at both CA1 (Fig. 2.11A) and CA3 (Fig. 2.11B) hippocampal regions. Instead, LCN2 was upregulated in the GFAP-positive cells at 1 day (Fig. 2.11C, D), 3 days (Fig. 2.11E, F) and 2 weeks (Fig. 2.11G, H) post-KA injection in the CA1 and CA3 lesioned regions of the hippocampus.

LCN2 had high immunoreactivity at 2 weeks post-KA injection, correlating with the high LCN2 mRNA and protein levels detected. Furthermore, at 2 weeks post-KA injection, reactive astrocytes were more pronounced compared to earlier timepoints, characterised by the large cell bodies, thick hypertrophic processes and increased expression of GFAP.

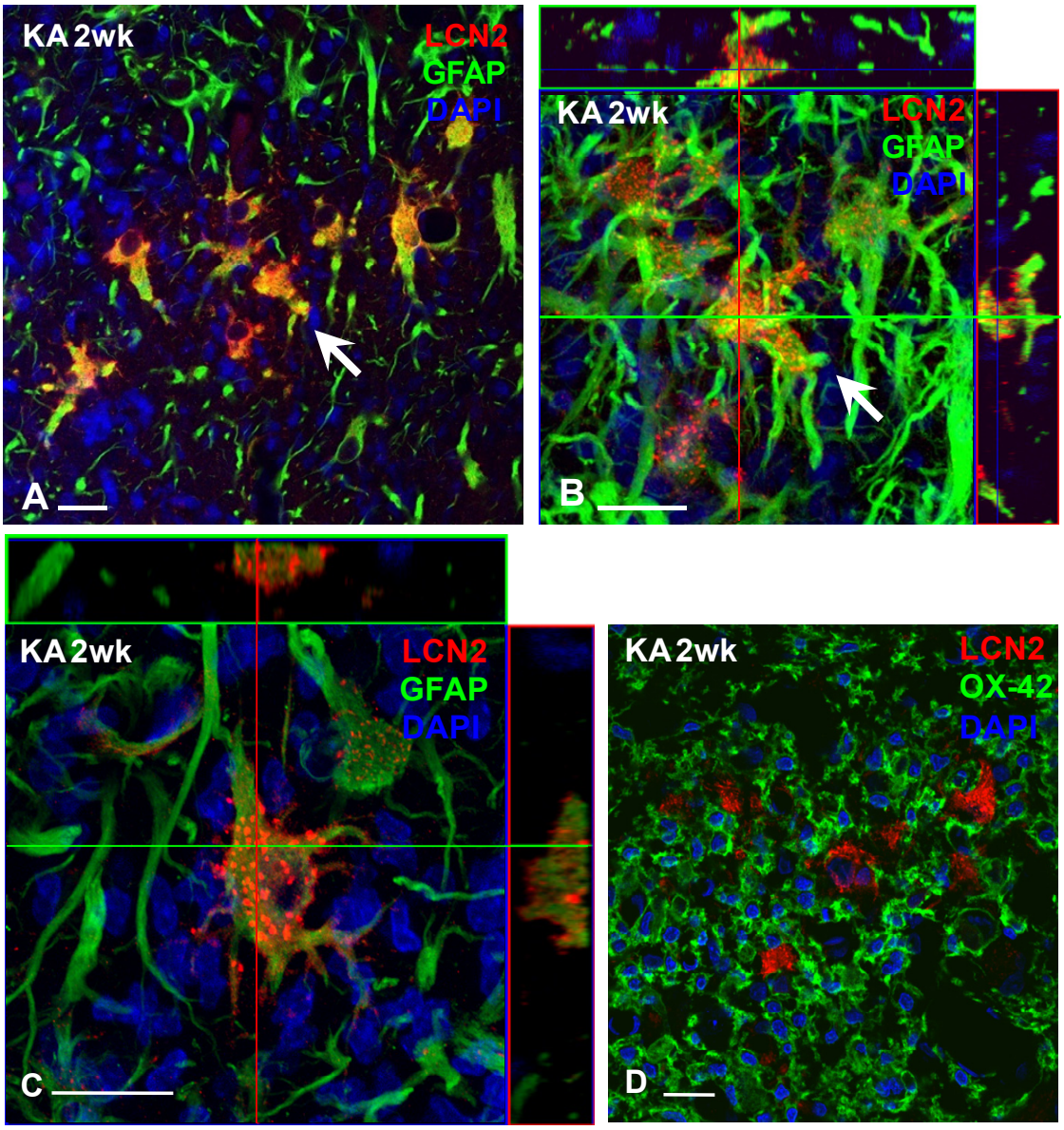

Fig. 2.10 Confocal micrographs of colocalisation of LCN2 with GFAP-positive cells. Right hippocampus at 2 weeks post-KA injection was double-labelled with LCN2 (red) and GFAP (green), a marker for astrocytes. (A) 40x magnification showed majority of the GFAP-positive cells were LCN2-positive. (B) *z*-series reconstruction of the cells indicated by the white arrows in (A) at 63x magnification, indicating LCN2 was expressed in the astrocytes. (C) Orthogonal projections through CA1 lesioned region at higher magnification demonstrate that LCN2 staining comprised of intense dots. LCN2 is present in astrocytes. (D) No colocalisation was observed between LCN2 and OX-42, a marker for microglia, indicates that LCN2 is not present in microglia. Scale=20 μm.

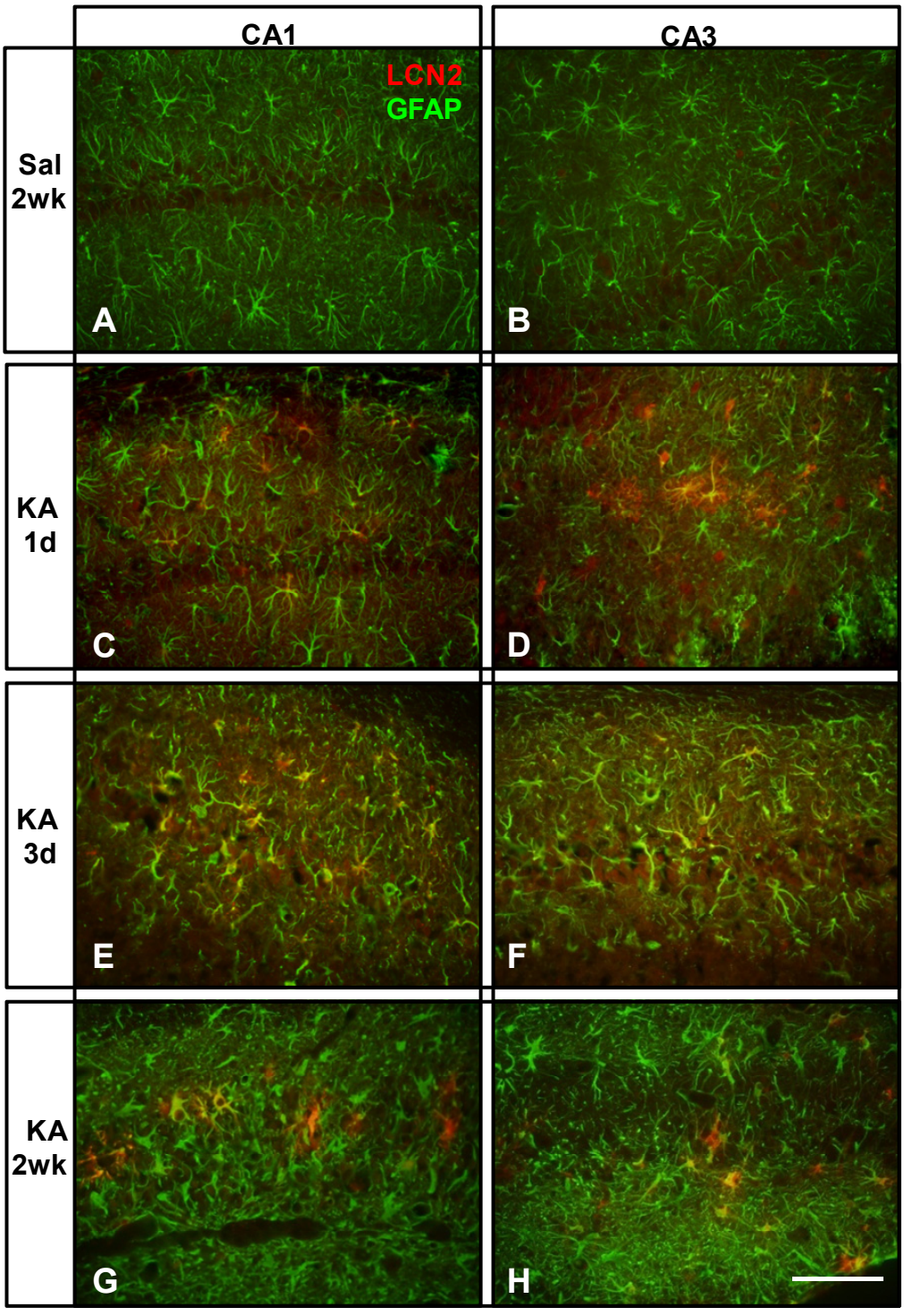

Fig. 2.11. Changes in LCN2 expression with GFAP-positive cells after KA injury. Negligible LCN2 staining was observed in (A) CA1 and (B) CA3 in 2 weeks post-saline injection hippocampus. Immunofluorescence staining for LCN2 (red) colocalised with GFAP (green) at (C,D) 1 day (E,F) 3 days and (G,H) 2 weeks post-KA injection and was upregulated in CA1 and CA3 lesioned regions. Scale=100 μm.

2.3.3. Changes in mRNA expression of other lipocalins in the rat hippocampus after KA injury

The mRNA expression of other lipocalins together with LCN2 was surveyed by real-time RT-PCR after KA injury in order to determine if the upregulation is specific to LCN2. The other lipocalins included apolipoprotein D (apoD), prostaglandin D2 synthase (PGDS), retinol binding protein 4 (Rbp4) and lipocalin 5 (LCN5).

At 3 days post-KA injection, LCN2 mRNA levels were 9.7- ($p < 0.001$) and 8.4- ($p < 0.01$) fold relative to the saline-injected controls in the right (Fig. 2.12A) and left (Fig. 2.12B) hippocampus, respectively. At 2 weeks post-KA injection, LCN2 mRNA levels continued to rise to 16.3- ($p < 0.01$) and 8.5- ($p < 0.01$) fold relative to the saline-injected controls, in the right (Fig. 2.12C) and left (Fig. 2.12D) hippocampus, respectively.

At 3 days post-KA injection, apoD mRNA expression was 1.6-fold ($p < 0.001$) in the right hippocampus relative to the saline-injected controls (Fig. 2.12A). In contrast, significant decreases in mRNA levels were observed with Rbp4 (0.43 fold, $p < 0.01$), LCN5 (0.23 fold, $p < 0.01$) and PGDS (0.34 fold, $p < 0.001$) relative to saline-injected controls at this timepoint (Fig. 2.12A). The left hippocampus showed a similar trend as the right hippocampus. PGDS mRNA levels decreased (0.49 fold, $p < 0.01$) relative to saline-injected controls (Fig. 2.12B). At 2 weeks post-KA injection, other than LCN2, the other lipocalins had no significant differences in the right or left hippocampus (Fig. 2.12C and D).

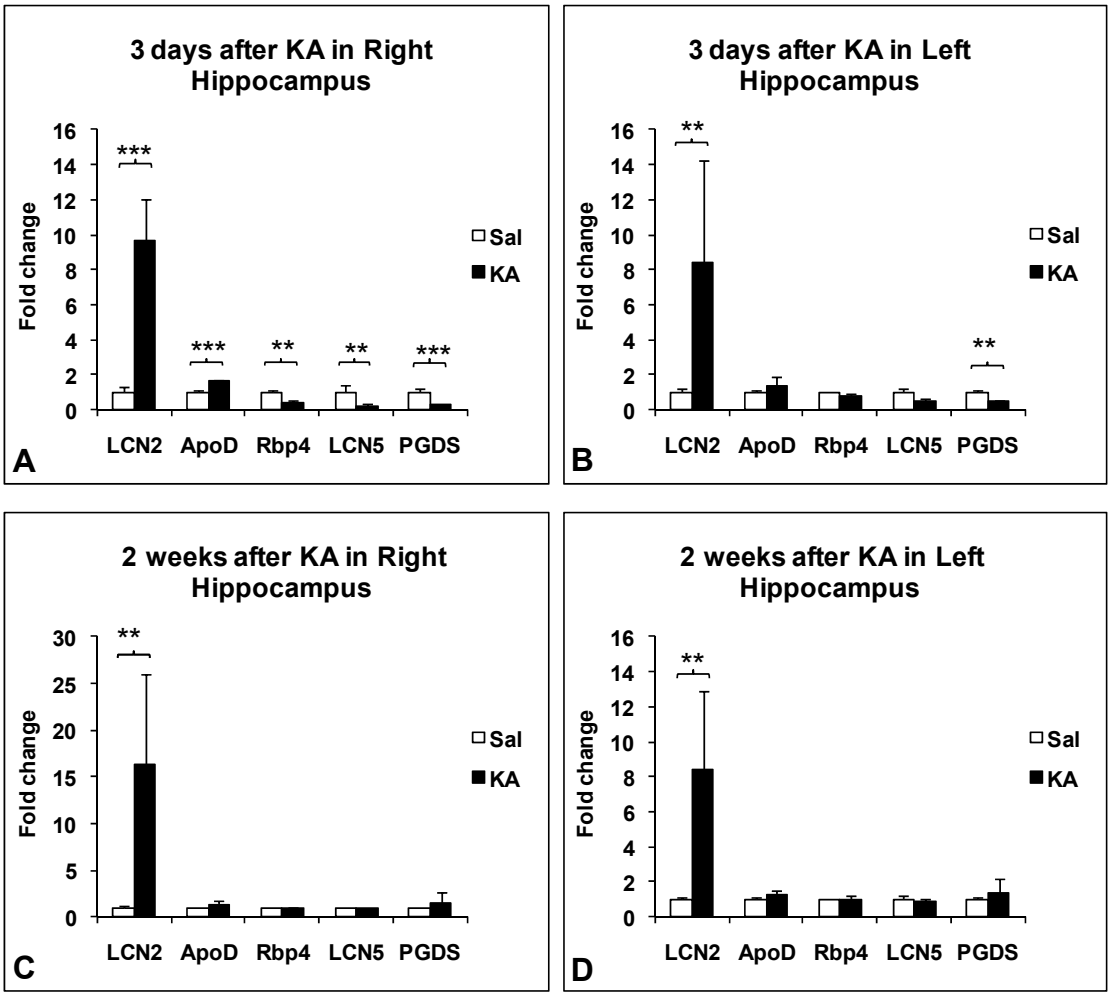

Fig. 2.12. Changes in mRNA expression of LCN2 and other lipocalins in the rat hippocampus after KA injury. Real-time RT-PCR analysis of the lipocalins of the right hippocampus: LCN2, apoD, Rbp4, LCN5 and PDGS at (A, B) 3 days and (C, D) 2 weeks post-KA injection. LCN2 mRNA levels changed from 9.7-fold (***$p < 0.001$) at 3 days post-KA injection to 16.3-fold (**$p < 0.01$) at 2 weeks post-KA injection of the right hippocampus, relative to their respective saline-injected controls. The increase in mRNA expression was specific to LCN2 as the significant changes in apoD, Rbp4, LCN5 and PDGS mRNA levels observed at 3 days post-KA injection returned to normal baseline at 2 weeks post-KA injection. Analysed by Student's t-test, asterisks indicate significant difference (*$p < 0.05$, **$p < 0.01$, ***$p < 0.001$). Data are expressed as mean ± SEM, $n = 4$ per treatment group.

2.4. DISCUSSION

The present study aimed to bridge the knowledge gap between understanding of LCN2 in the periphery and in the CNS by examining the distribution and expression of LCN2 among different brain parts in normal rat brain and analysing changes in expression in the KA-lesioned hippocampus. The distribution of LCN2 was surveyed across various parts of the brain in both the left and right hemispheres. Since LCN2 is known as a bacteriostatic agent, and often upregulated during infections (Flo et al., 2004), it may be expressed in those areas of the brain that bacteria can access easily. Interestingly, the hippocampus has the lowest expression of LCN2, possibly because it is folded deep in the temporal lobe and more inaccessible to bacterial infections. The low basal expression of LCN2 in the hippocampus was also confirmed with RT-PCR and western blot analysis. The olfactory bulb expressed the highest level of LCN2 mRNA, followed by the cerebellum, brainstem, thalamus and hypothalamus, consistent with the trend observed in protein expression.

The olfactory bulb and the brainstem are connected to the olfactory, respiratory and oral mucosa by the olfactory and trigeminal nerves, and there is evidence that these could be entry portals for microorganisms (Thorne et al., 2004). The vestibulocochlear nerve not only projects to the brainstem but axons of the vestibular nerve also terminate in the cerebellum. Hence, it is possible that the high basal expression of LCN2 in the olfactory bulb, brainstem and cerebellum may help the CNS defend against pathogens by sequestering iron and bacterial siderophores. These high LCN2-expressing regions were then investigated for LCN2's cellular localisation. In the olfactory bulb, cerebellum and brainstem, colocalisation of LCN2 with GFAP, a marker of astrocytes, was observed, thus it can be concluded that

LCN2 is expressed in the astrocytes. This is consistent with the study in which LCN2 is expressed by primary astrocytes *in vitro* (Lee et al., 2009).

The expression of LCN2 was suggested to be an innate immune response to prevent bloodborne bacteria from disseminating into the CSF and brain as intraperitoneal injection of lipopolysaccharide (LPS) resulted in the increase in LCN2 protein in the choroidal epithelia and endothelial cells of blood vessels in the brain parenchyma (Marques et al., 2008). LPS is a component of the outer membrane of Gram negative bacteria and is commonly used to induce inflammation in the CNS and periphery (Block et al., 2007; Choi et al., 2008; Gibbons and Dragunow, 2006; Ip et al., 2011). Previously, microarray analysis showed upregulation of LCN2 mRNA in the hippocampus after icv injection of lipopolysaccharide (LPS) in C57BL/6 mice (Bonow et al., 2009). In view of the potential differences between LCN2 orthologues (Kjeldsen et al., 2000), icv LPS injections were performed on rats. Similar to the mouse models, LCN2 mRNA and protein levels increase significantly in the LPS-treated hippocampi by 20 times compared to saline-injected controls. The elevation of LCN2 may be dependent on Toll-like receptor 4 (TLR4), as TLR4-deficient mice had low levels of LCN2 expression relative to the C57BL/6 wild-type, with a 200-fold and a 20-fold increase in LCN2 mRNA and protein expression, respectively, after LPS intraperitoneal administration (Flo et al., 2004).

To induce neurodegeneration, KA icv injection was performed and LCN2's mRNA and protein expression increased steadily from earlier timepoints - 1 day and 3 days and peaked at the later timepoint, 2 weeks post-KA injection. Since LCN2 expression was highly upregulated at 2 weeks post-KA injection, which has pronounced reactive gliosis occurring, suggests that the elevation of LCN2 may be associated with reactive gliosis as LCN2 was demonstrated to induce reactive astrocytosis in primary astrocytes *in vitro* (Lee et al., 2009)

This inference about LCN2 and reactive gliosis was further confirmed with low magnification of LCN2 immunofluorescence at the degenerating hippocampus. LCN2 upregulation was only observed in lesioned areas visualised with Nissl staining. Nissl staining was performed for KA/saline-treated sections to ensure the icv KA injection was effective in inducing neurodegeneration prior to any further analysis. In 3 days and 2 weeks post-KA injection samples, hippocampal lesions were observed in CA1 and CA3 regions. In contrast, at 1 day post-KA injection, hippocampal lesions were only observed in the CA3 region. There may be delayed onset of neuronal death, therefore neurodegeneration may not have been completed by 1 day post-KA injection. Hence the most vulnerable region, CA3, was first affected due to high density of KA receptors localised at that region (Nadler et al., 1980a; Patel et al., 1986). The CA2 hippocampal region was mostly unaffected at all timepoints similar to previous KA lesioning studies (McGeer and McGeer, 1982; Sperk et al., 1983). Hence, the upregulation of LCN2 in the CA1 and CA3 hippocampal lesions further suggests its expression in glial cells, which are known to be upregulated in the lesioned areas during neurodegeneration (Wang et al., 2005; Zheng et al., 2011).

Furthermore, immunoperoxidase staining of 2 weeks post-KA injection sections also showed intense LCN2 immunoreactivity in cells with large cell bodies, thick processes which are characteristic of astrocytes at the lesion sites (CA1 and CA3 regions) of the hippocampus. Thus, double immunolabelling was performed to determine the cellular localisation of LCN2 using sections from 2 weeks post-KA injection since they have high LCN2 expression. As speculated, LCN2 colocalised with GFAP, but not other glia markers, such OX-42 (marker for microglia). Therefore, LCN2 is expressed in astrocytes, but not microglia. This is consistent with the enhanced secretion of LCN2 by primary astrocytes into culture media with LPS treatment *in vitro* (Lee et al., 2009), indicating expression of LCN2 from astrocytes upon insult. Since LCN2 was secreted by primary astrocytes (Lee et al., 2009), the

LCN2 staining of round intense dots from the high magnifications of the orthogonal projections could be vesicles or other intracellular organelles for transport of LCN2 to the cell surface to be secreted out, either to act on itself (autocrine function) or other cells, depending on the localisation of the LCN2 receptors. Furthermore, LCN2 was reported to be expressed in primary microglial cultures and BV-2 microglial cell line *in vitro* (Lee et al., 2007) and we likewise found LCN2 mRNA to be expressed in BV-2 microglial cells by RT-PCR (in *Appendix 1A*), but LCN2 was not detected in microglia *in vivo*. The discrepancies may be due to differences between *in vitro* and *in vivo* conditions.

With the knowledge that LCN2 is expressed in the reactive astrocytes, the expression changes of LCN2 throughout the different timepoints were studied with double immunolabelling of LCN2 and GFAP. In all saline-injected controls at all timepoints, negligible LCN2 staining was observed, again correlating with the low LCN2 expression physiologically. Upregulation of LCN2 in the astrocytes was observed in the lesioned areas as early as at 1 day post-KA injection. Corresponding to the LCN2 mRNA and protein expression levels, LCN2 staining was most intense at 2 weeks post-KA injection, likely due to the increase of reactive astrocytosis. Hyperproliferation of glia usually occurs after neuronal death (Wang et al., 2005). Expression of GFAP, a marker for astrogliosis, was shown to increase steadily, even at one day after intrahippocampal injection of KA (Bendotti et al., 2000; Zheng et al., 2011), and upregulation of reactive astrocytes was observed to peak at 1 month post-KA icv injection (Mitchell et al., 1993).

Since LCN2 is a member of the lipocalin family, it would be valid to question whether this distinct upregulation was only specific to LCN2 or to other lipocalins as well. Four more well-studied lipocalins were examined, which are apolipoprotein D (apoD), prostaglandin D2 synthase (PGDS), retinol binding protein 4 (Rbp4) and

lipocalin 5 (LCN5). ApoD binds arachidonic acid (Morais Cabral et al., 1995), cholesterol (Patel et al., 1997), pregnenolone and progesterone (Vogt and Skerra, 2001). PGDS is a PGD2-producing enzyme as well as a binding protein for biliverdin, bilirubin, retinaldehyde and retinoic acid (Urade and Hayaishi, 2000). Rbp4 is a binding protein for all-*trans* retinoic acid and is elevated in patients with Type 2 diabetes (Graham et al., 2006). Lipocalin 5 is a binding protein for retinoic acid and is a major secreted protein in the epididymis (Ong et al., 2000).

Although at 3 days post-KA injection, there was a significant increase in apoD and decreases in Rbp4, LCN5 and PGDS mRNA levels relative to saline-injected controls, these changes did not persist till 2 weeks. An interesting point to note is the changes in apoD mRNA levels were consistent with a previous study that showed apoD immunoreactivity to peak at 3 days after KA injection but return to baseline levels by 7 days post-injection (Ong et al., 1997). Of the lipocalins, only LCN2 mRNA expression continued to increase from 3 days to 2 weeks post-KA injection in the right hippocampus. The increase of LCN2 mRNA expression in the left hippocampus could be due to diffusion of KA from the right to the left lateral ventricle after icv injection.

From the data presented in this chapter, the pronounced upregulation was found to be unique to LCN2, but not other lipocalins. Also, it is possible to speculate that if the CNS is threatened by bacterial infections, LCN2 will be greatly expressed by the astrocytes in the olfactory bulb, cerebellum and brainstem as a CNS defence response. This is the same context as the upregulation of LCN2 with the administration of LPS. Due to the bacterial origin of LPS, the mammalian host release LCN2 as an innate immune response to scavenge iron from bacteria, protecting the host from “bacterial infection”. Like LCN2, lactoferrin, another mammalian iron-binding protein, is a bacteriostatic agent which binds iron directly to

inhibit bacterial growth (Ellison, 1994). In the mammalian host, LCN2 complements the activity of lactoferrin by binding ferric siderophore complexes rather than free iron, targeting the iron that has been earmarked for bacterial use (Clifton et al., 2009; Goetz et al., 2002). Therefore, LCN2-deficient mice were reported to have increased susceptibility to bacterial infections (Berger et al., 2006; Flo et al., 2004). The bacteriostatic property of LCN2 demonstrated by NGAL's dramatic 20-fold inhibition on *E.coli* growth was negated with the addition of iron to saturate NGAL. This indicates that the main function of LCN2 in the anti-bacterial innate immune response is to limit iron by sequestering ferric siderophores (Berger et al., 2006; Goetz et al., 2002).

However, these are the roles of LCN2 in conditions of bacterial infections. How about in non-bacterial infection conditions? Unlike LPS, KA does not have bacterial origin. Since previously lipocalins were classified primarily as transport proteins (Flower, 1996), could LCN2 transport iron or an unknown endogenous ligand? Thus, other than its bacteriostatic property, it would be interesting to know if LCN2 has any involvement in neurodegeneration, in order to substantiate its pronounced upregulation after KA injury. Therefore, in the next chapter, the expression of LCN2 receptors will be investigated after KA injury, as the cellular localisation of these receptors will be pertinent to postulate the role of LCN2 in KA-induced neurodegeneration.

CHAPTER 3

EXPRESSION OF LCN2R

IN NORMAL AND KA-LESIONED HIPPOCAMPUS

3.1. INTRODUCTION

With the discovery that LCN2 is expressed in the astrocytes in the brain, the next question is – what does LCN2 bind to in the hippocampus? Recently, two cellular receptors for LCN2 have been identified - megalin and 24p3R (Devireddy et al., 2005; Hvidberg et al., 2005).

Megalin, a multi-ligand receptor, was shown to bind NGAL with high affinity by surface plasmon resonance analysis and mediates NGAL's cellular uptake. Megalin was also detected to bind siderophore-NGAL with similar affinity (Hvidberg et al., 2005). Other than binding NGAL/LCN2, megalin binds lactoferrin, another iron-binding protein secreted from human neutrophils (Willnow et al., 1992). Megalin is not new to the CNS as its involvement in CNS development and Alzheimer's disease (AD) has been well-studied. It is expressed early in the development (McCarthy et al., 2002) and involved in the formation of brain structures (Spoelgen et al., 2005; Willnow et al., 1996). In the adult, megalin is only expressed at the choroid plexus (Carro et al., 2005), the ependymal cells of the lateral ventricles (Gajera et al., 2010) and in the spinal cord (Wicher et al., 2006). Megalin-deficient mice have a low survival rate (1 in 50) and die immediately after birth from respiratory insufficiency, exhibiting brain malformations (Marzolo and Farfan, 2011; Willnow et al., 1996).

Megalin is also implicated in neurodegenerative conditions such as Alzheimer's disease (AD). It is involved in the endocytic uptake of numerous ligands, including many known carriers of amyloid beta (Aβ) (Christensen and Birn, 2002) and participates in Aβ clearance (Carro et al., 2005; Deane et al., 2004; Hammad et al., 1997; Zlokovic, 1996). In AD patients and the elderly, a reduced level of megalin expression was reported (Dietrich et al., 2008), suggesting a reduction of protective effects of megalin on the brain.

The other LCN2 receptor, 24p3R, was cloned by Green and colleagues for 24p3 (murine orthologue of LCN2) (Devireddy et al., 2005). Ligand-cell binding experiments and internalisation assays showed that only 24p3R-expressing HeLa cells could bind to ^{32}P-labelled 24p3 and internalise it into the cells. This was not observed in HeLa cells, which do not express 24p3R (Devireddy et al., 2005). Therefore, 24p3R/LCN2R is necessary for binding and internalisation of 24p3/LCN2. In addition, 24p3R-expressing HeLa cells internalise apo-24p3 to export intracellular ^{55}Fe into the extracellular medium, decreasing intracellular iron levels. The low intracellular iron level was suggested to trigger Bim-dependent apoptosis in the 24p3R-expressing cells (Devireddy et al., 2005). Following the discovery of 24p3R, the Bim-dependent apoptotic function of LCN2 mediated by 24p3R was also observed in primary astrocytes and C6 glioma cells (Devireddy et al., 2005; Lee et al., 2009). Although it has been established that 24p3R binds both apo-24p3 (iron-free) and holo-24p3 (iron-loaded), the affinity of 24p3R for neither was measured.

LCN2R is widely expressed in many organs (such as kidney, liver, testes and heart), but its mRNA expression is highest in the brain. It is noteworthy that among brain-derived cells surveyed, primary neurons have higher LCN2R mRNA expression than the primary astrocytes or C6 glioma cells (Bennett et al., 2011).

Suk and colleagues (2009) have detected both megalin and 24p3R (murine orthologue of LCN2R) in brain-derived cells. LCN2 was reported to sensitise primary astrocytes and C6 glioma cells to apoptotic stimuli. Since 24p3R mRNA expression was detected in both cell types, while megalin was only expressed in the primary astrocytes, this suggests that the pro-apoptotic effect of LCN2 was mediated by 24p3R. In addition, 24p3R was also expressed in primary microglia, BV-2 cells, primary cortical neurons and B35 neuroblastoma (Lee et al., 2007; 2011).

In this thesis, the focus will be placed on the rat orthologue of 24p3R, LCN2R, rather than megalin. This is firstly because LCN2R has been well-characterised with LCN2, as compared to the interaction of megalin with LCN2, especially in iron transport and apoptosis. Secondly, being a promiscuous receptor with many ligands, it would be difficult to distinguish LCN2's effect through megalin without interference from the effects of other ligands. Although megalin's protective effect on AD suggests a possible role in KA-induced neurodegeneration, in view of the potential confounding factors and the unavailability of a specific antibody for megalin, cellular localisation studies were focused on LCN2R instead.

Since little is known about LCN2R physiologically and in conditions of neurodegeneration, this chapter will examine if LCN2R is present *in vivo* and more importantly - its cellular localisation. The effect of LCN2, mediated by LCN2R would be different depending on the cellular localisation of LCN2R in the hippocampus. For instance, if LCN2R was expressed on astrocytes, the LCN2 produced could bind to the LCN2R expressed on the same cells to mediate an autoregulatory function as suggested by Lee et al. (2009). On the other hand, if LCN2 receptors were expressed on neurons or microglia, the function of LCN2 may be different. These results would be important in postulating the possible mechanism or function of LCN2 in KA-induced neurodegeneration.

3.2. MATERIALS AND METHODS

3.2.1. Animals and kainate (KA) injections

Male Wistar rats weighing approximately 200 g each were anaesthetised by intraperitoneal injection of ketamine (75 mg/kg) and xylazine (10 mg/kg). KA (1.2 µl of 1 mg/ml) was stereotaxically injected into the right lateral ventricle (coordinates: 1.0 mm caudal to bregma, 1.5 mm lateral to the midline, 4.5 mm from the surface of the cortex) using a microlitre syringe (5 µl Hamilton syringe, Model no.: 88000, 24 gauge needle, outer diameter of needle: 0.57 mm, inner diameter of needle: 0.31 mm). Experimental control rats were injected with 1.2 µl of normal saline instead of KA. All procedures involving animals were approved by the Institutional Animal Care and Use Committee, NUS.

3.2.2. Real-time RT-PCR

A total of 24 animals were used, four KA-injected animals versus four saline-injected control animals were sacrificed at 1 day, 3 days and 2 weeks after injection. Three animals were also sacrificed to study LCN2R in the normal hippocampus. Tissues were freshly dissected from the brain and immersed into RNAlater (Ambicon, CA, USA), flash frozen and kept at -80°C until analysis. Total RNA was isolated using TRIzol reagent (Invitrogen, CA, USA) according to the manufacturer's protocol, and RNeasy Mini Kit (Qiagen Inc., CA, USA) was used to purify the RNA. The samples were reverse transcribed using High-Capacity cDNA Reverse Transcription Kits (Applied Biosystems, CA, USA). The reaction conditions were 25°C for 10 min, 37°C for 120 min and 85°C for 5 min. Real-time PCR amplification was carried out using the 7500 Real-time PCR system (Applied Biosystems, CA, USA) with Taq-Man Universal PCR Master Mix (Applied Biosystems, CA, USA) and gene-specific primers

and probes according to manufacturer's protocols (Assay ID: Slc22A17/LCN2R (Rn00598583_m1)). β-actin (Part no: 4352340E) was used as an internal control. All primers and probes were synthesised by Applied Biosystems. The PCR conditions were: an initial incubation of 50°C for 2 min and 95°C for 10 min followed by 40 cycles of 95°C for 15 s and 60°C for 1 min. All reactions were carried out in triplicates. The threshold cycle, CT, which correlates inversely with the levels of target mRNA, was measured as the number of cycles at which the reporter fluorescence emission exceeds the preset threshold level. The amplified transcripts were quantified using the comparative CT method (Livak and Schmittgen, 2001), with the formula for relative fold change = $2^{-\Delta\Delta CT.}$ The mean was calculated, and possible significant differences were analysed using Student's t-test. $p < 0.05$ was considered significant. RT-PCR was conducted on rat hippocampal tissues using specific primers to Slc22A17/LCN2R transcript (Applied Biosystems, Assay ID: Rn00598583_m1). DNA gel electrophoresis was performed to separate the PCR products in a 1.5% agarose gel. The DNA bands were stained with ethidium bromide and visualised under UV irradiation.

3.2.3. Western blotting

Three KA-injected rats and three saline-injected control animals were sacrificed at 1 day, 3 days and 2 weeks after injection. Three normal rats were also sacrificed to analyse LCN2R protein levels in the untreated rat brain. The rats were anaesthetised by intraperitoneal injection of ketamine and xylazine and decapitated. The tissues were quickly removed and homogenised in cold lysis buffer containing Tris–HCl, pH 7.4, 10 mM EDTA, 150 mM NaCl, 0.5% Triton X-100 with protease inhibitor cocktail (Roche Diagnostics, Indianapolis, IN, USA) and placed on the shaker for 1 hr at 4°C. After centrifugation at 12,000g for 30 min, the supernatant was

collected, and protein concentration was determined using the BCA protein assay kit (Pierce Biotechnology, Rockford, IL, USA). Prior to gel electrophoresis, the protein lysates were denatured by heating the sample in the presence of SDS and DTT for 10 min at 95-100°C.

Total protein (60 µg) was resolved in 12% SDS-polyacrylamide gel under reducing conditions and electro-transferred to a nitrocellulose membrane (Biorad, CA, USA). Non-specific binding sites on the membrane were blocked by incubation with 5% non-fat milk for 1 hr. The membrane was then incubated overnight with polyclonal rabbit anti-Slc22A17/LCN2R antibody at 1:2000 (Cat no. 4651, Prosci Incorporated, Poway, CA, USA). After washing with 0.1% Tween-20 in TBS, the membrane was incubated with horseradish peroxidase-conjugated goat anti-rabbit immunoglobulin lgG (1:10,000; Thermo Fisher Scientific, Rockford, IL, USA) for 1 hr at room temperature. The protein was visualised with SuperSignal West Pico chemiluminescent substrate (Thermo Fisher Scientific, Rockford, IL, USA) according to the manufacturer's instructions. Blots were treated with stripping buffer (Restore Western Blot Stripping Buffer, Thermo Fisher Scientific, Rockford, IL, USA) at room temperature for 10 min before reprobing of membrane with antibody to β-actin (Sigma, St. Louis, MO, USA). Exposed films were scanned with at least 300 dpi and the mean optical density of the protein bands of LCN2R was analysed by densitometry using ImageJ (NIH, Maryland, USA), and normalised to β-actin. The mean was calculated, and possible significant differences were analysed using Student's t-test. $p < 0.05$ was considered significant.

3.2.4. Double immunofluorescence labelling

A total of 24 animals were used, four KA-injected animals versus four saline-injected control animals were sacrificed at 1 day, 3 days and 2 weeks after injection

to study the effect of KA lesions. Three untreated rats were used to study the cellular localisation of LCN2R in the normal hippocampus. The rats were anaesthetised by intraperitoneal injection of anaesthetic comprising ketamine and xylazine and transcardially perfused with Ringer solution, followed by 4% paraformaldehyde in 0.1M phosphate buffer (pH 7.4). The brains were dissected out, and blocks containing the hippocampus were sectioned coronally at 20 µm using a freezing microtome. Sections were soaked in phosphate buffered saline (PBS) for 30 min to remove traces of sucrose and permeabilised with PBS-0.3% Triton X-100 for 10 min. They were then blocked with 5% donkey/goat serum in PBS-0.3% Triton X-100 for 1 hr, followed by incubation with rabbit polyclonal antibody to Slc22A17/LCN2R at 1:500 (Cat no. 4651, Prosci Incorporated, Poway, CA, USA) and mouse monoclonal antibody to OX-42 (1:200, Chemicon, Temecula, CA, USA) or mouse monoclonal MAP2a (1:200, Sigma-Aldrich, MO, USA) or goat polyclonal antibody to LCN2 at 1:200 (AF3508, R&D systems, MN, USA) overnight at 4°C. Specificity of the Slc22A17/LCN2R antibody was verified by pre-incubating 10 µg/ml (5x) and 20 µg/ml (10x) of Slc22A17 peptide (Prosci Incorporated, Poway, CA, USA) with 2 µg/ml of Slc22A17/LCN2R antibody overnight. The sections were washed in PBS, and incubated for 1 hr at room temperature in 1:200 dilution of donkey anti-goat IgG (H+L) Alexa Fluor 488 and donkey anti-rabbit IgG (H+L) Alexa Fluor 555 or goat anti-rabbit IgG (H+L) Alexa Fluor 555 and goat anti-mouse IgG (H+L) Alexa Fluor 488 (Invitrogen, CA, USA). The sections were then washed and mounted with ProLong® Gold antifade reagent with DAPI (Invitrogen, Carlsbad, CA, USA) and captured using a fluorescence microscope (Olympus BX51; Olympus Corporation, Tokyo, Japan) and a laser scanning confocal microscope (LSM 510, Carl Zeiss Göttingen, Germany). Colocalisation was established by analysing the overlap between the different labels by orthogonal reconstruction throughout the entire *z*-stack (LSM 510, Carl Zeiss Göttingen, Germany).

3.3. RESULTS

3.3.1. Expression of LCN2R in the normal hippocampus

3.3.1.1. LCN2R mRNA and protein expression in the hippocampus

To investigate if LCN2R is present in the normal hippocampus, RT-PCR and western blot analysis were conducted. In the right hippocampus, RT-PCR revealed a PCR product of 98bp (Fig. 3.1A). Western blot analysis of the right hippocampi of three normal rats showed discrete bands slightly under the 75kDa ladder, due to glycosylation of LCN2R. This indicates that LCN2R mRNA and protein were present in the normal rat hippocampus.

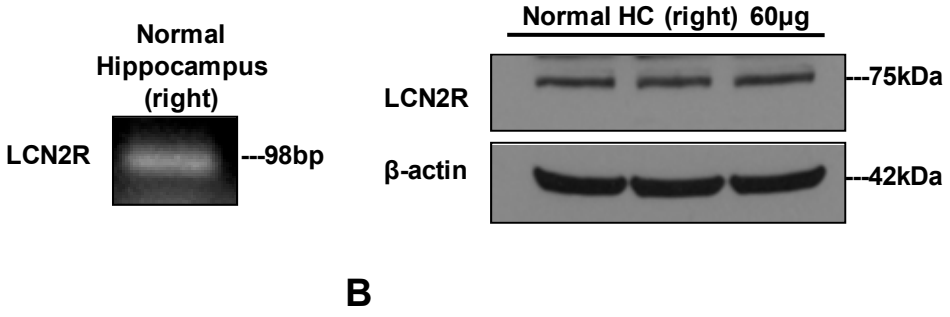

Fig. 3.1. LCN2R mRNA and protein expression in the right hippocampus of normal rat brain. (A) RT-PCR was conducted on the cDNA of the right hippocampus from a normal rat with specific primers to LCN2R transcript. (B) 60 µg of right hippocampus lysate from three individual normal animals were loaded for western blot analysis and probed with anti-LCN2R.

3.3.1.2. Cellular expression of LCN2R in the hippocampus

LCN2R labelling was observed in neuronal-like cells of the normal rat hippocampal sections, in the CA hippocampal regions (from CA1, CA2, CA3 to CA4) (Fig. 3.2A, D, G, J) and the cells of the dentate gyrus (Fig. 3.2.M). Colocalisation of LCN2R with MAP2a (Fig. 3.2B, E) indicates that it was localised in the neurons (Fig. 3.2C, F). Control experiments were performed by incubating the LCN2R antibody

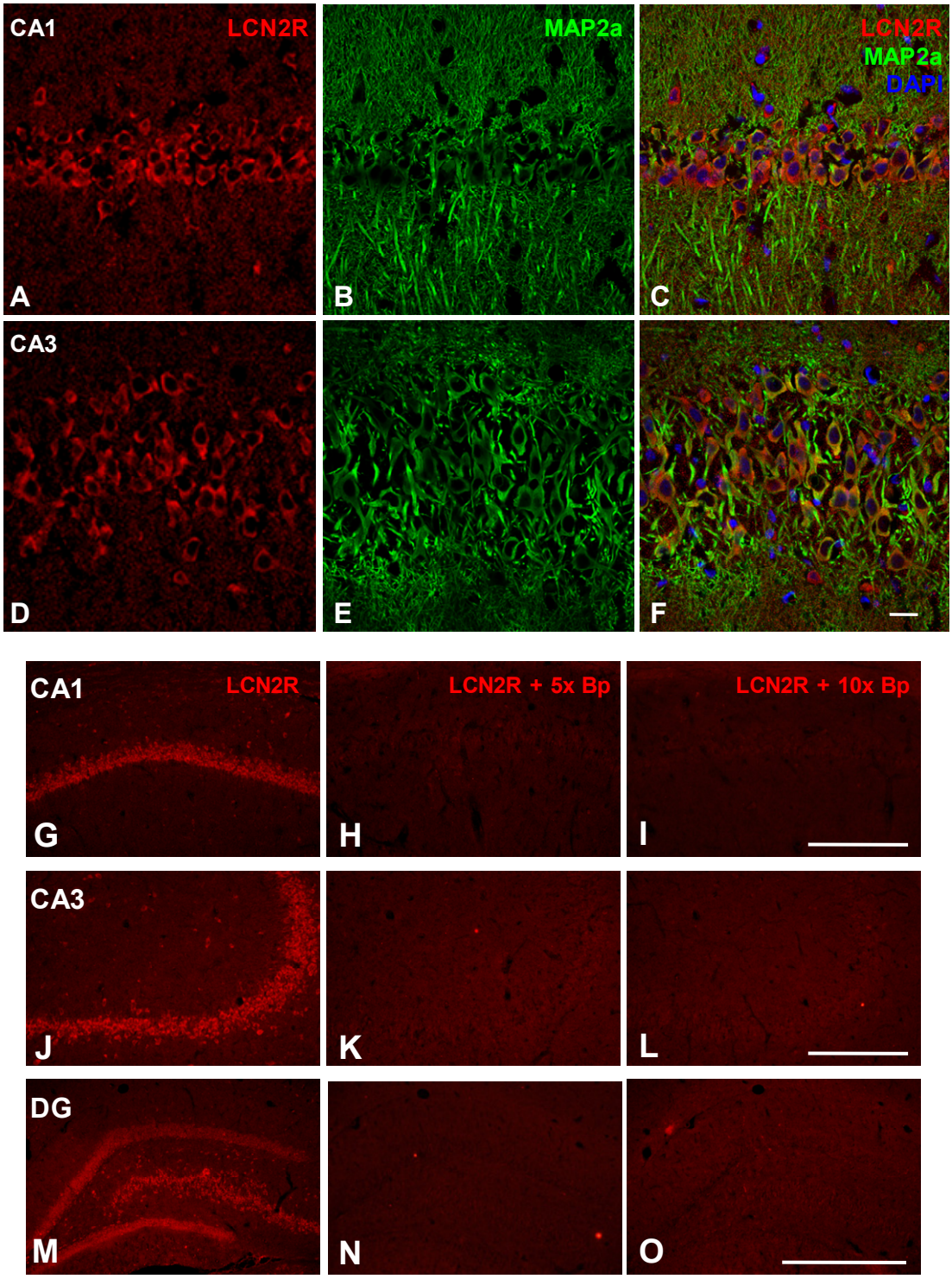

Fig. 3.2. Cellular expression of LCN2R in normal hippocampus. Hippocampal sections are double-labelled with (A, D) LCN2R and (B, E) MAP2a, indicating colocalisation at both (C) CA1 and (F) CA3 regions of the hippocampus. Scale=20 µm. Sections are pre-incubated with LCN2R antibody with (H, K and N) 5x and (I, L and O) 10x excess of blocking peptide, blocking LCN2R positive staining at (G) CA1, (J) CA3 hippocampal regions and (M) the dentate gyrus, indicating the specificity of the antibody. G-L: scale=200 µm; M-O: scale=500 µm.

together with its blocking peptide in 5x and 10x excess. The antigen-absorbed LCN2R antibody showed absence of staining for the normal rat hippocampal sections, in the CA1 (Fig. 3.2H and I), CA3 (Fig. 3.2K and L) hippocampal regions and dentate gyrus (Fig. 3.2N and O). This indicates the specificity of the LCN2R antibody in the neurons.

3.3.2. Expression of LCN2R in the Kainate-lesioned brain

3.3.2.1. mRNA expression changes of LCN2 receptors after LPS and KA treatment

Previously in *Chapter 2*, LCN2 mRNA and protein expression was greatly upregulated by 20-fold in LPS-treated hippocampi *(Fig. 2.5).* Since LCN2 has two known receptors, real-time RT-PCR was performed to examine any mRNA expression changes in LCN2R and megalin. In LPS-treated right hippocampi, LCN2R and megalin mRNA expression was 0.68- ($p < 0.01$) and 0.74- ($p < 0.01$) fold relative to the saline-injected controls, respectively (Fig. 3.3A).

As a comparison to LPS-treatment, mRNA expression of the LCN2 receptors was also studied at 2 weeks post-KA injection, which had the highest upregulation of LCN2 (relative to controls) among all timepoints. In KA-treated hippocampi, mRNA levels of LCN2R and megalin were 0.32- ($p < 0.01$) and 0.50- ($p < 0.001$) fold relative to the saline-injected controls in the right hippocampi, respectively (Fig. 3.3B).

In both KA and LPS treatment, the downregulation of the LCN2 receptors could be attributed to loss of neurons after treatment. Since LCN2R had the greatest decrease in mRNA expression after KA injury, further studies will be done on different timepoints of KA injection in the next section *(Section 3.3.2.2.)* to understand the expression changes of LCN2R.

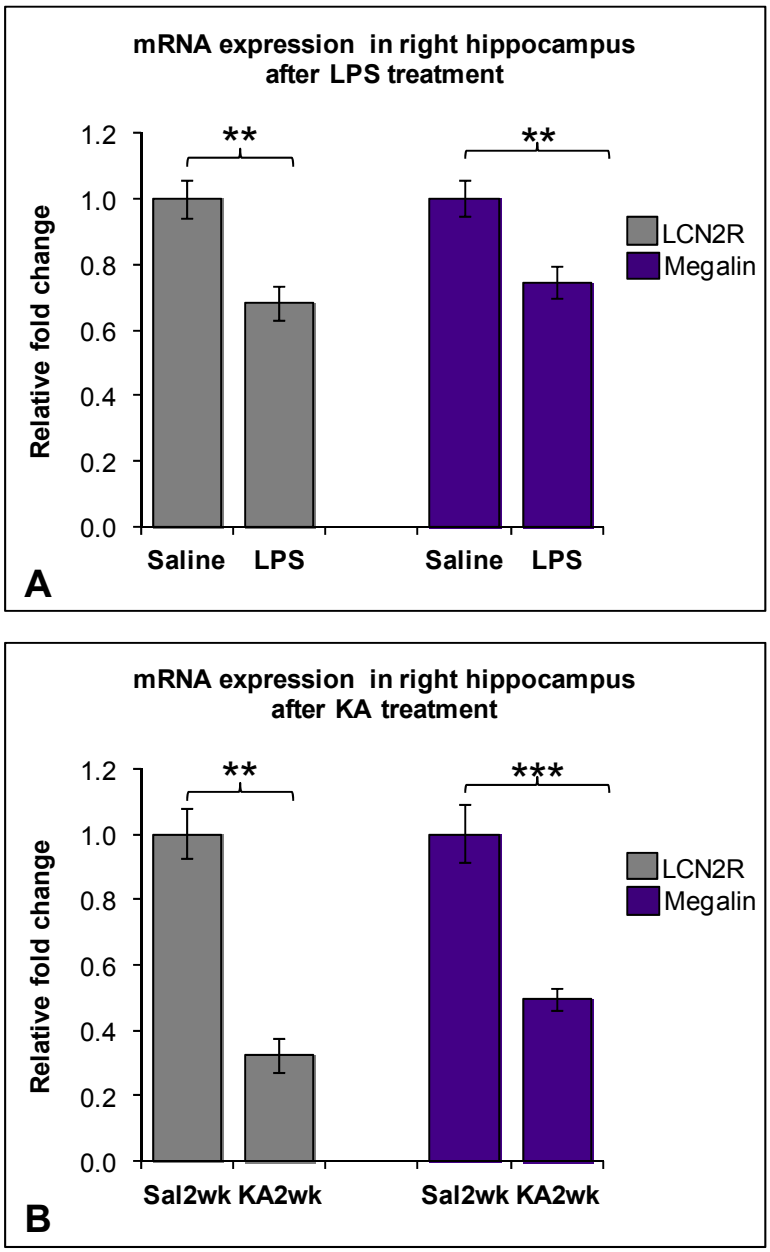

Fig. 3.3. mRNA expression changes of LCN2 receptors, LCN2R and megalin, after LPS and KA treatment. (A) Real-time RT-PCR analysis on mRNA changes of LCN2R and megalin at 24 hrs post-LPS and -saline injection. (B) Real-time RT-PCR analysis on mRNA changes of LCN2R and megalin at 2 weeks post-KA and –saline injection. The right hippocampus of each animal was analysed. Analysed by Student's t-test, asterisks indicate significant difference (*$p < 0.05$, **$p < 0.01$, ***$p < 0.001$). Data are expressed as mean ± SEM, $n = 4$ per treatment group.

3.3.2.2. Changes in LCN2R mRNA and protein expression in the rat hippocampus after KA injury

Real-time RT-PCR indicated that LCN2R mRNA expression was 0.28- (p < 0.001), 0.22- (p < 0.001) and 0.30- (p < 0.001) fold at 1 day, 3 days and 2 weeks post-KA injection relative to their controls, respectively (Fig. 3.4).

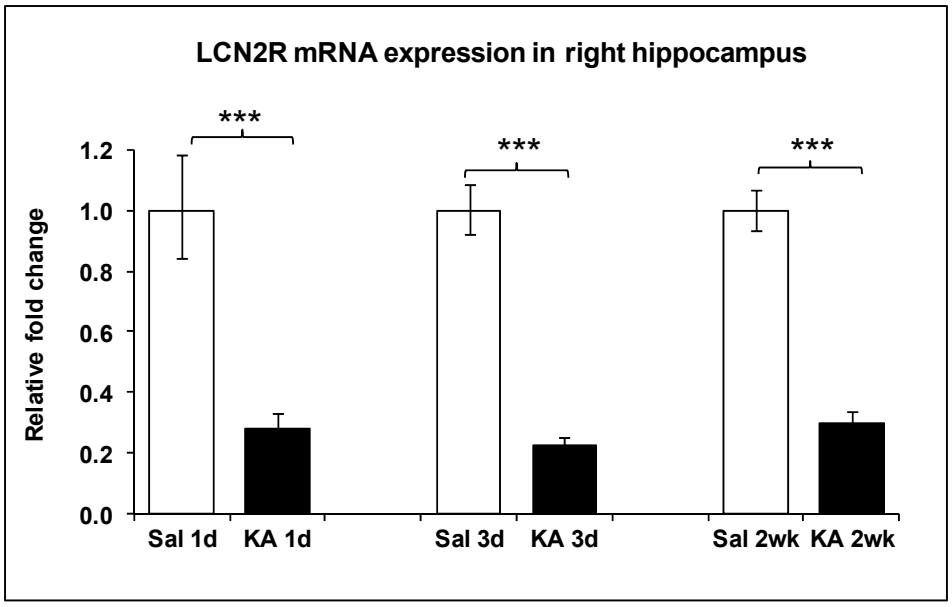

Fig. 3.4. LCN2R mRNA expression downregulated after KA injury. Real-time RT-PCR analysis of LCN2R mRNA expression in the right hippocampus at 1 day, 3 days and 2 weeks post-KA and -saline injection. Analysed by Student's t-test, asterisks indicate significant difference (*p < 0.05, **p < 0.01, ***p < 0.001). Data are expressed as mean ± SEM, n = 4 per treatment group.

The decrease in LCN2R in KA-treated animals was further validated by western blot analysis (Fig. 3.5). All KA-treated samples had lighter bands than their respective saline-injected controls (Figure 3.5A-C). Decrease in LCN2R protein expression was revealed to be significant at all timepoints by densitometric analysis. LCN2R protein expression was 0.53 times (p < 0.001) lower at 1 day post-KA injection compared to the saline-injected controls. At 3 days and 2 weeks post-KA injection, LCN2R protein expression further decreased to 0.13 (p < 0.01) and 0.18 (p < 0.05) times relative to their saline-injected controls, respectively. Densitometric analysis of the LCN2R protein bands were normalised to β-actin (identical to the β-

actin bands from *Fig. 2.7A-C*). Hence, after KA injury, LCN2R mRNA and protein expression were reduced significantly.

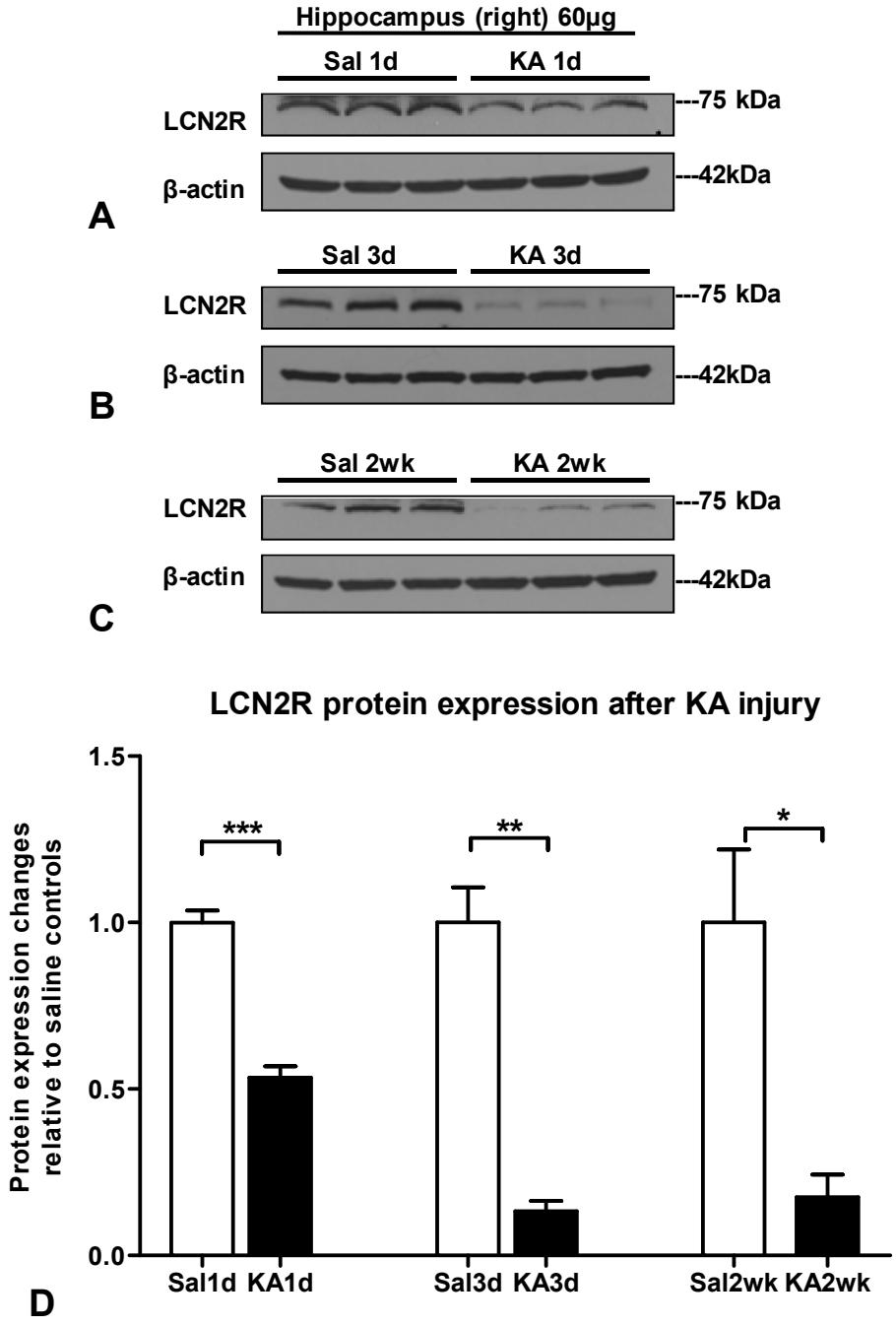

Fig. 3.5. LCN2R protein expression downregulated after KA injury. Western blot analysis of LCN2R protein expression in the right hippocampus at (A) 1 day, (B) 3 days and (C) 2 weeks post-KA vs -saline icv injection. *n* = 3 per treatment group. (D) Densitometric analysis of LCN2R protein expression. LCN2R was downregulated after KA injury. Values are normalised with the saline-injected controls of the respective timepoints. Analysed by Student's t-test, asterisks indicate significant difference (*$p < 0.05$, **$p < 0.01$, ***$p < 0.001$). Data are expressed as mean ± SEM, *n* = 3 per treatment group.

3.3.2.3. Changes in LCN2R immunoreactivity in the rat hippocampus after KA injury

Immunofluorescence staining of LCN2R was detected on the neurons of the hippocampus in the saline-injected controls (Fig. 3.6A, B), similar to the staining observed in the normal (untreated) hippocampus *(Fig. 3.2)*. After KA injury, LCN2R staining was reduced in the neurons, but upregulated in other cell types in the lesioned areas. To identify the cell type, sections were colabelled with LCN2R and OX-42 (marker for microglia).

Immunostaining for OX-42 (as shown in the inserts in their respective timepoints) illustrates the change in morphology of the microglia. With time, the morphology of the microglia transformed from that of ramified microglia to activated and reactive microglia. In the hippocampus of normal (untreated) and saline-injected control animals, the ramified cells possess a small oval cell body and numerous processes of small diameter radiating from the soma. With KA insult, activated microglia were observed with larger cell bodies and with shorter and stouter processes (Davis et al., 1994; Stoll and Jander, 1999; Streit et al., 1999; 2000) (Fig. 3.6).

At 1 day post-KA injection, LCN2R was localised at the pyramidal neurons of the intact CA1 region and did not colocalise with the ramified microglia (Fig. 3.6C). The microglia had similar morphology to those observed in the 2 weeks post-saline injection controls. In contrast, at the CA3 region, sparse LCN2R staining colocalised with OX-42 in the hippocampal lesioned area (Figure 3.6D). At 3 days post-KA injection, LCN2R was upregulated together with OX-42 in both CA1 and CA3 lesioned areas (Figure 3.6 E-F). Intense upregulation of LCN2R and OX-42 was also observed in the lesioned areas of 2 weeks post-KA injection sections (Figure 3.6G-H). Among the three timepoints, the upregulation of LCN2R and OX-42 positive cells

was the greatest at 2 weeks post-KA injection. At all timepoints, LCN2R colocalised with OX-42 in the lesioned areas.

Forty times magnifications of the CA1 hippocampal region of 3 days (Fig. 3.7A) and 2 weeks (Fig. 3.7C) post-KA injection samples indicate that majority of the LCN2R positive cells were immunolabelled with OX-42. Orthogonal projections through CA1 lesioned region at higher magnification demonstrate that LCN2R was present in the OX-42-positive cells at both timepoints (Fig. 3.7B, D), confirming LCN2R's upregulation in the microglia after KA injury.

3.3.2.4. Immunoreactivity at CA1-CA2 region in KA-treated sections

In the previous section, LCN2R was shown to be expressed in neurons in normal/saline conditions and upregulated in microglia in lesioned areas. Hence, the immunoreactivity of LCN2R was examined at higher magnifications at the CA1 to CA2 region to further confirm the change in cellular localisation after KA injury. As observed previously, in the CA1 hippocampal lesioned area of 2 weeks post-KA injection samples, LCN2R positive cells colocalised with the OX-42 positive microglia cells (Fig. 3.8A). Interestingly, in the non-lesioned CA2 hippocampal region, LCN2R was expressed in the intact pyramidal neurons instead (Fig. 3.8A). This confirms that LCN2R is expressed in the microglia in lesioned areas, and remained localised in the intact neurons after KA injury.

At 2 weeks post-KA injection, LCN2 was highly upregulated in the astrocytes *(Chapter 2)* and its receptor, LCN2R, was also greatly upregulated in microglia at this timepoint. Hence, to examine the relationship between LCN2 and LCN2R, double immunolabelling was performed on 2 weeks post-KA injection sections.

Similar to Figure 3.8A, LCN2R was present in neurons of the CA2 region, and had lower expression in the lesioned area, while LCN2 was upregulated in the astrocytes of the lesioned CA1 region (Fig. 3.8B).

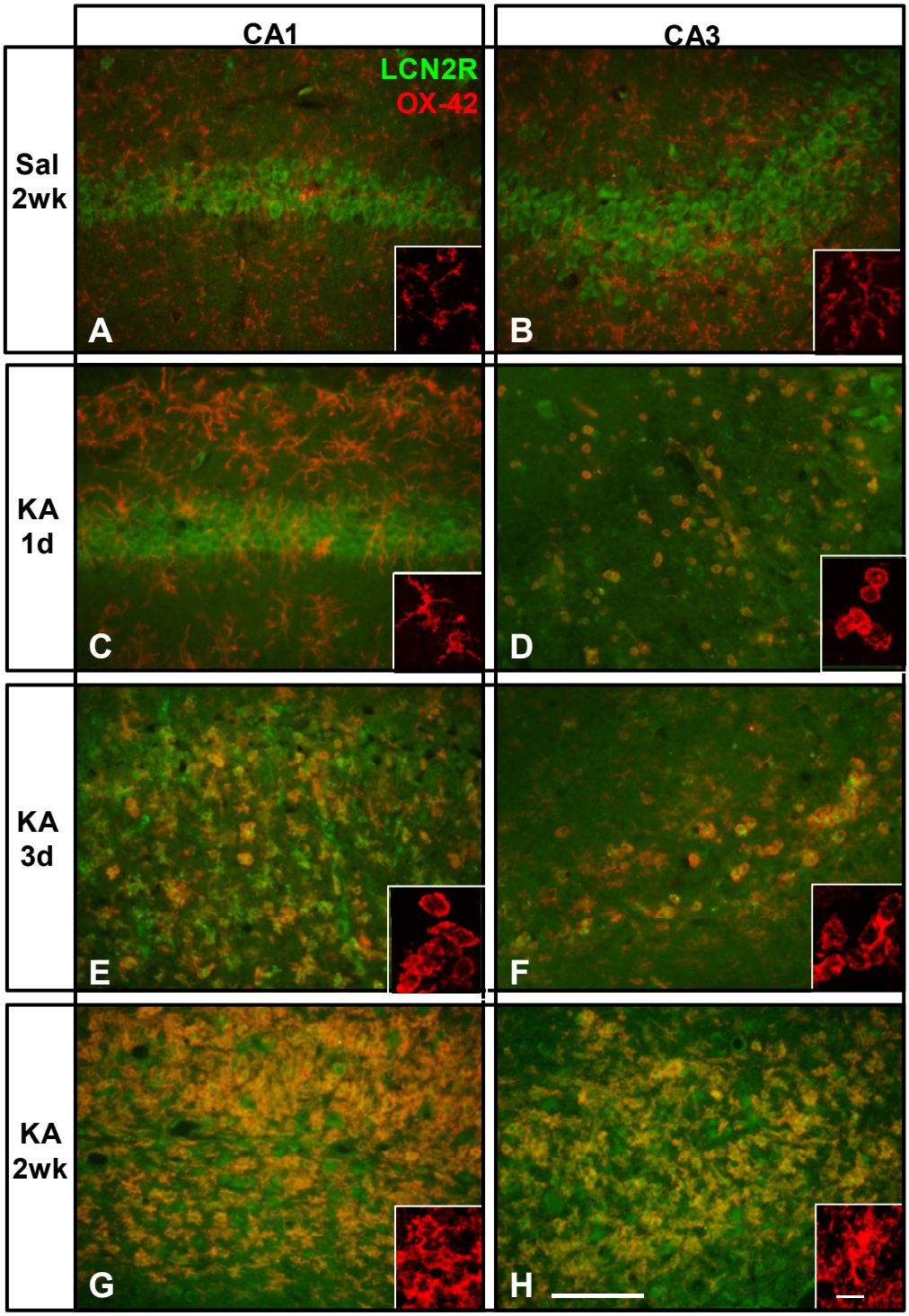

Fig. 3.6. Changes in cellular localisation of LCN2R in the rat hippocampus after KA injury. Hippocampal sections were double-labelled with LCN2R (green) and OX-42 (red), a marker for microglia. (A, B) In 2 weeks post-saline injection samples, immunostaining of LCN2R at the neurons in CA1 and CA3 regions and did not colocalise with OX-42. (C) LCN2R was expressed at the pyramidal neurons at CA1, but (D) colocalised with OX-42 at CA3 in 1 day post-KA injection samples. LCN2R colocalise with OX-42 in the CA1 and CA3 regions in (E, F) 3 days and (G, H) 2 weeks post-KA injection samples. Scale=100 μm, Inserts in A-H shows morphology of microglia labelled with OX-42 at the timepoint. Scale in inserts=10 μm.

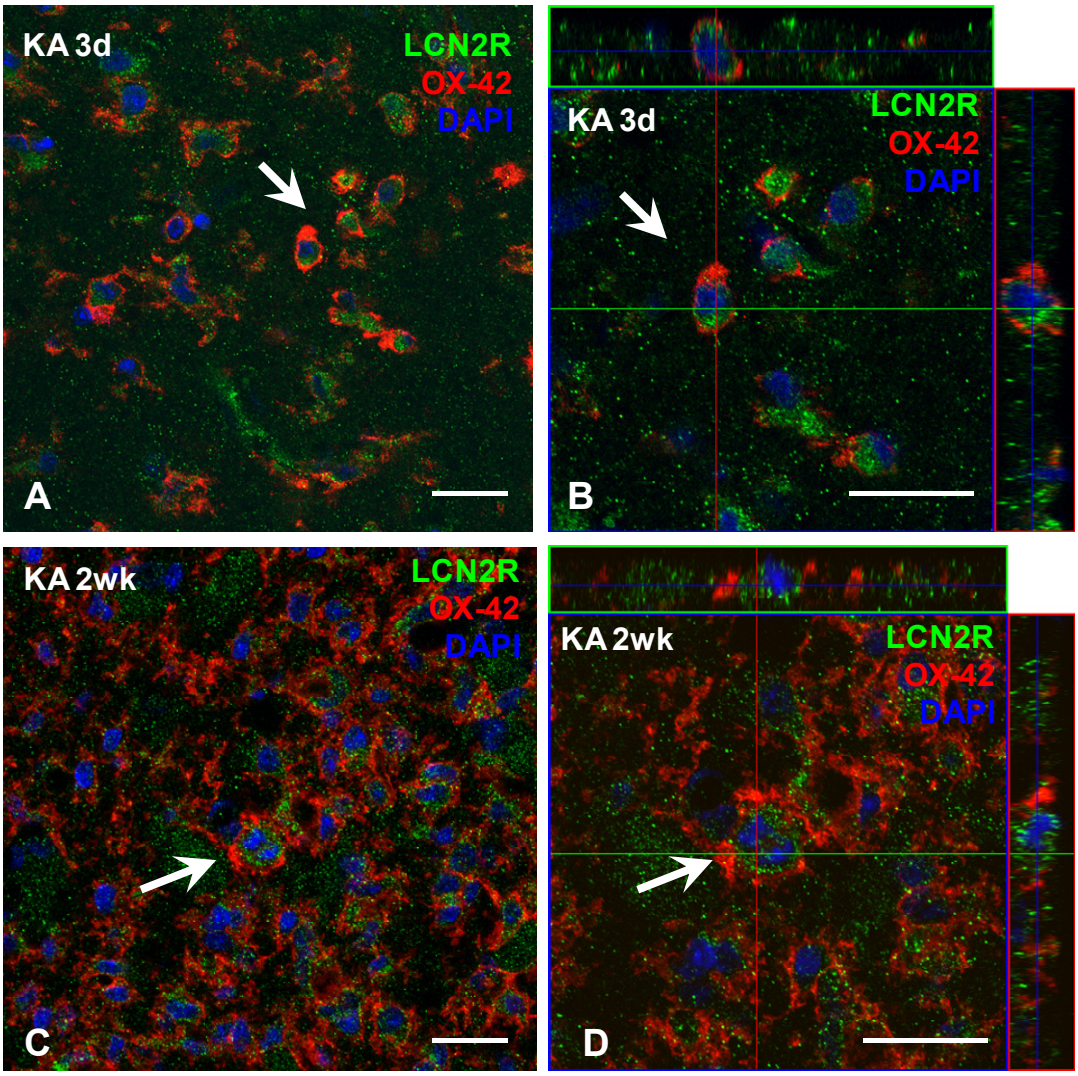

Fig. 3.7. Confocal micrographs of colocalisation of LCN2R with OX-42 positive cells. Right hippocampus at (A, B) 3 days and (C, D) 2 weeks post-KA injection was double-labelled with LCN2R (green) and OX-42 (red), a marker for microglia. (A, C) 40x magnification showed LCN2R positive cells are OX-42 positive. (B, D) 63x magnifications of orthogonal projections through CA1 lesioned region of the cells indicated by the white arrows in (A) and (C). LCN2R is present in microglia. Scale=20 µm.

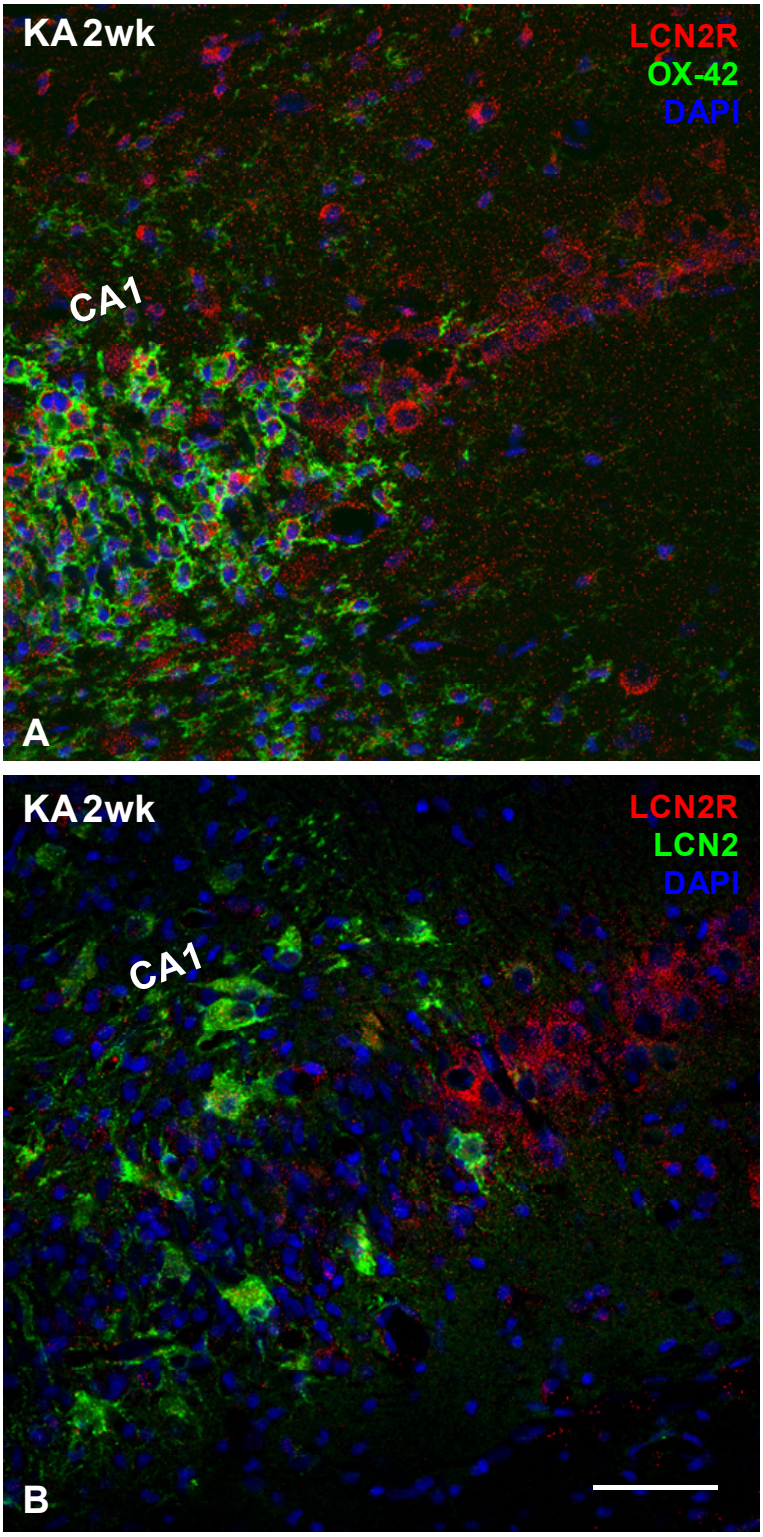

Fig. 3.8. Immunoreactivity at CA1-CA2 region in KA-treated sections. (A) Colocalisation studies of LCN2R (red) and OX-42 (green). LCN2R was localised at intact pyramidal neurons (CA2 region) and upregulated in the microglia of the CA1 lesioned area. (B) Colocalisation studies of LCN2 (green) and LCN2R (red). LCN2R was predominantly expressed in the intact neurons at CA2 region, while LCN2 was upregulated in the astrocytes at CA1. Scale=50 μm.

3. 4. DISCUSSION

The present study was carried out to examine the expression and cellular localisation of LCN2R physiologically and after KA injury to help investigate a possible function of LCN2 in KA-induced neurodegeneration. For the first time, the two known LCN2 receptors, LCN2R and megalin, were detected in the intact hippocampus and LCN2R was observed to have changes in cellular localisation after KA injury.

In *Chapter 2*, a tremendous upregulation (20-fold increase) of LCN2 mRNA and protein expression were observed after LPS treatment. As a preliminary finding, real-time RT-PCR was performed to detect the difference in LPS and KA treatments on the LCN2 receptors. With LPS treatment, megalin and LCN2R mRNA expression decreased significantly by 26% and 32% respectively. At 2 weeks post-KA injection, the significant downregulation of both receptors were even more pronounced; megalin's mRNA expression decreased by 50% while LCN2R's mRNA expression decreased by almost 70%.

In both treatments, LCN2 receptors were significantly downregulated and the decrease in LCN2R was more pronounced than megalin, suggesting that LCN2R could be more sensitive to insults. In the normal rat, LCN2R was detected in neurons as it colocalised with MAP2a at the hippocampal formation and at the dentate gyrus. The staining of LCN2R was specific as it was abolished with the addition of blocking peptide. Since LCN2R was localised at the neurons, the decrease in expression is likely due to neuronal loss after KA-induced neurodegeneration. Furthermore, KA-treated samples have a greater decrease of LCN2 receptors compared to the LPS-treated samples because in the KA-induced neurodegeneration model, excitotoxicity causes neuronal loss either through necrosis or apoptosis (Nishiyama et al., 1996; Pollard et al., 1994b; Portera-Cailliau et al., 1997; Wang et al., 2005), while LPS-

induced inflammatory mediators indirectly cause neuronal damage (Boje and Arora, 1992; Choi et al., 2008; Jeohn et al., 1998). Therefore, the neuronal loss sustained due to KA injury is expected to be greater than in LPS treatment. These results further strengthen the evidence for LCN2R localisation on neurons physiologically.

With this preliminary understanding, we next investigated LCN2R at 1 day, 3 days and 2 weeks post-KA injection to understand the progression of its possible expression changes at different phases of neurodegeneration. After KA injury, LCN2R mRNA expression decreased significantly by 70-80%, likely due to neuronal damage. Similarly, LCN2R protein levels also decreased significantly by 47% in 1 day post-KA injection hippocampi and 87% and 82% in 3 days and 2 weeks post-KA injection hippocampi respectively. Higher LCN2R protein levels were observed 1 day post-KA injection, likely due to the delayed onset of neurodegeneration after KA injection (Sperk et al., 1983; Tokuhara et al., 2007). Thus at later timepoints, most neurons have undergone degeneration. Hence, LCN2R protein levels were similar at 3 days and 2 weeks post-KA injection.

Interestingly, although mRNA and protein levels of LCN2R were reduced significantly after KA injury, intense immunoreactivity for LCN2R was observed in OX-42 positive microglial cells in lesioned areas of KA-treated sections. Although OX-42 labels all types of microglia, LCN2R colocalised only with activated microglia characterised by its amoeboid morphology, which is different from its resting, ramified form. This is evident from the double immunofluorescence staining of LCN2R with OX-42 at 1 day post-KA injection samples: Only the CA3 hippocampal subfield was lesioned, as shown in the Nissl staining in Figure 2.8B *(Chapter 2)*. Hence, upregulation and colocalisation of OX-42 and LCN2R was observed in the lesioned area. In contrast, the CA1 hippocampal region was intact, hence LCN2R staining was localised at the pyramidal neurons and did not colocalise with the ramified microglia.

This resembles the neuronal expression of LCN2R at the neurons and ramified microglia in saline-injected controls. Expression of LCN2R and OX-42 increase steadily at the lesioned sites from 1 day to 3 days and peaked at 2 weeks post-KA injection. The morphological and expression changes of microglia observed in the present study corresponds with previous studies which shown upregulation of activated microglia at 1 day after icv KA injection, increasing in number gradually to peak at 1 month before declining (Jorgensen et al., 1993; Mitchell et al., 1993). Thus, it is possible that LCN2R expression may even be more highly upregulated in the activated microglia at 1 month post-KA injection.

The cellular localisation of LCN2R was further confirmed by examining the intersection between the lesioned CA1 region and the intact CA2 hippocampal regions of 2 weeks post-KA injection sections at high magnifications. LCN2R was expressed at the neurons in the intact CA2 region and at the activated microglia in the lesioned CA1 region, further confirming the decrease of LCN2R in neurons to the upregulation in activated microglia after KA injury. The punctate staining of LCN2R observed here is also congruent with localisation of LCN2R in a punctate distribution in LCN2R stable HEK cell lines (Bennett et al., 2011).

The expression of LCN2R in the neurons and microglia observed here is consistent with the previous studies reporting the expression of LCN2R in primary microglia, BV-2 microglial cells, primary cortical neurons and B35 neuroblastoma cells (Lee et al., 2007; 2011). Although, LCN2R was also expressed in murine primary astrocytes and C6 glioma cells (Lee et al., 2009), the same was not observed in the astrocytes *in vivo*. This discrepancy could be due to differences in species (in orthologues) or *in vitro* and *in vivo* differences. LCN2R neuronal staining also corresponded with the high LCN2R mRNA expression detected in primary neurons (Bennett et al., 2011).

It is noteworthy to point out that despite the pronounced increase of LCN2R immunoreactivity in the activated microglia after KA injury, especially at 2 weeks post-KA injection, the overall LCN2R mRNA and protein expression still decreased. This phenomenon indicates that LCN2R is highly expressed in the neurons and the decrease in expression could not be compensated by the further upregulation of LCN2R in the activated microglia. The abundant expression of LCN2R in the neurons suggests its involvement in physiological conditions.

Taken together, during KA-induced neurodegeneration, upregulation of LCN2 in the astrocytes may result in the secretion of LCN2 into the extracellular environment as LCN2 was reported to be secreted by primary astrocytes into the culture media (Lee et al., 2009). The released LCN2 could bind the receptors on the neighbouring effector cells, in this case, either the LCN2R expressing-activated microglia or -intact neurons. LCN2-induced apoptosis mediated by LCN2R had been reported in mouse primary microglia, cortical neurons, BV-2 microglial cells, B35 neuroblastoma and 24p3R-expressing HeLa cells (Devireddy et al., 2005; Lee et al., 2007; 2011). Could the same be observed *in vivo*? For the first time, the cellular localisation of both LCN2 and LCN2R were elucidated in the hippocampus. Nonetheless, the effect of the astrocytic expression of LCN2 on the LCN2R-expressing neurons and activated microglia are still unknown and will be examined in *Chapters 4 and 5*.

CHAPTER 4

EXPRESSION OF BIM

IN KA-LESIONED HIPPOCAMPUS

4.1. INTRODUCTION

In the previous chapters *(Chapter 2 and 3),* it was established that after KA-induced injury, LCN2R expression was decreased in the neurons, but upregulated in the activated microglia, at the lesioned site. This was accompanied by an upregulation of LCN2 in the astrocytes.

Recent studies have suggested LCN2 and LCN2R to have a role in apoptosis. Addition of LCN2/24p3 (murine orthologue of LCN2) was internalised by 24p3R-expressing cells, resulting in apoptosis (Devireddy et al., 2005). In most neurodegenerative diseases, and in the KA-induced neurodegeneration model, neuronal loss is often associated with apoptosis, together with other types of neuronal death, such as necrosis, and more recently autophagy (Jellinger, 2010; Pollard et al., 1994b; Przedborski et al., 2003).

Furthermore, the pro-apoptotic effect of 24p3/LCN2 was shown to be associated with Bim as Bim was increased with 24p3/LCN2 treatment in 24p2R-expressing HeLa cells, primary astrocytes, C6 glioma cells and B35 neuroblastoma (Devireddy et al., 2005; Lee et al., 2009; 2011). The pro-apoptotic effect of 24p3/LCN2 was abolished by stable knockdown of Bim. This confirms that LCN2's pro-apoptotic effect on cells was Bim-dependent. Nonetheless, the same was not observed in primary microglia and BV-2 microglial cells, indicating LCN2's apoptotic role may have other pathways (Lee et al., 2007). Although it appears that the Bim-dependent apoptotic effect of LCN2 may be dependent on cell type, it is still intriguing to investigate whether LCN2 and LCN2R have an effect on apoptosis in KA-induced neurodegeneration via Bim.

Bim is a pro-apoptotic member of the Bcl-2 homology domain 3 (BH3) subfamily of the Bcl-2 family. The Bcl-2 family consists of both anti- and pro-apoptotic

proteins, which share sequence homology with the conserved region known as the Bcl-2 homology (BH) domains (Danial, 2007; Youle and Strasser, 2008). The anti-apoptotic members are Bcl-2, Bcl-X_L and Bcl-w proteins, while the pro-apoptotic members are categorised into multidomain proteins, such as Bax and Bak; and the BH3-only proteins, including Bim, Bid and Puma (Danial, 2007). The members of BH3 subfamily are important initiators of the intrinsic (mitochondrial) pathway, by activating Bax/Bak either through direct or indirect binding to anti-apoptotic Bcl-2 members (Cheng et al., 2001; Wei et al., 2001). As it can bind all anti-apoptotic Bcl-2 members, Bim is known as one of the potent members in the BH-3 subfamily (O'Connor et al., 1998). Bim has three major isoforms generated by alternative splicing, namely the Bim_{EL} (extra-long), Bim_L (long) and Bim_S (short) (O'Connor et al., 1998). The Bim_{EL} form is detected in the rat brain and is most common in neurons (Shibata et al., 2002; Whitfield et al., 2001), unlike Bim_L and Bim_S, which are detected in rat C6 glioma cells but not in rat brain (Shinoda et al., 2004). Bim is usually sequestered to the microtubule-associated dynein motor complex and when released, it associates with 14-3-3 to be translocated to the mitochondria to promote activation of Bax/Bak-dependent apoptosis via neutralisation of anti-apoptotic proteins (Puthalakath et al., 1999; Shinoda et al., 2004).

Furthermore, Bim has been demonstrated to promote neurodegeneration in various experimental paradigms. Upregulation of Bim was observed in hippocampal injury in seizure models induced by intra-amygdala KA injection (Murphy et al., 2010; Shinoda et al., 2004). Bim was also reported to be induced in growth factor (NGF) withdrawal-induced apoptosis in sympathetic neurons (Putcha et al., 2001). In trophic factor deprivation (TFD), c-Jun N-terminal kinases (JNKs) caused induction and phosphorylation of Bim to induce a Bim-dependent cell death (Putcha et al., 2003).

In KA-induced excitotoxicity, triggers from the intrinsic pathway were evident, such as the release of cytochrome-c and disruption of mitochondrial membrane potential (Wang et al., 2005). Therefore, together with the previous studies on the pro-apoptotic effect of Bim in various neurodegeneration models, LCN2 and LCN2R may have an effect on apoptosis in KA-induced neurodegeneration via Bim, a pro-apoptotic protein in the intrinsic pathway. This chapter will examine Bim expression changes and especially its cellular localisation after KA injury to determine if it has any association with LCN2R-expressing microglia and neuronal cells.

4.2. MATERIALS AND METHODS

4.2.1. Animals and kainate (KA) injections

Male Wistar rats weighing approximately 200 g each were anaesthetised with intraperitoneal injection of ketamine (75 mg/kg) and xylazine (10 mg/kg). KA (1.2 µl of 1 mg/ml) was stereotaxically injected into the right lateral ventricle (coordinates: 1.0 mm caudal to bregma, 1.5 mm lateral to the midline, 4.5 mm from the surface of the cortex) using a microlitre syringe (5 µl Hamilton syringe, Model no.: 88000, 24 gauge needle, outer diameter of needle: 0.57 mm, inner diameter of needle: 0.31 mm). Experimental control rats were injected with 1.2 µl of normal saline instead of KA. All procedures involving animals were approved by the Institutional Animal Care and Use Committee, NUS

4.2.2. Real-time RT-PCR

A total of 24 animals were used, four KA-injected animals versus four saline-injected control animals were sacrificed at 1 day, 3 days and 2 weeks after injection. Tissues were freshly dissected from the brain and immersed into RNAlater (Ambicon, CA, USA), flash frozen and kept at -80°C until analysis. Total RNA was isolated using TRIzol reagent (Invitrogen, CA, USA) according to the manufacturer's protocol, and RNeasy Mini Kit (Qiagen Inc., CA, USA) was used to purify the RNA. The samples were reverse transcribed using High-Capacity cDNA Reverse Transcription Kits (Applied Biosystems, CA, USA). The reaction conditions were 25°C for 10 min, 37°C for 120 min and 85°C for 5 min. Real-time PCR amplification was carried out using the 7500 Real-time PCR system (Applied Biosystems, CA, USA) with Taq-Man Universal PCR Master Mix (Applied Biosystems, CA, USA) and gene-specific primers and probes according to manufacturer's protocols (Assay ID: Bim

(Rn00674175_m1)). β-actin (Part no: 4352340E) was used as an internal control. All primers and probes were synthesised by Applied Biosystems. The PCR conditions were: an initial incubation of 50°C for 2 min and 95°C for 10 min followed by 40 cycles of 95°C for 15 s and 60°C for 1 min. All reactions were carried out in triplicates. The threshold cycle, CT, which correlates inversely with the levels of target mRNA, was measured as the number of cycles at which the reporter fluorescence emission exceeds the preset threshold level. The amplified transcripts were quantified using the comparative CT method (Livak and Schmittgen, 2001), with the formula for relative fold change = $2^{-\Delta\Delta CT}$. The mean was calculated, and possible significant differences were analysed using Student's t-test. $p < 0.05$ was considered significant.

4.2.3. Western blotting

Three KA-injected rats and three saline-injected control animals were sacrificed at 1 day, 3 days and 2 weeks after injection. The rats were anaesthetised by intraperitoneal injection of ketamine and xylazine and decapitated. The right hippocampi were quickly removed and homogenised in cold lysis buffer containing Tris–HCl, pH 7.4, 10 mM EDTA, 150 mM NaCl, 0.5% Triton X-100 with protease inhibitor cocktail (Roche Diagnostics, Indianapolis, IN, USA) and placed on the shaker for 1 hr at 4°C. After centrifugation at 12,000g for 30 min, the supernatant was collected, and protein concentration was determined using the BCA protein assay kit (Pierce Biotechnology, Rockford, IL, USA). Prior to gel electrophoresis, the protein lysates were denatured by heating the sample in the presence of SDS and DTT for 10 min at 95-100°C.

Total protein (60 µg) was resolved in 12% SDS-polyacrylamide gel under reducing conditions and electro-transferred to a nitrocellulose membrane (Biorad, CA, USA). Non-specific binding sites on the membrane were blocked by incubation with 5% non-fat milk for 1 hr. The membrane was then incubated overnight with monoclonal rabbit goat anti-Bim antibody at 1:1000 (Cell Signaling Technology, MA, USA). Specificity of the Bim antibody was verified by pre-incubating 230 ng/ml (10x) and 460 ng/ml (20x) of recombinant Bim peptide (Cell Signaling Technology, MA, USA) with 23 ng/ml Bim antibody overnight. After washing with 0.1% Tween-20 in TBS, the membrane was incubated with horseradish peroxidase-conjugated goat anti-rabbit immunoglobulin IgG (1:10,000; Thermo Fisher Scientific, Rockford, IL, USA) for 1 hr at room temperature. The protein was visualised with SuperSignal West Pico chemiluminescent substrate (Thermo Fisher Scientific, Rockford, IL, USA) according to the manufacturer's instructions. Blots were treated with stripping buffer (Restore Western Blot Stripping Buffer, Thermo Fisher Scientific, Rockford, IL, USA) at room temperature for 10 min before reprobing of membrane with antibody to β-actin (Sigma, St. Louis, MO, USA). Exposed films were scanned with at least 300 dpi and the mean optical density of the protein bands of LCN2R was analysed by densitometry using ImageJ (NIH, Maryland, USA), and normalised to β-actin. The mean was calculated, and possible significant differences were analysed using Student's t-test. $p < 0.05$ was considered significant.

4.2.4. Double immunofluorescence labelling

A total of 24 animals were used, four KA-injected animals versus four saline-injected control animals were sacrificed at 1 day, 3 days and 2 weeks after injection to study the effect of KA lesions. The rats were anaesthetised by intraperitoneal injection of anaesthetic comprising ketamine and xylazine and transcardially perfused

with Ringer solution, followed by 4% paraformaldehyde in 0.1M phosphate buffer (pH 7.4). The brains were dissected out, and blocks containing the hippocampus were sectioned coronally at 20 µm using a freezing microtome. Sections were soaked in phosphate buffered saline (PBS) for 30 min to remove traces of sucrose and permeabilised with PBS-0.3% Triton X-100 for 10 min. Antigen retrieval was performed by incubating the sections in 1% sodium dodecyl sulfate (SDS) for 5 min, followed by PBS washes. They were then blocked with 5% goat serum in PBS-0.3% Triton X-100 for 1 hr, followed by incubation with rabbit monoclonal antibody to Bim at 1:100 (Cell Signaling Technology, MA, USA) and/or mouse monoclonal antibody to OX-42 (1:200, Chemicon, Temecula, CA, USA) or mouse monoclonal antibody to NeuN (1:200, Millipore, MA, USA) overnight at 4°C. Specificity of the Bim antibody was verified by pre-incubating 2.3 µg/ml (10x) of recombinant Bim peptide (Cell Signaling Technology, MA, USA) with 0.23 µg/ml Bim antibody overnight. The sections were washed in PBS, and incubated for 1 hr at room temperature in 1:200 dilution of goat anti-rabbit IgG (H+L) Alexa Fluor 555 and/or goat anti-mouse IgG (H+L) Alexa Fluor 488 (Invitrogen, CA, USA). The sections were then washed and mounted with ProLong® Gold antifade reagent with DAPI (Invitrogen, Carlsbad, CA, USA) and captured using a fluorescence microscope (Olympus BX51; Olympus Corporation, Tokyo, Japan) and a laser scanning confocal microscope (LSM 510, Carl Zeiss Göttingen, Germany). Colocalisation was established by analysing the overlap between the different labels by orthogonal reconstruction throughout the entire *z*-stack (LSM 510, Carl Zeiss Göttingen, Germany).

4.2.5. *In situ* cell death detection (TUNEL assay)

TUNEL assay was performed on tissues from 1 day, 3 days and 2 weeks post-kainate treated animals in accordance with the manufacturer's instructions for the *in situ* cell death detection kit, Fluorescein (Roche, Mannheim, Germany).

Colocalisation of Bim and TUNEL assay was done by performing immunofluorescence staining of Bim before performing TUNEL assay. Sections were incubated with rabbit anti-Bim monoclonal antibody overnight at 4°C, then incubated for 1 hr at room temperature in 1:200 dilution of goat anti-rabbit IgG (H+L) Alexa Fluor 555 (Invitrogen, CA, USA). After PBS-0.1% Triton-X washes, sections were incubated with Proteinase K (10 µg/ml in 10 mM Tris/HCl, pH 7.4) at 37°C for 30 min. Sections were washed twice with PBS. For positive controls, DNAse I recombinant was added at (30U/ml) at 37°C for 30 min to induce DNA strand breaks. Sections were then incubated with TUNEL reaction mixture with 40 µl/section, at 37°C for 1 hr. Negative controls were incubated with label solution without the enzyme solution. The sections were then washed and mounted with ProLong® Gold antifade reagent with DAPI (Invitrogen, Carlsbad, CA, USA) and captured using a fluorescence microscope (Olympus BX51; Olympus Corporation, Tokyo, Japan). Colocalisation was established using a laser scanning confocal microscope (LSM 510, Carl Zeiss Göttingen, Germany) to analyse the overlap between the different labels by orthogonal reconstruction throughout the entire *z*-stack (LSM 510, Carl Zeiss Göttingen, Germany).

4.3. RESULTS

4.3.1. mRNA expression of Bim in kainate-lesioned hippocampus

At 1 day post-KA injection, real-time RT-PCR showed that there is no significant difference between KA- and saline-injected hippocampus in Bim mRNA expression. In contrast, Bim mRNA expression was 1.4- ($p < 0.01$) and 2.1- ($p < 0.01$) fold in the right hippocampus at 3 days and 2 weeks post-KA injury relative to their saline-injected controls, respectively (Fig. 4.1).

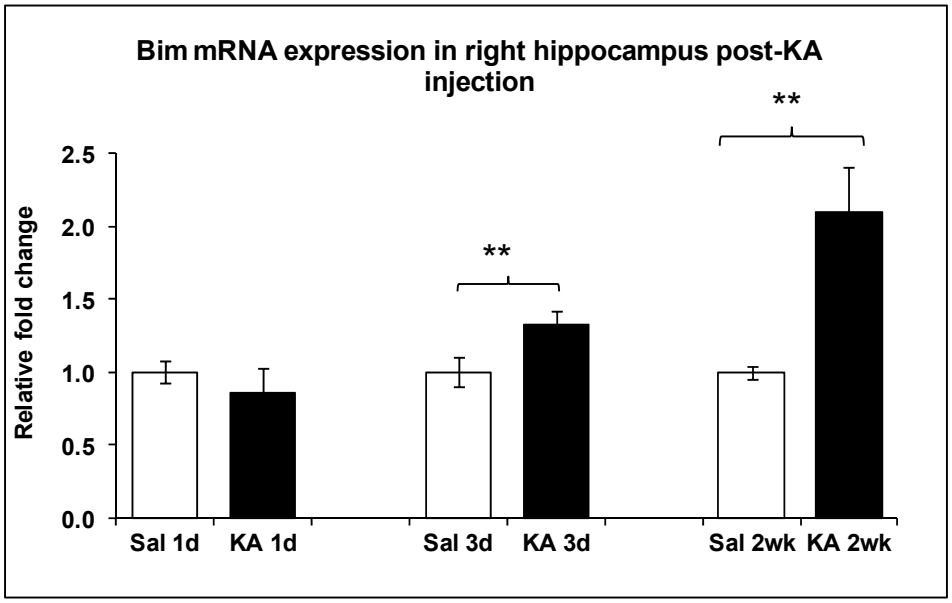

Fig. 4.1. Bim mRNA expression upregulated after KA injury. Real-time RT-PCR analysis of Bim mRNA expression at the right hippocampi at 1 day, 3 days and 2 weeks post-KA injection, relative to their saline-injected controls. Bim mRNA levels increased significantly at 3 days and 2 weeks post-KA injection. Analysed by Student's t-test, asterisks indicate significant difference (*$p < 0.05$, **$p < 0.01$, ***$p < 0.001$). Data are expressed as mean ± SEM, $n = 4$ per treatment group.

4.3.2. Protein expression of Bim in kainate-lesioned hippocampus

To validate the mRNA changes in Bim expression, western blot analysis was performed with hippocampal lysate from the right side of the brain, i.e. site of icv injection. At 1 day post-KA injection, there is no obvious difference in intensity of the bands between treated and saline-injected animals (Fig. 4.2A). At 3 days post-KA injection, denser bands at 23kDa were observed for KA-treated samples relative to the saline-injected controls (Fig. 4.2B). The increase in band intensity was even more pronounced in 2 weeks post-KA injection hippocampi (Fig. 4.2C). Densitometric analysis revealed no significant differences between 1 day post-KA and saline injection samples. In contrast, significant increases in Bim protein levels were detected at 3 days and 2 weeks post-KA injection with 2.5- ($p < 0.01$) and 5.0- ($p < 0.01$) fold in KA-treated samples relative to the saline controls, respectively (Fig. 4.2E).

This upregulation of Bim protein levels validates the increase in mRNA levels from real-time RT-PCR results. Control experiments performed by incubating blots with 10x and 20x antigen-absorbed Bim antibody showed absence of bands for 2 weeks post-KA injection hippocampal lysates, indicating specificity of the Bim antibody (Fig. 4.2D).

4.3.3. Regional expression of Bim in kainate-lesioned hippocampus

Since Bim mRNA and protein expression were greatly expressed at 2 weeks post-KA injection, sections from this timepoint were used to perform the control experiments. Upregulation of Bim was detected at the subiculum (Fig. 4.3A), CA1 (Fig. 4.3C) and CA3 (Fig. 4.3E) lesioned areas of the right hippocampus. Sections incubated with pre-incubated Bim antibody with 10x excess blocking peptide (2.3 µg/ml) showed an absence of staining at the subiculum (Fig. 4.3B), CA1 (Fig. 4.3D),

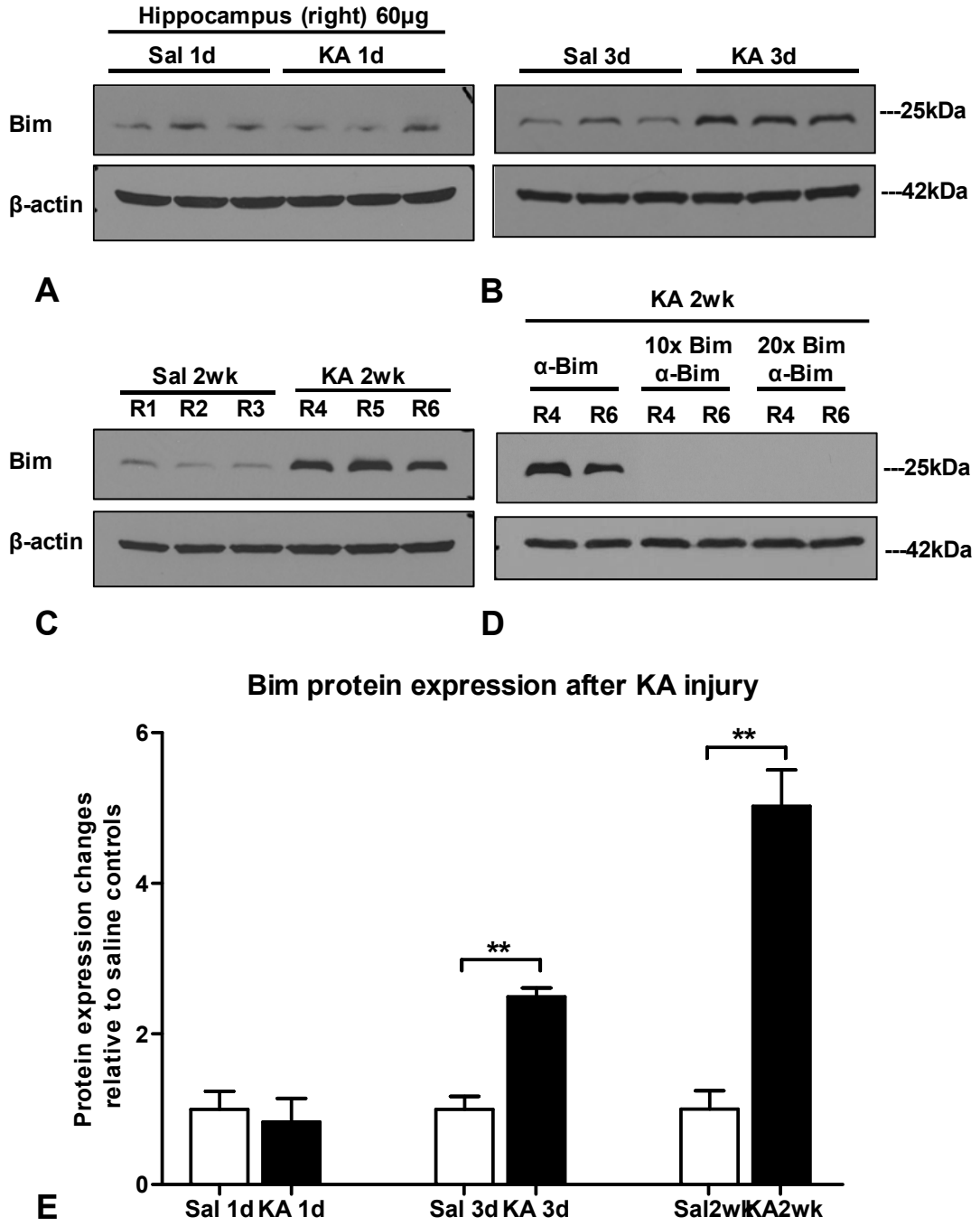

Fig. 4.2. Bim protein expression changes after KA injury. Western blot analysis of Bim protein expression in the right hippocampi at (A) 1 day, (B) 3 days and (C) 2 weeks post-KA vs. -saline icv injection. (D) 2 weeks post-KA treated hippocampi lysates, R4 and R6 were used for three sets of incubation conditions for the blocking experiments. Lane 1 and 2 from the left: Incubated with 23 ng/ml of Bim antibody. Lane 3 and 4: Incubated with Bim antibody pre-absorbed with 230 ng/ml of blocking peptide. Lane 5 and 6: Incubated with Bim antibody pre-absorbed with 460 ng/ml of blocking peptide. (E) Densitometric analysis of Bim protein expression in (A-C) 1 day, 3 days and 2 weeks post-KA vs. saline-injected controls. Values are normalised with the saline-injected controls at the respective timepoints. Analysed by Student's t-test, asterisks indicate significant difference (*$p < 0.05$, **$p < 0.01$, ***$p < 0.001$). Data are expressed as mean ± SEM, $n = 3$ per treatment group.

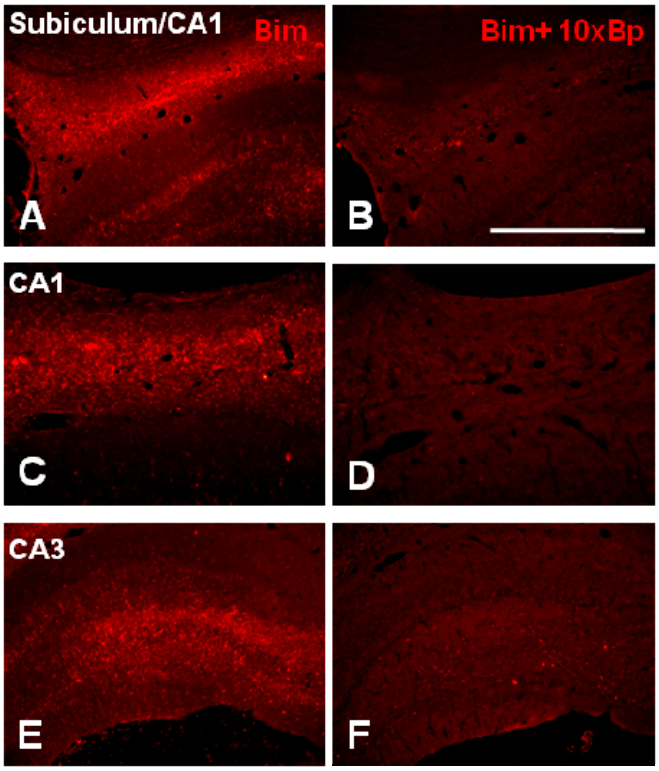

Fig. 4.3. Regional expression of Bim in 2 weeks post-KA injection lesioned hippocampus. Immunoreactivity of Bim (red) was upregulated at (A) subiculum/CA1, (C) CA1 and (E) CA3 regions of the right hippocampus. (B, D and F) Sections incubated with pre-absorbed Bim antibody with 10x excess blocking peptide showed absence of positive Bim staining. Scale=500 μm.

and the CA3 (Fig. 4.3F) hippocampal regions. This indicates the specificity of the Bim antibody. Immunoreactivity of Bim in the lesioned area suggests that the upregulated Bim could be localised in glial cells since gliosis are usually observed in the lesioned areas where neurons are damaged. Next, double immunofluorescence was performed to identify the localisation of Bim.

4.3.4. Cellular expression of Bim in kainate-lesioned hippocampus

Double immunofluorescence was carried out to identify the cellular localisation of Bim after KA injury. Negligible Bim staining was observed in all the saline-injected controls, as represented by 2 weeks post-saline injection

hippocampus (Fig. 4.4A). In contrast, 1 day (Fig. 4.4B), 3 days (Fig. 4.4C) and 2 weeks (Fig. 4.4D) post-KA injection hippocampal sections had increased Bim immunoreactivity and colocalisation of Bim and OX-42, a marker for microglia. After KA injury, OX-42 positive cells had an amoeboid morphology unlike the ramified cells observed in saline controls, indicating activation of microglia (as described in *Chapter 3, Results, Section 3.3.2.3*). The 2 weeks post-KA injection sections had the greatest upregulation of Bim and OX-42 positive cells in the lesioned hippocampal regions. Orthogonal projections through CA1 lesioned region at a higher magnification demonstrate that Bim was present in the OX-42-positive activated microglia (Fig. 4.4E).

Only in 1 day post-KA injection sections, upregulation of Bim was also observed in neuronal-like cells in addition to the OX-42 immunopositive cells. Hence, double immunofluorescence of Bim and NeuN (marker for neurons) was performed. In 1 day post-saline injection controls, no Bim was detected (Fig. 4.5A-C), but it was upregulated in NeuN positive cells in KA-treated sections in the CA1 (Fig. 4.5D-F) and CA3 (Fig. 4.5G-I) hippocampal regions. Orthogonal projections through the CA1 lesioned region at higher magnification demonstrate that upregulated Bim was localised in the NeuN positive pyramidal neurons at the CA1 and CA3 hippocampal regions of 1 day post-KA injection hippocampal sections (Fig. 4.5J).

Therefore upregulated Bim was detected in the activated microglia of the CA1 and CA3 hippocampal lesioned areas at all timepoints after KA injury; and detected in the pyramidal neurons in 1 day post-KA injection samples only.

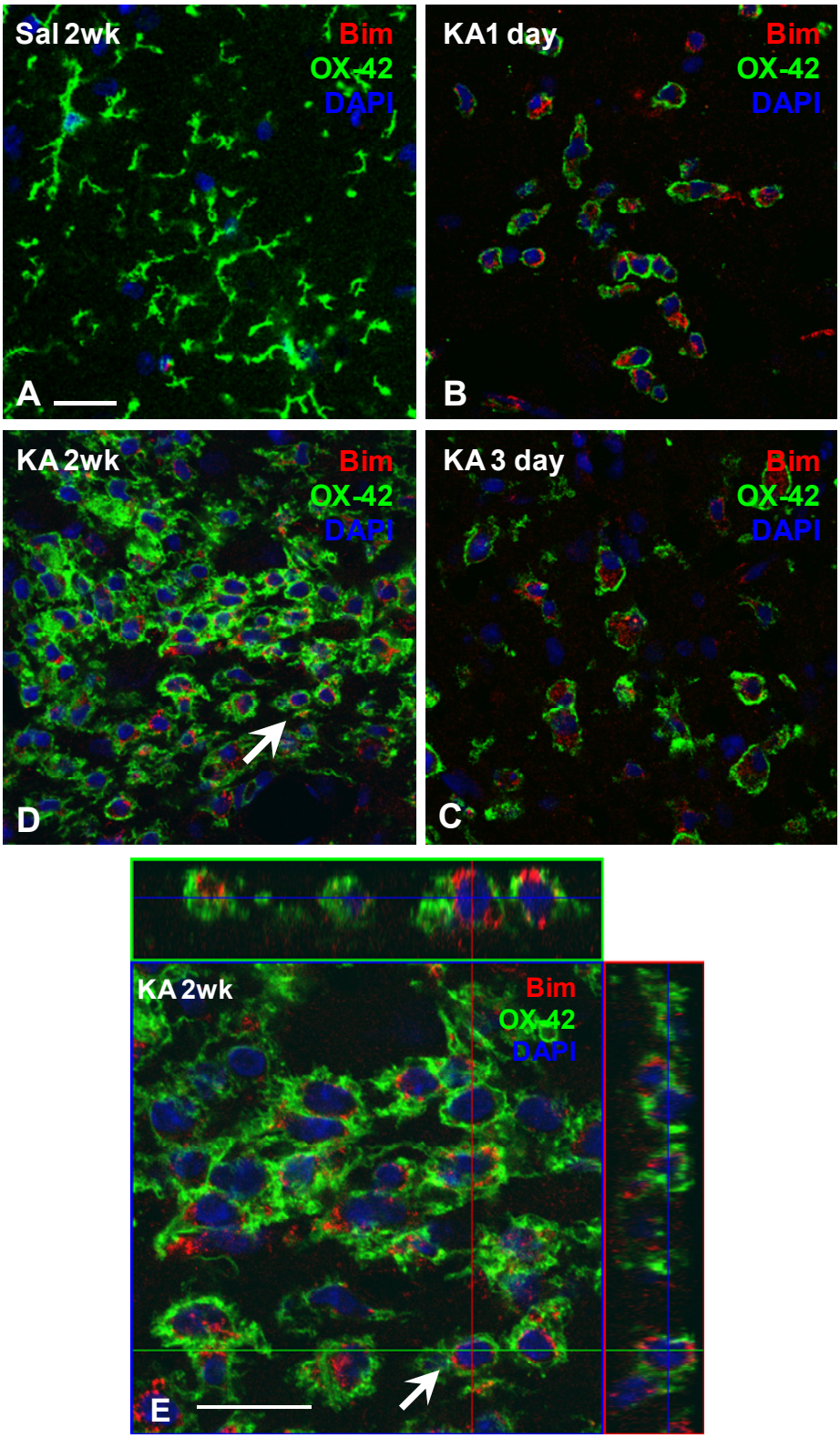

Fig. 4.4. Confocal micrographs of upregulation of Bim in activated microglia after KA injury. (A) In 2 weeks post-saline injection controls, negligible Bim staining was observed. At (B) 1 day, (C) 3 days and (D) 2 weeks post-KA injection, upregulated Bim (red) colocalised with OX-42 (green). (E) Orthogonal projections through CA1 lesioned region at higher magnification demonstrate that Bim was upregulated in the OX-42-positive cells. Confocal micrographs were taken from CA1 region of the right hippocampus. Scale=20 μm.

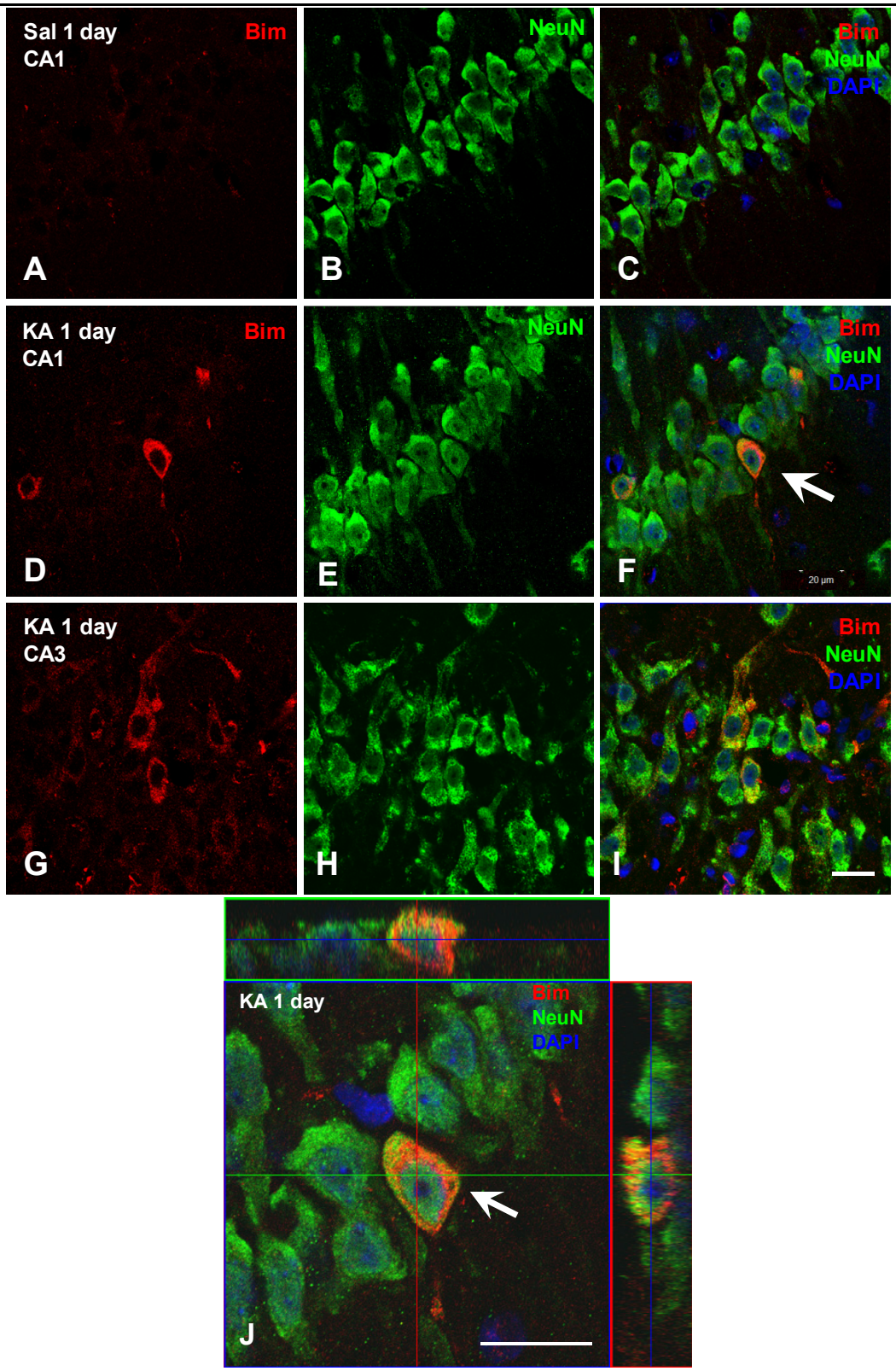

Fig. 4.5. Confocal micrographs of upregulation of Bim in neurons at 1 day post-KA injury. Hippocampal sections were incubated with anti-Bim (red) and anti-NeuN (green) antibody. (A-C) No Bim staining detected in the CA1 region of a 1 day post-saline injection sample. In KA-treated sections, Bim staining colocalised with NeuN in (D-F) CA1 and (G-I) CA3 regions of the hippocampus. (J) Orthogonal projections through CA1 lesioned region at higher magnification demonstrate that Bim is present in the NeuN-positive cells. Scale=20 µm.

4.3.5. Apoptotic condition in hippocampus after KA injury

Since Bim is a pro-apoptotic protein, TUNEL assay was performed to determine if the upregulation of Bim in the activated microglia and neurons would lead to apoptosis. There was an absence of TUNEL positive cells at 2 weeks post-KA injection (Fig. 4.6E and F). In 3 days post-KA injection samples, some TUNEL staining was observed at the pyramidal neurons in the CA1 and CA3 regions (Fig. 4.6C and D) and was more pronounced in 1 day post-KA injection samples (Fig. 4.6A and B). Orthogonal projections through CA1 lesioned region in 1 day post-KA injected samples demonstrate that TUNEL positive cells were Bim positive, indicating that the Bim positive cells were apoptotic (Fig. 4.7A-C).

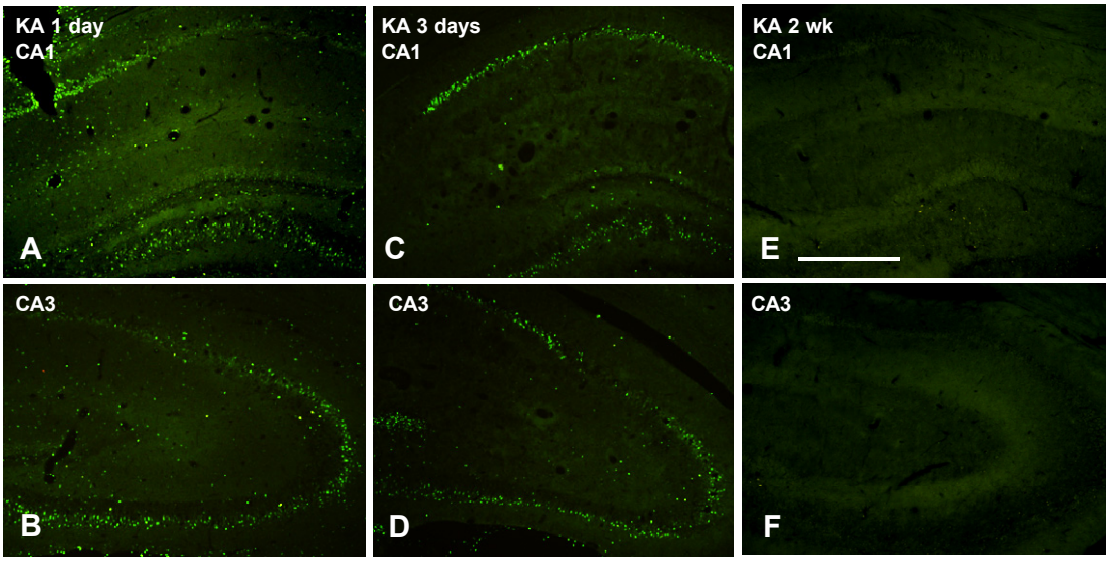

Fig. 4.6. Fluorescent micrographs of TUNEL assay of the lesioned hippocampus after KA injury. *In situ* cell death detection kit was applied to right hippocampal sections to indicate the apoptotic status. Positive TUNEL staining (green) is an indication of apoptosis. CA1 and CA3 regions in (A, B) 1 day post-KA injection, (C, D) 3 day post-KA injection and (E, F) 2 weeks post-KA injection sections. 1 day and 3 days post-KA injection sections have TUNEL positive cells, while 2 weeks post-KA injection sections have no TUNEL staining. Scale=500 μm.

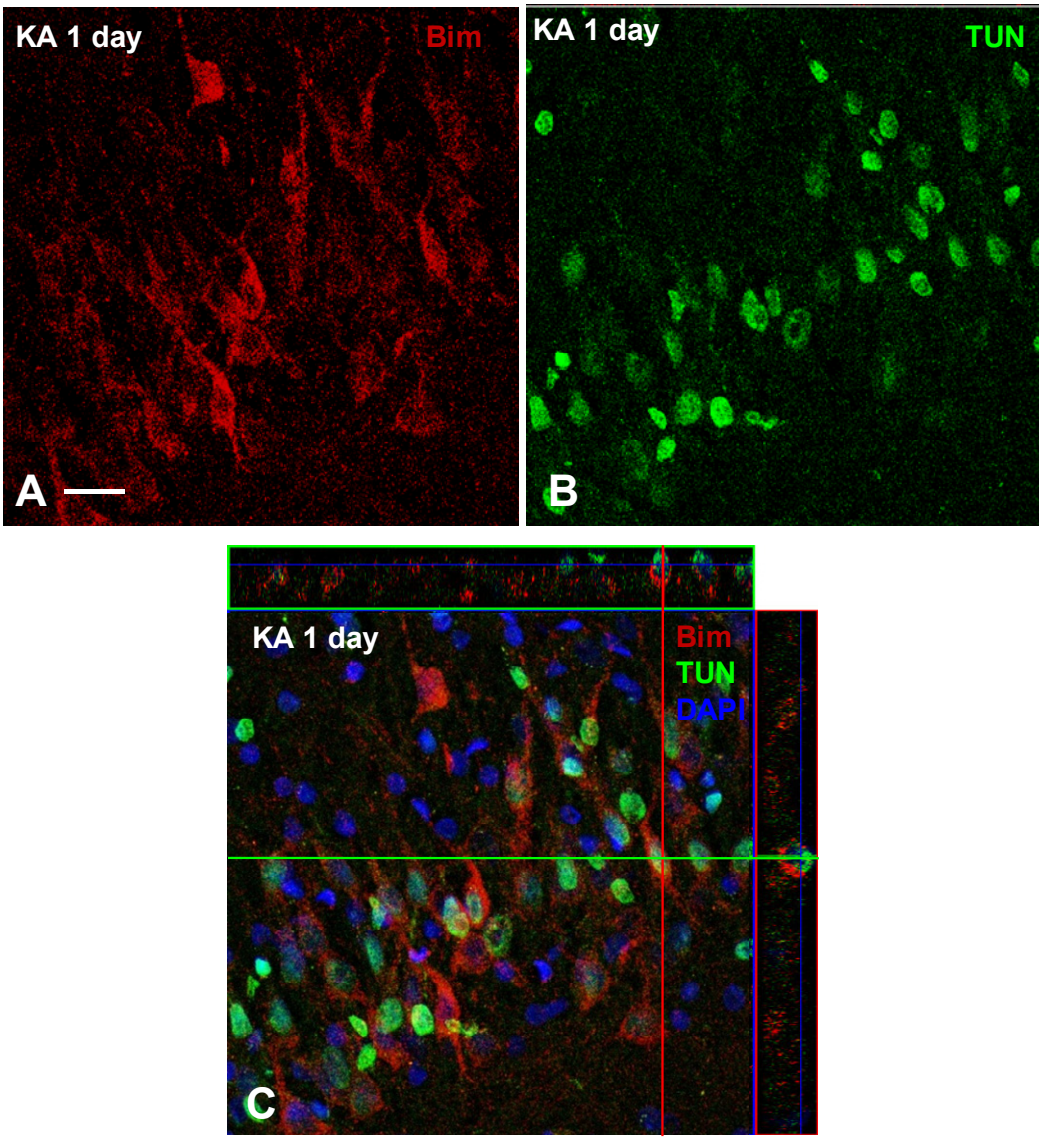

Fig. 4.7. Confocal micrograph of colocalisation of Bim with TUNEL staining in 1 day post-KA injection sections. 1 day post-KA injection hippocampal sections were stained with (B) TUNEL assay (green) and double-labelled with (A) anti-Bim antibody (red). (C) Orthogonal projections through CA3 lesioned region demonstrate that Bim was present in the TUNEL-positive cells. Scale=20 μm.

4.4. DISCUSSION

The present study was carried out to examine the expression and cellular localisation of Bim after KA injury. In this chapter, an association was made between Bim and the LCN2R-expressing cells, which is in line with this thesis's hypothesis that LCN2 and LCN2R may have an effect on Bim-mediated apoptosis in KA-induced neurodegeneration.

Although Bim has three major isoforms generated by alternative splicing, namely Bim_{EL} (extra-long), Bim_{L} (long) and Bim_{S} (short) (O'Connor et al., 1998), only Bim_{EL} can be detected in the rat hippocampus, while the other two were absent, consistent with the single band at 23kDa detected in the present study, similar to the observations made by Shinoda and colleagues (2004). Significant upregulation of mRNA and protein levels of Bim were detected at 3 days and 2 weeks post-KA injury, while no obvious change was detected at 1 day post-KA injury. Another study on icv KA injection in rats showed downregulation of Bim immunopositive cells at 6, 12 hours, and the highest at 24 hours, which coincide with the greatest increase in Fluoro-Jade-stained cells (indicator of neurodegeneration) (Korhonen et al., 2003). The reduction of Bim expression before 24 hours could be attributed to neuronal loss as Bim was detected in hippocampal neurons (O'Reilly et al., 2000).

In saline-injected control sections, low levels of expression of Bim were observed, consistent with reports of low Bim expression in normal physiological conditions (Murphy et al., 2010; O'Reilly et al., 2000). In contrast, upregulation of Bim was observed in all KA-treated sections, with intense immunoreactivity at 2 weeks post-KA injection when there was a 5.0 times increase in protein expression. Proteins upregulated at later timepoints after KA injury were often associated with gliosis (Zagulska-Szymczak et al., 2001) and indeed Bim was upregulated in activated microglia, characterised by their amoeboid morphology, in the lesioned areas of the

hippocampus at all timepoints after KA injury. In addition, at 1 day post-KA injection, other than in the activated microglia, upregulated Bim was also observed in the NeuN immunopositive neurons. Taken together, increased Bim expression was observed in the activated microglia and neurons. Interestingly, the cellular localisation of Bim coincided with the LCN2R-expressing cells, i.e. the activated microglia and neurons. Since the elevation of Bim expression was observed in the LCN2R-expressing cells, upregulation of Bim could be a downstream effect of the interaction between LCN2 and LCN2R.

To examine if the upregulated Bim had any apoptotic effect on the expressing cells, TUNEL assay was performed. Negative TUNEL staining was observed at 2 weeks post-KA injection. Despite having the highest Bim mRNA and protein expression, the Bim expressing-activated microglia were not apoptotic. The upregulation of Bim in activated microglia might be a pro-apoptotic signal to clear the microglia as a self-regulatory mechanism in the inflammatory site after KA injury. Bim's gradual increase in expression from 1 day to 2 weeks post-KA injection indicates that it may increase further at later timepoints. Therefore, at 2 weeks post-KA injection, it might be too early to detect clearing or apoptosis of activated microglia as they have been shown to peak in numbers at one month post-KA injection before declining (Jorgensen et al., 1993; Mitchell et al., 1993). Alternatively, Bim may have other unknown functions in the activated microglia other than mediating apoptosis in the intrinsic pathway.

In contrast, the TUNEL positive cells observed at 1 day and 3 days post-KA injection outlined the pyramidal neurons from CA1 to CA3 region, indicating the apoptotic cells were likely to be neuronal cells. Many studies have shown great increases in the number of Fluoro-Jade positive cells and TUNEL positive cells among the pyramidal neurons 1 day post-KA administration (Korhonen et al., 2003;

Shinoda et al., 2004) and detection of activated caspase 3 in the CA1 lesioned hippocampus 12 hours after excitotoxic injury in mice, which later peaked at 24 hours (Theofilas et al., 2009). This evidence further supports the present TUNEL positive staining at 1 day post-KA injection, indicating apoptosis was present. Furthermore, the majority of these apoptotic cells were Bim immunopositive, indicating that Bim-expressing neurons were apoptotic. Upregulation of neuronal Bim was only detected at 1 day, but not 3 days or 2 weeks post-KA injection possibly because the Bim-expressing neurons would have undergone apoptosis and could not be detected at later timepoints. Although LCN2R was expressed in both activated microglia and neurons, upregulation of Bim may have differential effects on them; Bim-expressing neurons were apoptotic, but not Bim-expressing activated microglia.

It is interesting to note that although upregulation of Bim was observed in the activated microglia and neurons at 1 day post-KA injection, the upregulation was not reflected in the mRNA and protein expression, i.e. there was no significant difference between KA-treated and saline controls. As mentioned in previous studies, Bim could be downregulated due to neuronal damage, but its significance could have been negated by the increase in expression in the activated microglia and surviving neurons.

In the present study, the increase in Bim mRNA and protein expression observed after KA injury is consistent with upregulation of Bim after intra-amygdala KA injection and KA treatment on hippocampal cultures (Murphy et al., 2010; Shinoda et al., 2004). However, no difference was detected between Bim-deficient and wild-type control mice after intrahippocampal KA injection (Theofilas et al., 2009), which contradicted with another group that showed decreased hippocampal cell death from Fluoro-Jade staining of Bim-deficient mice compared to the wild-type controls (Murphy et al., 2010). Furthermore, Bim knockdown protected mouse

organotypic hippocampal cultures after KA-induced cell death (Murphy et al., 2010). Since neurodegeneration was still observed in the Bim-deficient mice despite lacking Bim expression, this indicates that other BH3-only proteins could compensate for Bim's absence or the involvement of other mechanisms in contributing to the intrinsic and/or extrinsic pathway, leading to apoptosis.

In this chapter, through the expression and localisation of Bim, LCN2R and Bim were found to be upregulated in the same cell types. Also, the LCN2R-expressing neurons with upregulated Bim were found to be apoptotic. It is tempting to conclude that, at 1 day post-KA injection, LCN2 released by the astrocytes could interact with the LCN2R-expressing neurons to upregulate Bim, to trigger apoptosis. Unfortunately, such a conclusion would be premature as it is unclear if the upregulation of Bim is a downstream effect of LCN2 and LCN2R's interaction. The increase in Bim could be due to other pro-apoptotic triggers downstream of KA-induced excitotoxicity. Therefore, it is important to investigate the effect of LCN2 on Bim-dependent apoptosis, mediated by the receptor LCN2R, which will be examined in the following chapter, *Chapter 5*.

CHAPTER 5

EXPRESSION OF LCN2 AND LCN2R

IN PRIMARY HIPPOCAMPAL NEURONS

5.1. INTRODUCTION

In the previous chapters we have seen that Bim was significantly upregulated at 3 days and 2 weeks post-KA injection, and coincidentally was localised in the LCN2R-expressing neurons and activated microglia. Also, the LCN2R-expressing neurons with upregulated Bim were found to be apoptotic. Yet it is unclear if the apoptosis and upregulation of Bim in the neurons was a consequence of LCN2 and LCN2R's interaction. Therefore, this chapter aims to examine if LCN2 and LCN2R interact at the hippocampal neurons, and if they do, then to examine their localisation. The pertinent question of whether LCN2 has a direct role in upregulating Bim expression to trigger apoptosis in the neurons (Bim-dependent apoptosis) will also be addressed in this chapter.

Besides mediating apoptosis, LCN2 is well-known as an iron-trafficking protein. Other than its role in sequestering iron-bacterial siderophore complexes to limit iron availability to the pathogen, LCN2 could bind iron and deliver it into the mammalian cells via endocytosis (Mori et al., 2005; Yang et al., 2002b). NGAL (human orthologue of LCN2):enterochelin can capture ^{55}Fe and deliver it to the mouse kidney's proximal tubule *in vivo*, whereas without NGAL, ^{55}Fe was detected at the liver instead (Schmidt-Ott et al., 2006). Furthermore, the import of iron into the cells could regulate iron-responsive genes, such as the upregulation of ferritin and downregulation of transferrin receptor 1 (Devireddy et al., 2005; Yang et al., 2002b) and decreased levels of iron-regulatory protein IRP2 and conversion of IRP1 to cytosolic aconitase (Devireddy et al., 2010).

Recently, a link was established between apoptosis and intracellular iron levels: Iron-loaded LCN2 (holo-LCN2) could import iron into the cell, increasing intracellular iron and thus inhibiting apoptosis. Iron-free LCN2 (apo-LCN2) could cause iron export via binding with intracellular endogenous mammalian

siderophore(s) complexed with intracellular iron (Richardson, 2005). The decrease in intracellular iron activates Bim, the pro-apoptotic protein, to stimulate apoptosis (Devireddy et al., 2005). Therefore, the iron status of LCN2 affects the intracellular iron level, which in turn determines the apoptotic status of the cell, i.e. the iron status of LCN2 accounts for the distinct biological effects on the cell. For instance, holo-NGAL was more effective than apo-NGAL in inducing epithelial characteristics in 4T1-Ras-transformed mesenchymal tumour cells (Hanai et al., 2005); and holo-NGAL upregulated the expression of the iron-dependent reporter construct, but inhibited the iron-repressed genes while apo-NGAL resulted in an opposite effect (Li et al., 2004).

Furthermore, LCN2-induced cell death sensitisation in B35 neuroblastoma, C6 glioma and BV-2 microglial cells was abolished upon the addition of the siderophore:iron complex (Lee et al., 2007; 2009; 2011). The siderophore:iron complex can associate with apo-LCN2 to form holo-LCN2 to import iron into the cells. Thus, by increasing intracellular iron levels, holo-LCN2 inhibits apoptosis. This indicates that the pro-apoptotic effect of LCN2 could be affected by the iron status of LCN2, which is consistent with the mechanism proposed by Green, Devireddy and colleagues (2005). Therefore, the effect of LCN2:Fe:siderophore (holo-LCN2) should be studied in comparison with LCN2 (apo-LCN2) to detect if they exert different or opposite effects on the cells as suggested by many studies.

Due to the possible interactions that can occur among different cell types, to isolate the effect of LCN2 on neurons among all the other cell types, primary hippocampal neurons were cultured. This chapter aims to investigate the effect of iron on Bim-dependent apoptosis on the neurons by comparing apo-LCN2 and holo-LCN2 conditions.

5.2. MATERIALS AND METHODS

5.2.1. Primary hippocampal neuronal culture

Primary neuronal cultures were obtained from hippocampi of newborn Wistar pups, by procedures approved by the Institutional Animal Care and Use Committee, NUS. Each set of primary hippocampal neuron isolation consisted of 6 hippocampi from 3 newborn pups. In all, 3 sets of cells were obtained from 9 newborn pups, *n*= 3. Brains were removed and placed in Dissection Medium (Hank's balanced salts solution (HBSS, 0.01 M HEPES/NaOH). The hippocampi were dissected, cut into halves, and digested with papain in HBSS (1.5 mM $CaCl_2$, 0.2 ug/ul of L-cysteine, 0.5 mM EDTA, 20 units/ml DNase I, 15 units/ml papain) at 37°C for 30 min followed by mechanical trituration using a 1 ml pipette tip. Tubes were then clapped twice between hands to provide additional mechanical force for cell dissociation. Dissociated cells were harvested by centrifugation and resuspended in Neurobasal-A medium (supplemented with B27, 2 mM GlutaMAX-1 and 1% penicillin-streptomycin) for plating.

Cells were seeded at 20,000 cells/coverslip in 24-well plates for Duolink assays; 160,000 cells/well in 12-well plates for RNA extraction for real-time RT-PCR analysis; 28,750 cells/well in 96-well plates for cell survival assays and were cultured at 37°C in a humidified 5% CO_2 incubator. Plates were coated with 0.01% poly-L-lysine solution (Sigma, St. Louis, MO, USA) at 37°C overnight and washed with cell culture grade PBS and water and left to dry before plating of cells. The primary cultures were used on days *in vitro* (DIV) 10 for immunocytostaining of LCN2R and treatment for Duolink assays, real-time RT-PCR analysis and cell survival assays. HBSS, HEPES/NaOH, penicillin/streptomycin, GlutaMAX-1, sodium pyruvate, B27 supplement, and Neurobasal-A were from Invitrogen (Carlsbad, CA, USA); DNase I was from Roche (Roche Diagnostic GmbH, Mannheim, Germany); papain and

Glucose D-(+) were from Sigma-Aldrich (MO, USA); and $CaCl_2$ was from Merck (NJ, USA).

5.2.2. Immunocytochemistry

Immunocytochemistry for LCN2R was performed on primary hippocampal neurons on DIV 10. The cells on the coverslips were fixed with 4% paraformaldehyde for 10 min, followed by permeabilisation with PBS-01% Triton X-100 for 5 min. Cells were then blocked with 3% BSA in PBS for 1 hr at room temperature, followed by incubation with rabbit polyclonal antibody to Slc22A17/LCN2R at 1:2000 (Cell Signaling Technology, MA, USA) and mouse monoclonal MAP2a (1:200, Sigma-Aldrich, MO, USA) overnight at 4°C. The cells were washed in PBS, and incubated for 1 hr at room temperature in 1:200 dilution of goat anti-rabbit IgG (H+L) Alexa Fluor 555 and goat anti-mouse IgG (H+L) Alexa Fluor 488 (Invitrogen, CA, USA). The cells were washed with PBS and mounted with ProLong® Gold antifade reagent with DAPI (Invitrogen, Carlsbad, CA, USA). Colocalisation was examined using a laser scanning confocal microscope by analysing the overlap between the different labels by orthogonal reconstruction throughout the entire *z*-stack (LSM 510, Carl Zeiss, Göttingen, Germany).

5.2.3. Treatment of primary hippocampal neurons

Primary hippocampal neurons were treated on DIV 10 for Duolink assays, real-time RT-PCR analysis and cell survival assays. Recombinant rat LCN2 (rLCN2) used for treatment was purchased from R&D systems (Minneapolis, MN, USA). To obtain the tricomplex, rLCN2:Fe:Ent, five-fold molar excess of ferric enterochelin (0.7 kDa) (EMC Microcollections, Tübingen, Germany) was pre-incubated with rLCN2

protein as suggested by Lee and colleagues (2007, 2009) for 1 hr at 4°C. Different incubation times 30 min, 1 hr, 2 hr and overnight at 4°C all showed presence of LCN2:Fe:Ent complex as detected by native polyacrylamide gel electrophoresis. The MES buffer (25 mM MES and 150 mM NaCl, pH 6.5) used to reconstitute the lyophilised rLCN2 protein was used as the vehicle for controls.

5.2.4. Native polyacrylamide gel electrophoresis

500 ng of recombinant rat LCN2 (rLCN2) (Minneapolis, MN, USA) and rLCN2 preincubated with five-fold molar excess of ferric enterochelin (0.7 kDa) (EMC Microcollections, Tübingen, Germany) were loaded for native gel electrophoresis. Bromophenol blue was added to the proteins to facilitate loading of the proteins into 10% polyacrylamide gels (without SDS). Tris-glycine buffer without SDS, at pH 7.4 and pH > 8.0 were used as the running and transfer buffer respectively. Post-transfer denaturation of the electro-transferred proteins was done with 10% SDS in TBS buffer at 70°C for 10 min. Reducing agents were avoided in the procedures prior to the post-transfer denaturation. Blocking of the membrane was performed with 5% non-fat milk for 1 hr. The membrane was then incubated overnight with polyclonal goat anti-LCN2 antibody at 1:200 (AF3508, R&D systems, Minneapolis, MN, USA). After washing with 0.1% Tween-20 in TBS, the membrane was incubated with horseradish peroxidase-conjugated mouse anti-goat immunoglobulin IgG (1:10,000; Thermo Fisher Scientific, Rockford, IL, USA) for 1 hr at room temperature. The protein was visualised with SuperSignal West Pico chemiluminescent substrate (Thermo Fisher Scientific, Rockford, IL, USA) according to the manufacturer's instructions.

5.2.5. Duolink *in situ* proximity ligation assay (PLA)

On DIV 10, primary hippocampal neurons plated 20,000 cells/coverslip were treated with 20 µg/ml rLCN2, rLCN2:Fe:Ent or MES buffer as vehicle control for 24 hrs. On DIV 11, they were fixed with 4% paraformaldehyde for 10 min, followed by permeabilisation with PBS-01% Triton X-100 for 5 min. Cells were then blocked with 3% BSA in PBS for 1 hr at room temperature, followed by incubation with rabbit polyclonal antibody to Slc22A17/LCN2R at 1:2000 (Cell Signaling Technology, MA, USA) and goat polyclonal antibody to LCN2 at 1:200 (AF3508, R&D systems, MN, USA) overnight at 4°C. After PBS washes, cells were incubated with secondary antibodies conjugated with oligonucleotides (PLA probes MINUS and PLA probe PLUS) and incubated for 1 hr at 37°C. The PLA probe anti-rabbit MINUS binds to the rabbit LCN2R antibody, while the PLA probe anti-goat PLUS binds to the goat LCN2 antibody. After several washes, the ligation solution was added to the cells for 30 min at 37°C which consists of ligase and two oligonucleotides which hybridised the two PLA probes and joined them to a closed circle if they are in close proximity (less than 40 nm apart) which was amplified via rolling circle amplification (RCA) using a polymerase with the addition of the amplification solution for 100 min at 37°C. The RCA product hybridised to the fluorescently labelled oligonucleotides produced a distinct fluorescent spot. *In situ* PLA was performed according to the instructions provided by the manufacturer (OLINK Bioscience, Uppsala, Sweden).

After performing the Duolink assay, cells were incubated with mouse monoclonal MAP2a (1:200, Sigma-Aldrich, MO, USA) for 1 hr at room temperature. After several PBS washes, cells were incubated for 1 hr at room temperature in 1:200 dilution of goat anti-mouse IgG (H+L) Alexa Fluor 488 (Invitrogen, CA, USA). The cells were then washed and mounted with Duolink mounting medium (OLINK Bioscience, Uppsala, Sweden). Duolink and MAP2a colocalisation were examined

using a laser scanning confocal microscope, by analysing the overlap between the different labels by orthogonal reconstruction throughout the entire *z*-stack (LSM 510, Carl Zeiss, Göttingen, Germany).

5.2.6. Real-time RT-PCR analysis

Primary hippocampal neurons plated (160,000 cells/well) on 12-well plates were treated with rLCN2, rLCN2:Fe:Ent or vehicle control (MES buffer) on DIV 10 for 24, 48 or 72 hrs. Total RNA was isolated using PureLink™ RNA Mini Kit (Invitrogen, Carlsbad, CA, USA) according to the manufacturer's protocol, with DNaseI treatment (Roche Diagnostic GmbH, Mannheim, Germany). Quantitation of RNA was performed with the NanoDrop. The samples were reverse transcribed using High-Capacity cDNA Reverse Transcription Kits (Applied Biosystems, CA, USA). The reaction conditions were 25°C for 10 min, 37°C for 120 min and 85°C for 5 min. Real-time RT-PCR amplification was carried out using the 7500 Real-time PCR system (Applied Biosystems, CA, USA) with Taq-Man Universal PCR Master Mix (Applied Biosystems, CA, USA) and gene-specific primers and probes according to manufacturer's protocols (Assay ID: Bim (Rn00674175_m1)). β-actin (Part no.: 4352340E) was used as an internal control. All primers and probes were synthesised by Applied Biosystems. The PCR conditions were: an initial incubation of 50°C for 2 min and 95°C for 10 min followed by 40 cycles of 95°C for 15 s and 60°C for 1 min. All reactions were carried out in triplicates. The threshold cycle, CT, which correlates inversely with the levels of target mRNA, was measured as the number of cycles at which the reporter fluorescence emission exceeds the preset threshold level. The amplified transcripts were quantified using the comparative CT method (Livak and Schmittgen, 2001), with the formula for relative fold change = $2^{-\Delta\Delta CT}$. Fold change was normalised to untreated cells (added with media) of each set of hippocampal

neurons. The mean was calculated from 3 sets of neurons and possible significant differences with treatment and time effects were analysed by two-way ANOVA using SPSS version 12 (SPSS Inc., Chicago, IL, USA). Since the effect of time on treatment effects was not the aim of the study, to examine the effect of different treatments at a particular timepoint, different treatments at 24, 48 and 72 hrs were further investigated by three separate one-way ANOVAs and were followed-up by Tukey's HSD post-hoc comparisons. $p < 0.05$ was considered significant.

5.2.7. Cell survival assay: MTS assay

Primary hippocampal neurons plated (28,750 cells/well) in 96-well plates were pre-treated with rLCN2, rLCN2:Fe:Ent or MES buffer (vehicle) on DIV 10 for 48 hrs. 20 and 50 µg/ml of rLCN2 were used in both rLCN2 and rLCN2:Fe:Ent treatments. Cells were then post-treated with 2 µg/ml tunicamycin (Sigma-Aldrich MO, USA) or PBS (vehicle) for 24 hrs (Table 1).

Dose of pre-treatment (µg/ml)	Pre-treatment (48 hrs)	Post-treatment (24 hrs)
-	Vehicle	PBS
20	rLCN2	PBS
20	rLCN2:Fe:Ent	PBS
-	Vehicle	Tunicamycin
20	rLCN2	Tunicamycin
20	rLCN2:Fe:Ent	Tunicamycin
-	Vehicle	PBS
50	rLCN2	PBS
50	rLCN2:Fe:Ent	PBS
-	Vehicle	Tunicamycin
50	rLCN2	Tunicamycin
50	rLCN2:Fe:Ent	Tunicamycin

Table 1. Treatment groups to investigate the effect of LCN2 and LCN2:Fe:Ent on cell survival.

The cell survival assay was performed on DIV 13 with CellTiter 96® Aqueous Non-Radioactive Cell Proliferation Assay (MTS assay) (Promega, WI, USA). Since primary hippocampal neurons are non-dividing, the cell proliferation assay was utilised as a cell survival assay instead. CellTiter 96® AQueous One Solution reagent was added according to manufacturer's instructions and incubated at 37ºC. Using a spectrophotometric plate reader (Infinite M200, Tecan), readings were recorded at 1, 2, 3 and 4 hours after incubation at 490 nm with reference wavelength at 630 nm. Absorbance values were normalised to vehicle controls of each set of hippocampal neurons and the mean was calculated from 3 sets of neurons. To investigate the effect of the different pre-treatments (i.e. effect of different pre-treatments on the same dose of rLCN2 and same post-treatment), four separate one-way ANOVAs were performed using SPSS version 12 (SPSS Inc., Chicago, IL, USA), followed-up by Tukey's HSD post-hoc comparisons. $p < 0.05$ was considered significant.

5.3. RESULTS

5.3.1. LCN2R expression in the primary hippocampal neurons

LCN2R staining was observed in primary hippocampal neurons (Fig. 5.1A). Colocalisation of LCN2R with MAP2a (Fig. 5.1B) indicates that LCN2R was localised at the neurons (Fig. 5.1C), similar to observations made in the hippocampus of normal animals *(Chapter 3, Fig. 3.2)*. At higher magnification, orthogonal projections demonstrate that the punctate staining of LCN2R was mostly present on the projections and on the surface of the MAP2a-positive cells (Figure 5.1D).

5.3.2. Interaction of LCN2 with LCN2R

Duolink assay was performed firstly, to investigate if the two proteins, LCN2 and its receptor, LCN2R, interact and secondly, if they interact, the localisation of the interaction. In vehicle (MES)-treated cells (Fig. 5.2A), Duolink signals were not obvious. In rLCN2-treated (Fig. 5.2B) and rLCN2:iron:enterochelin (rLCN2:Fe:Ent)-treated (Fig. 5.2C) primary neurons, Duolink signals were present and colocalised with MAP2a staining. Thus, Duolink assay illustrates the presence of interaction between exogenous rLCN2 and endogenous LCN2R receptor expressed on the neurons *in vitro* when either rLCN2 or rLCN2:Fe:Ent was applied.

A native gel electrophoresis was carried out to examine the ability of the exogenous iron:enterochelin (Fe:Ent) to bind the recombinant LCN2 (rLCN2). The lane loaded with rLCN2:Fe:Ent has a shift in weight compared to the lane loaded with rLCN2 (Fig. 5.2D). The shift in the weight is due to the formation of the complex of rLCN2 with iron enterochelin (719 Da), an indication that the commercial rLCN2 is capable of binding to the iron:bacterial siderophore.

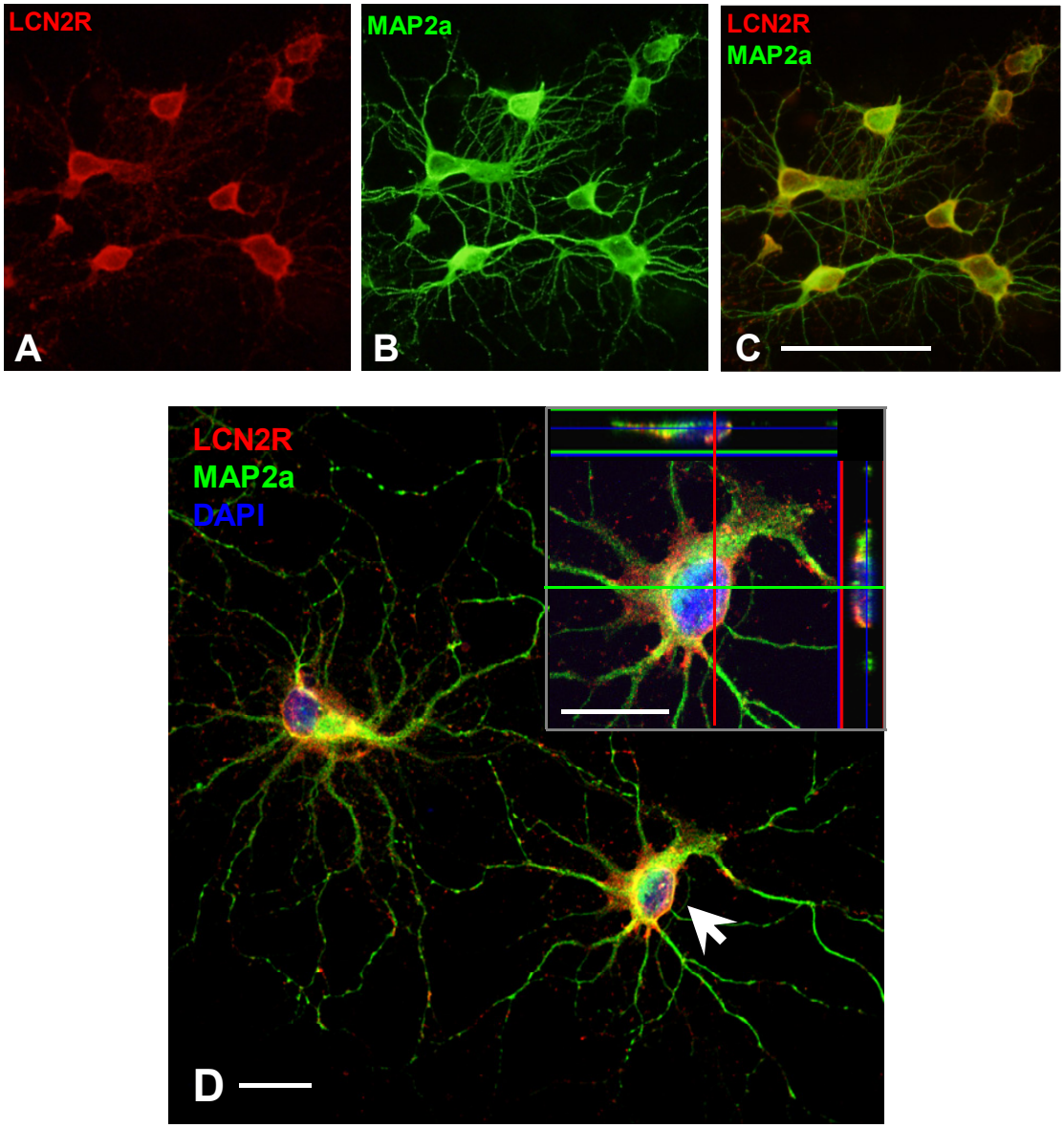

Fig. 5.1. LCN2R is present in the primary hippocampal neurons. Primary hippocampal neurons were cultured till DIV 10, fixed and double-labelled with LCN2R (red) and MAP2a (green). (A-C) Fluorescence micrographs of colocalisation of LCN2R with MAP2a under 20x low magnification. Scale=100 µm. (D) Confocal micrographs were taken at 40x magnification, and 63x for orthogonal projections in the insert, demonstrating that LCN2R was mostly present on the surface of the cell body and on the projections of the MAP2a-positive cells. Scale=20 µm. Scale in insert=20 µm.

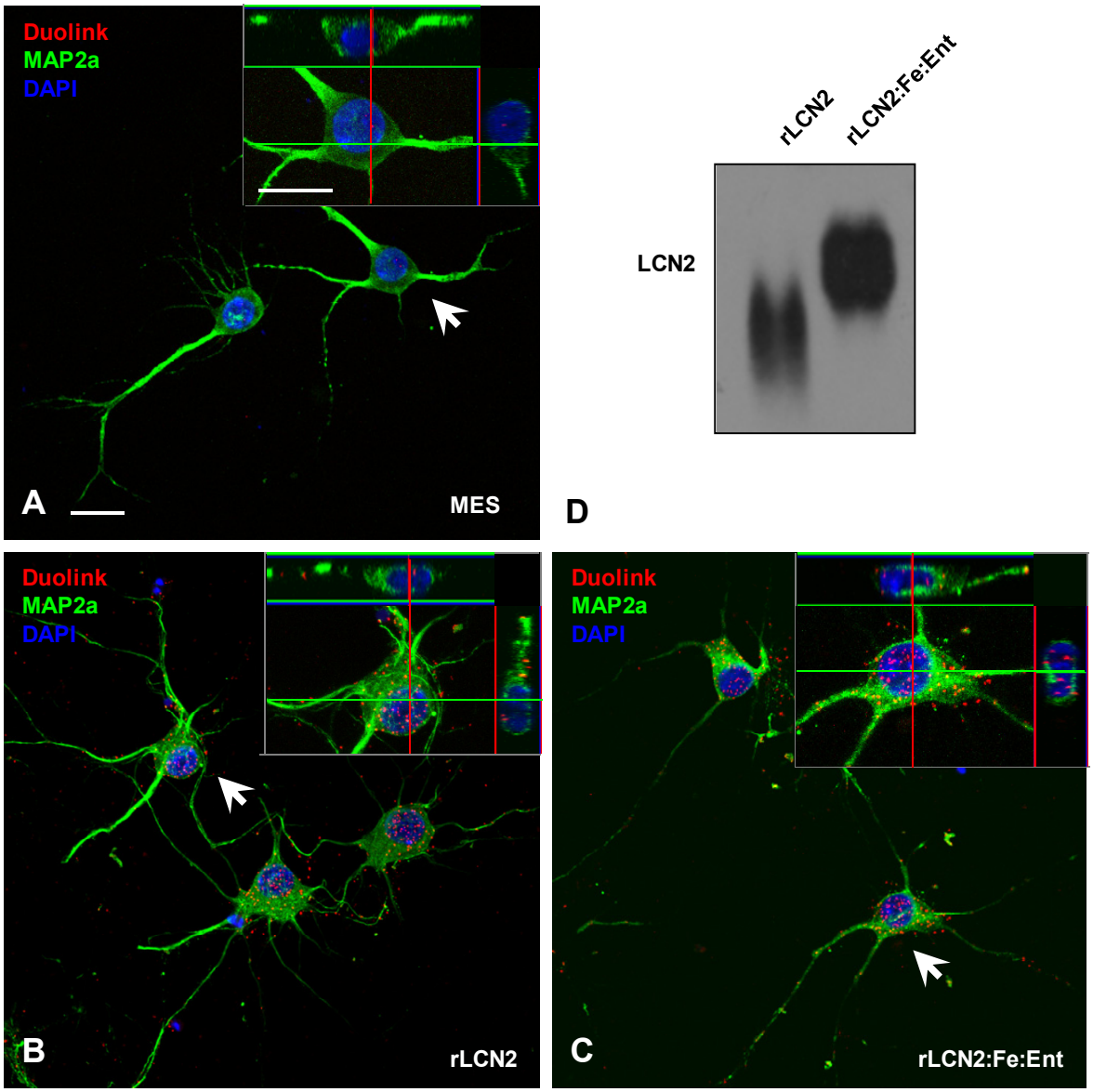

Fig. 5.2. Interaction of LCN2 with LCN2R in primary hippocampal neurons. Primary hippocampal neurons were cultured and treated on DIV 10 with (A) vehicle (MES buffer), (B) rLCN2, (C) rLCN2:iron:enterochelin (rLCN2:Fe:Ent) for 24 hrs. Cells were fixed and Duolink (red) was performed followed by MAP2a immunostaining (green). Confocal micrographs were taken at 40x magnification, while 63x magnification was used for orthogonal projections shown in the inserts. (A) Duolink signals were not obvious in vehicle (MES)-treated control cells, but were present and colocalised with MAP2a staining in (B) rLCN2-treated and (C) rLCN2:Fe:Ent-treated primary neurons. Scale=20 µm. Scale in inserts=20 µm. (D) Native gel loaded with rLCN2 protein and rLCN2:Fe:Ent (pre-incubated together for 1 hr prior to loading), probed with anti-LCN2 antibody. Upwards shift of weight (increase in weight) in the lane loaded with rLCN2:Fe:Ent, indicates the ability of rLCN2 to bind with the bacterial iron siderophore.

5.3.3. Effect of rLCN2 and rLCN2:Fe:Ent treatment on Bim mRNA expression

Primary hippocampal neurons at DIV 10 were treated with rLCN2 to mimic the effect of the LCN2 release in the lesioned hippocampus. Other than rLCN2, rLCN2:iron:enterochelin (rLCN2:Fe:Ent) was also used to investigate how the effect of LCN2:iron:siderophore would differ from that of LCN2. Bim mRNA expression changes were detected using real-time RT-PCR.

Two-way ANOVA revealed significant effects of the treatment [treatment: $F(2,18)=10.65$, $p<0.001$], the duration of treatment [time: $F(2,18)=8.08$, $p<0.01$] and a significant interaction between these effects [treatment x time: $F(4,18)=13.57$, $p<0.001$].

Follow-up one-way ANOVA for the effect of treatment at each treatment duration confirmed significant treatment effects on the changes in Bim mRNA levels at 24 hrs [treatment: $F(2,6)=33.10$, $p<0.001$], 48 hrs [treatment: $F(2,6)=5.69$, $p<0.05$], and 72 hrs [treatment: $F(2,6)=10.591$, $p<0.05$]. Follow-up one-way ANOVA for the effect of duration of treatment within each treatment group was not performed because the time course study of the various treatments was not the aim of the study.

Post-hoc Tukey's HSD tests confirmed that at 24 hrs of treatment, there were significant differences between rLCN2 and rLCN2:Fe:Ent ($p < 0.01$) and between rLCN2:Fe:Ent and vehicle control ($p < 0.001$). Bim mRNA expression was 1.3-fold in rLCN2:Fe:Ent-treated neurons relative to the vehicle controls. Similarly, at 48 hrs of treatment, post-hoc Tukey's HSD comparisons revealed that Bim mRNA levels increased significantly, being 1.2-fold ($p < 0.05$) relative to the vehicle controls, in rLCN2:Fe:Ent-treated neurons. Furthermore, at 72 hrs of treatment, significant

difference was only observed between rLCN2 and rLCN2:Fe:Ent (p < 0.01) as confirmed by post-hoc Tukey's HSD.

On the whole, no significant differences in Bim expression were observed between rLCN2-treated neurons with the vehicle controls at all timepoints. Instead, Bim mRNA levels were significantly increased at 24 and 48 hrs of rLCN2:Fe:Ent treatment (Fig. 5.3).

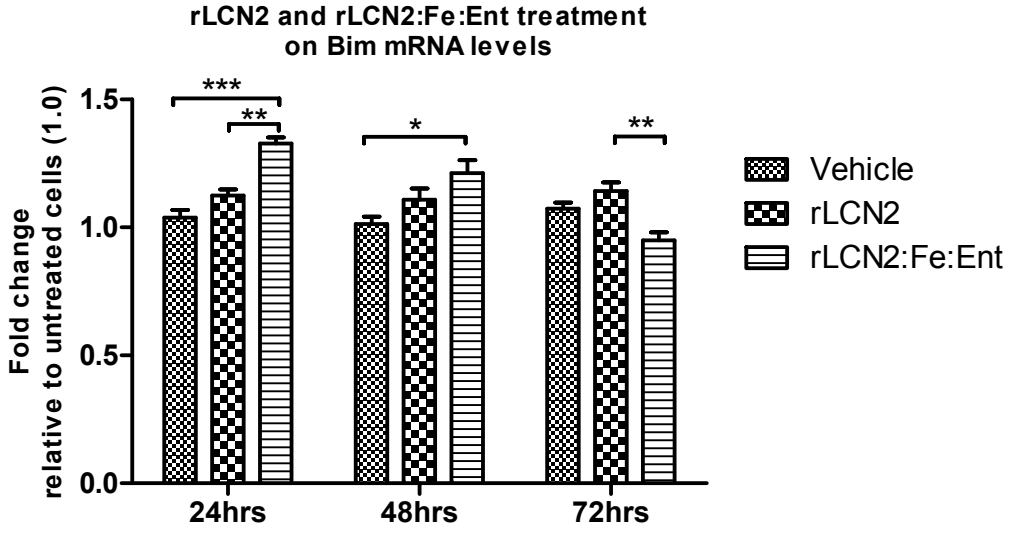

Fig. 5.3. Effect of rLCN2 and rLCN2:Fe:Ent treatment on Bim mRNA levels in primary hippocampal neurons. Primary hippocampal neurons were cultured and treated on DIV 10 with either media (untreated cells), vehicle (MES buffer), rLCN2, or rLCN2:Fe:Ent for 24, 48 or 72 hrs. Cells were harvested for RNA and real-time RT-PCR analysis was performed to determine the effect of treatment on Bim mRNA expression. Values are normalised with the untreated cells (Fold change= 1.0) at the respective timepoints to obtain the relative fold change. Analysed by 2-way ANOVA, follow-up one-way ANOVA for the effect of treatment at each timepoint. Tukey's HSD post-hoc comparisons at each timepoint revealed significant differences, indicated by (*p < 0.05, **p < 0.01, ***p < 0.001). Data are expressed as mean ± SEM, n = 3 per treatment group.

5.3.4. Effect of rLCN2 and rLCN2:Fe:Ent treatment on cell survival

In *Section 5.3.3* above, upregulation of Bim mRNA expression was observed in 24 and 48 hrs of rLCN2:Fe:Ent-treated neurons. Hence, a cell survival assay was

performed to determine if cell viability was affected. In addition, to examine if rLCN2:Fe:Ent (tricomplex) treatment has the ability to potentiate or desensitise neurons to apoptosis stress, an cytotoxic agent that triggers Bim-induced apoptosis was selected - tunicamycin. It is an ER-stress inducing agent known to upregulate Bim expression (Morishima et al., 2004; Puthalakath et al., 2007). Preliminary tunicamycin treatment was performed on primary hippocampal neurons. Bim mRNA levels were 2.7-fold ($p < 0.05$) with 24 hours of tunicamycin relative to untreated cells (Fig. 5.4A). MES-PBS-treated neurons had 93.2% of cell survival while MES-tunicamycin-treated neurons had 63.8% relative to the untreated cells. Hence, cell survival decreased about 30% after tunicamycin treatment (Fig. 5.4B).

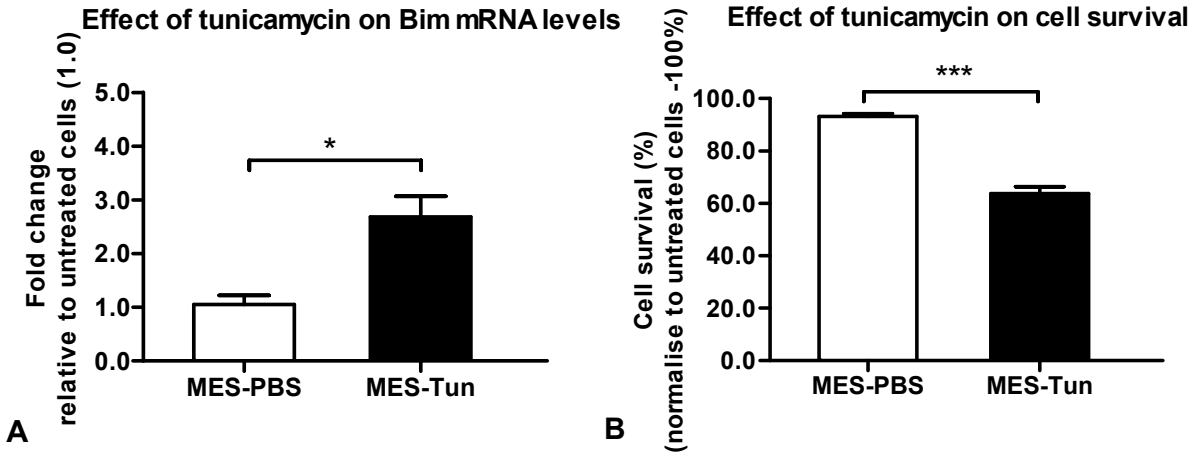

Fig. 5.4. Effect of tunicamycin on Bim mRNA levels and cell survival in primary hippocampal neurons. Primary neuronal cells were treated with 48 hrs of MES (vehicle) before 24 hrs of tunicamycin or PBS treatment. (A) Real-time RT-PCR analysis on primary neurons on the mRNA expression of Bim after tunicamycin (Tun) treatment, relative to untreated cells (Fold change=1.0). Upregulation of Bim mRNA expression was observed after tunicamycin treatment. (B) Cell survival assay (MTS assay) was performed on neurons. Tunicamycin caused decrease in cell survival. Cell survival was normalised to untreated cells (100%). Analysed by Student's t-test, asterisks indicate significant difference (*$p < 0.05$, **$p < 0.01$, ***$p < 0.001$). Data are expressed as mean ± SEM, $n = 3$ per treatment group.

After establishing that tunicamycin could upregulate Bim mRNA expression and cause decrease in cell survival, neurons were pre-treated with rLCN2 or

rLCN2:Fe:Ent (48hrs), and post-treated with tunicamycin (24hrs). Significant differences in cell survival were confirmed by performing four separate one-way ANOVA (Table 2):

	Pre-treatment	Post-treatment	One-way ANOVA	Post-hoc Tukey's HSD
1.	Vehicle or 20µg/ml rLCN2 or rLCN2:Fe:Ent	PBS	Significant $F(2,6)=14.20$, $p<0.01$	rLCN2 vs. rLCN2:Fe:Ent ($p<0.05$) rLCN2:Fe:Ent vs. vehicle control ($p<0.01$) rLCN2:Fe:Ent-treated neurons had decreased cell survival of 83.3% compared to the vehicle control (100%)
2.	Vehicle or 20µg/ml rLCN2 or rLCN2:Fe:Ent	Tunicamycin	Not significant $F(2,6)=0.67$, n.s.	-
3.	Vehicle or 50µg/ml rLCN2 or rLCN2:Fe:Ent	PBS	Significant $F(2,6)=7.34$, $p<0.05$	rLCN2 vs. rLCN2:Fe:Ent ($p<0.05$) rLCN2:Fe:Ent vs. vehicle control ($p<0.05$) rLCN2:Fe:Ent-treated neurons had decreased cell survival of 69.5% compared to the vehicle control (87.7%)
4.	Vehicle or 50µg/ml rLCN2 or rLCN2:Fe:Ent	Tunicamycin	Significant $F(2,6)=6.663$, $p<0.05$	rLCN2 vs. rLCN2:Fe:Ent ($p<0.05$)

Table 2. Statistical analysis of the effect of different treatments on cell survival.

One-way ANOVA indicated that the 1) pre-treatment (20 µg/ml of rLCN2 or tricomplex) had significant effects on cell survival with PBS post-treatment [pre-treatment: $F(2,6)=14.20$, $p<0.01$] and 2) no significant differences with tunicamycin post-treatment [pre-treatment: $F(2,6)=0.67$, n.s.]. For 50 µg/ml of rLCN2 and rLCN2:Fe:Ent, one-way ANOVA confirmed significant pre-treatment effects on cell

survival with 3) PBS post-treatment [pre-treatment: $F(2,6)=7.34$, $p<0.05$], and 4) tunicamycin post-treatment [pre-treatment: $F(2,6)=6.663$, $p<0.05$].

Post-hoc Tukey's HSD tests confirmed that there were significant differences in cell survival between 20 µg/ml of rLCN2 and rLCN2:Fe:Ent ($p < 0.05$); and between rLCN2:Fe:Ent with the vehicle control ($p < 0.01$). Neurons treated with rLCN2:Fe:Ent had lower cell survival of 83.3% compared to the vehicle controls (100%).

Similar to the trend observed in 20 µg/ml, when 50 µg/ml of rLCN2 and rLCN2:Fe:Ent were used, post-hoc Tukey's HSD tests confirmed that there were significant differences in cell survival between rLCN2 and rLCN2:Fe:Ent ($p < 0.05$); and between rLCN2:Fe:Ent with the vehicle control ($p < 0.05$). Neurons treated with rLCN2:Fe:Ent, had lower cell survival of 69.5% compared to the vehicle control (87.7%).

Post-hoc Tukey's HSD tests also confirmed that cell survival decreased significantly ($p < 0.05$) in the 50 µg/ml rLCN2:Fe:Ent-treated neurons in comparison to LCN2-treated neurons with tunicamycin post-treatment (Fig. 5.5).

On the whole, rLCN2:Fe:Ent-treated (and PBS post-treated) neurons decreased significantly in cell survival as compared to their vehicle controls. Treatment groups 1 and 3 (with PBS post-treatment) is comparable with the experimental conditions in *Section 5.3.3* which describes the upregulation of Bim mRNA expression after rLCN2:Fe:Ent treatment *(Fig. 5.3)*. Furthermore, no significant changes were observed in tunicamycin-treated cells as compared to their vehicle (MES) controls, indicating that rLCN2:Fe:Ent treatment does not potentiate or desensitise cell survival under ER stress-induced apoptosis.

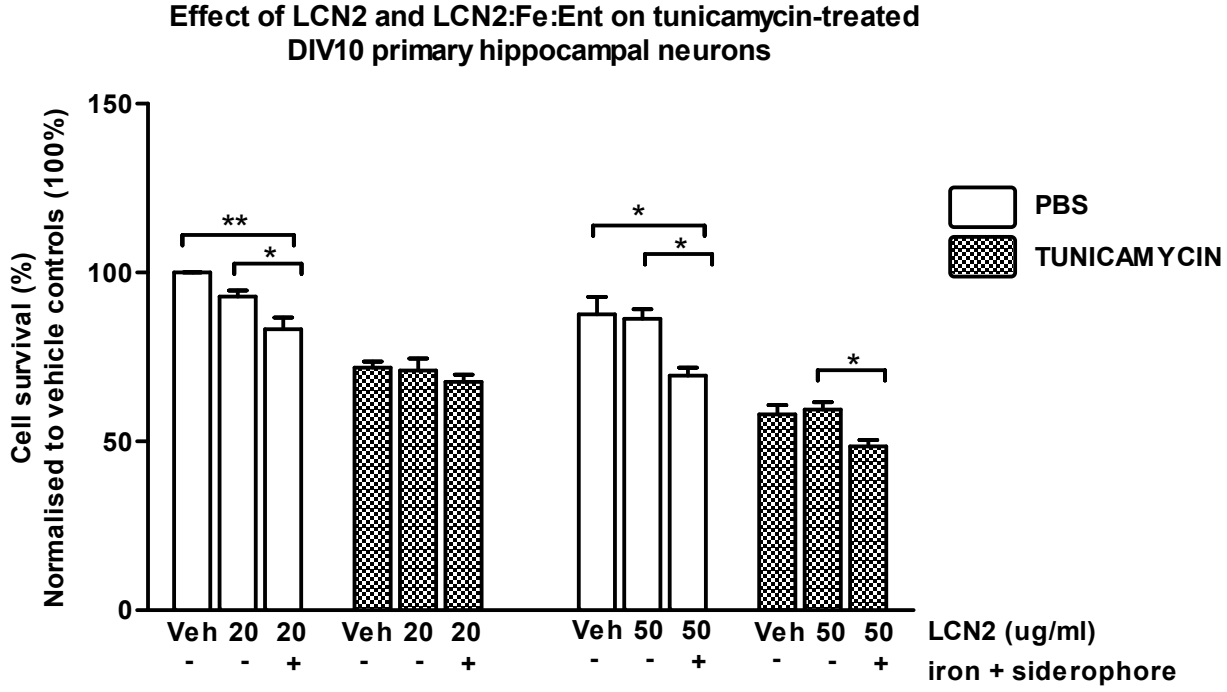

Fig. 5.5. Effect of rLCN2 and rLCN2:Fe:Ent treatment on primary hippocampal neurons on cell survival. Primary hippocampal neurons were plated on 96-well plates, cultured and pre-treated on DIV 10 with either media (untreated cells), vehicle (MES buffer), 20 µg/ml rLCN2, 50 µg/ml rLCN2, 20 µg/ml rLCN2:Fe:Ent or 50 µg/ml rLCN2:Fe:Ent, for 48 hrs. Cells were then treated with tunicamycin or vehicle (PBS) for 24 hrs. MTS assay was performed on DIV 13. Absorbance values are normalised with the untreated cells of its own set, and normalised values from three sets of cells were again normalised to the vehicle controls to 20 µg/ml of rLCN2/rLCN2:Fe:Ent (first bar from the left in the graph). Statistical analysis was performed with four separate 1-way ANOVA for each experimental setup to determine the effect of the pre-treatment on cell survival. Tukey's HSD post-hoc comparisons at each condition revealed significant differences, indicated by (*$p < 0.05$, **$p < 0.01$, ***$p < 0.001$). Data are expressed as mean ± SEM, $n = 3$ per treatment group.

5.4. DISCUSSION

In the previous chapters, upregulation of Bim was associated with apoptosis in the LCN2R-expressing neurons. However the link between LCN2, Bim and apoptosis is still unclear. Thus, in this chapter, the effect of LCN2 and iron-loaded LCN2 on Bim-dependent apoptosis on neurons was elucidated with *in vitro* assays.

After KA injury, Bim was upregulated in both the LCN2R-expressing activated microglia and neurons, which could potentially give identical or different responses upon LCN2 release. Therefore, in order to isolate the effect of LCN2 on the neurons, rat hippocampal neurons were cultured. Colocalisation of LCN2R with MAP2a indicated that the primary hippocampal neurons expressed LCN2R, identical to the neurons *in vivo (Chapter 3, Fig. 3.2)*. High magnification orthologonal projections of primary neurons revealed that LCN2R was mostly localised on the surface of the neurons and had punctate staining which was commonly observed for receptor proteins, such as GluR1-4 subunits of AMPA receptors, NR1 subunit of NMDA receptors, α2 and γ2 subunits of $GABA_A$ receptors (Andras et al., 2007; Kneussel et al., 1999; Mokin and Keifer, 2006; Nagy et al., 2004). LCN2R was also localised in a punctate distribution in LCN2R stable expressing HEK cell line (Bennett et al., 2011).

Since LCN2R was expressed on the primary neurons, cells were treated with recombinant LCN2 (rLCN2) and rLCN2:Fe:Ent to detect for protein interaction using the Duolink assay. The Duolink assay uses the *in situ* PLA technology which enables the detection, visualisation of protein interactions in cell samples. Primary antibodies raised in different species bind to the species-specific secondary antibodies, which are attached with a unique short DNA strand, also known as PLA probes. Only when the PLA probes are in close proximity (less than 40nm), the DNA strands interact and with ligation are amplified via rolling circle amplification with polymerase. The signal from the detected pair of PLA probes is visualised as an individual fluorescent dot.

Therefore, the Duolink provides insight to the presence of *in situ* protein interactions, the localisation of the interactions and quantity of interaction since each discrete dot represents a single interaction (Gullberg et al., 2004; Gustafsdottir et al., 2005; Weibrecht et al., 2010).

Interaction was detected between endogenous LCN2R and exogenous rLCN2 when applied in either rLCN2 or rLCN2:Fe:Ent and colocalised with MAP2a on the projections and surface of the neuron, and within the neuron. Here, the results illustrate the ability of LCN2R to bind and internalise LCN2, applied both as apo-LCN2 and as holo-LCN2, into the neurons, which is consistent with the receptor-mediated endocytosis proposed by others (Devireddy et al., 2005; Mori et al., 2005; Yang et al., 2002b).

LCN2 has been reported to colocalise with the divalent metal transporter (DMT1) which is found in late endosomes (Abergel et al., 2008; Yang et al., 2002b), and with Rab11, a well-established recycling endosome marker (Devireddy et al., 2005). Although these studies revealed LCN2 to be transported intracellularly via late endosomes or recycling endosomes, it is unclear in the present context and colocalisation studies could be done with late or recycling endosomal markers (Devireddy et al., 2005; Yang et al., 2002b). Vesicular intracellular staining observed in clones with highest expression of LCN2R among many LCN2R stable expressing HEK clones also supports the notion that LCN2R is internalised into the cytoplasm via vesicular or endosomal trafficking (Bennett et al., 2011). Furthermore, the absence of Duolink signals in vehicle-treated neurons indicates the absence of endogenous LCN2 in the neurons. This corresponds to the *in vivo* findings (*Chapter 2*) of the absence of LCN2 expression in other cell types, except in astrocytes. This also helps to confirm that the protein-to-protein interaction detected using Duolink was between the exogenous rLCN2 or rLCN2:Fe:Ent with the endogenous LCN2R.

To date, the extracellular mammalian siderophore has not been fully identified in the CNS, hence the bacterial siderophore, enterochelin, was used instead to act as a chaperone for iron to bind LCN2 so as to compare between apo-LCN2 (iron-free) and holo-LCN2 (iron-loaded). Various durations of incubation of rLCN2 with Fe:Ent were examined from 30 min to overnight. All durations produced a heavier band when compared to rLCN2 suggesting that LCN2 binds Fe:Ent readily due to the high affinity that LCN2 has for enterochelin (Abergel et al., 2008; Yang et al., 2002b). Therefore, primary neurons were treated with pre-incubated rLCN2 and Fe:Ent, and rLCN2 in order to see their effect on Bim expression and cell survival.

Devireddy et al. (2005) reported that the treatment of apo-24p3 (murine orthologue of LCN2) caused Bim-mediated apoptosis in 24p3R-expressing HeLa cells. Interestingly, the same was not observed in the rat hippocampal neurons. No significant differences in Bim expression was observed in rLCN2 (apo-LCN2)-treated neurons regardless of the duration of incubation of the recombinant protein in the culture media. Instead, holo-LCN2 (LCN2:Fe:Ent) resulted in significant increases in Bim mRNA levels at 24 and 48 hours (1.2- to 1.3-folds relative to vehicle controls) after treatment. At 72 hours after holo-LCN2 treatment, instead of upregulation of Bim mRNA as detected in earlier timepoints, there were no significant differences between holo-LCN2 and vehicle treated cells. By 72 hours, the effectiveness of rLCN2:Fe:Ent could be compromised. This is firstly because LCN2 was supplied as recombinant proteins which may be degraded by proteases from the cells after time. Secondly, the neurons with upregulated Bim mRNA expression at 24 and 48 hours could have already undergone apoptosis by 72 hours. Lastly, LCN2 was reported to traffic iron in acidic vesicles/endosomes and the low pH results in the dissociation of iron and degradation of enterochelin (Abergel et al., 2008). LCN2 has been shown to be non-degraded, suggesting its ability to be recycled (Yang et al., 2002b). Therefore, if the imported iron (from rLCN2:Fe:Ent complex) remained in the cells

earmarked for Bim-mediated apoptosis and with the availability of rLCN2 without enterochelin, import of iron will be discontinuous, resulting in the apo-LCN2 condition, instead of holo-LCN2 (Fig. 5.6). This speculation of the conversion of holo-LCN2 treatment to apo-LCN2 implies the absence of endogenous extracellular siderophores. Despite new progress in elucidation of mammalian siderophores (Bao et al., 2010; Devireddy et al., 2010), their existence in the primary neurons is still unknown. These plausible reasons may explain why Bim was not upregulated at 72 hours of holo-LCN2 treatment. Despite the anomaly observed at 72 hours, the trend observed at 24 and 48 hours of holo-LCN2 was consistent, indicating holo-LCN2 treatment results in upregulation of Bim mRNA expression.

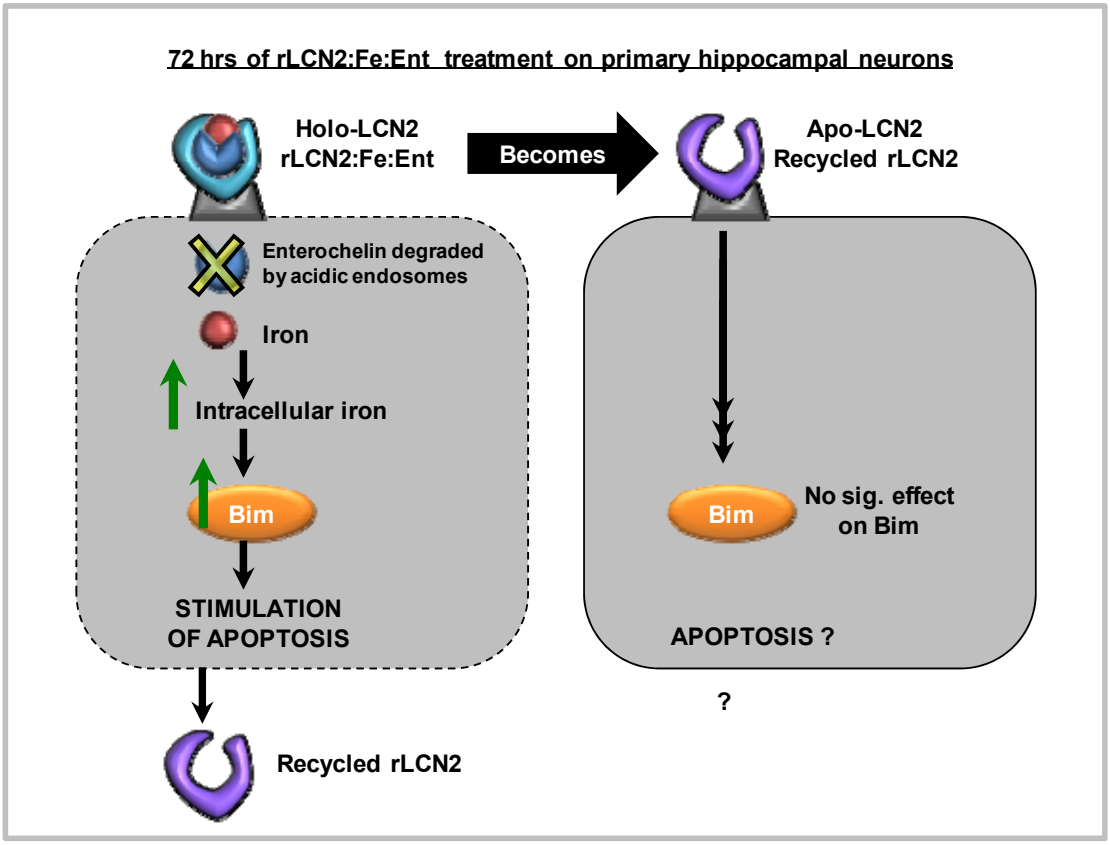

Fig. 5.6. Possible effects on Bim mRNA expression after 72 hours of rLCN2:Fe:Ent treatment on primary hippocampal neurons. With the degradation of enterochelin due to low pH in the endosomes, only rLCN2 is recycled. Since iron is imported into cells earmarked for apoptosis (depicted by the dotted cell membrane), this would result in an apo-LCN2 situation. The mechanism of apo-LCN2 remains unclear at this stage due to the insignificant effects on Bim. Hence, the possible effects of holo-LCN2 may be masked.

Significant decreases in cell survival were observed in cells treated with 20 μg/ml (16.8% decrease) and 50 μg/ml (18.2% decrease) of holo-LCN2 relative to vehicle controls. The decrease in cell survival was more pronounced at the higher dose of LCN2. Taken together with the previous result, holo-LCN2 leads to upregulation of Bim mRNA expression which stimulates apoptosis, resulting in decrease in cell survival. Since LCN2 was present in both apo- and holo-LCN2 treatment conditions, the pro-apoptotic effect of holo-LCN2 is likely to be attributed to the iron:enterochelin (Fe:Ent) complex as the critical factor to induce apoptosis in neurons.

Contrary to the present findings, LCN2 has been reported to sensitise microglia and astrocytes to cytotoxic agents, and the cell death sensitisation effect was abolished with the addition of iron:siderophore complex (Lee et al., 2007; 2009). This pro-apoptotic function of apo-LCN2 and anti-apoptotic function of holo-LCN2 *in vitro* is in line with the mechanism of holo-LCN2 increasing intracellular iron levels and inhibiting apoptosis as proposed by Devireddy et al. (2005). Yet, the present results show otherwise. This pro-apoptotic effect of holo-LCN2 may be specific to neurons, as previous studies have suggested LCN2 to have different biological effects depending on the cell type (Lee et al., 2009; Mori et al., 2005).

With the knowledge that holo-LCN2 is pro-apoptotic, how does holo-LCN2 induce apoptosis? Holo-LCN2 may deliver iron into the neurons and increase intracellular iron levels. This influx of iron may contribute to the pro-apoptotic effect of holo-LCN2. Iron is a strong promoter of free radical damage and thus most iron in the brain is sequestered by ferritin to keep intracellular iron levels in check (Thomas and Jankovic, 2004; Zecca et al., 2004). Damage to brain tissue releases iron which is capable of catalysing the generation of ROS, lipid peroxidation and autooxidation of neurotransmitters (Braughler et al., 1986; Halliwell and Gutteridge, 1985). In many

neurodegenerative diseases, iron homeostasis is often disrupted, which has been suggested to be a precursor of AD and iron accumulation has been found in regions affected by AD and PD in aged brains (McNeill and Chinnery, 2011). Therefore, if the excess iron imported by LCN2 is not sequestered by sufficient intracellular ferritin or regulated by iron regulatory mechanisms, free iron can cause cellular damage, upregulate Bim expression, stimulate apoptosis and decrease cell survival.

If holo-LCN2 delivers iron into the neurons to upregulate Bim, with a pro-apoptotic effect, it would be reasonable to postulate that apo-LCN2 might produce the opposite phenomenon, i.e. an anti-apoptotic effect, since studies have shown apo-LCN2 and holo-LCN2 to have opposite effects on apoptosis (Devireddy et al., 2005; Lee et al., 2007; 2009; 2011). Similar to the effect on Bim mRNA expression, no significant differences on cell survival was observed in apo-LCN2 treated neurons. There are a few possible explanations. Firstly, the effect of apo- and holo-LCN2 might not be opposite. In holo-LCN2, the presence of iron could enhance the effect of apo-LCN2. For instance, holo-LCN2 protected kidneys from ischaemia-reperfusion injury while apo-LCN2 only protected the injured kidneys partially (Mori et al., 2005). Also, holo-NGAL was more effective than apo-NGAL in inducing epithelial characteristics in 4T1-Ras-transformed mesenchymal tumour cells (Hanai et al., 2005). Secondly, the primary neurons were in physiological conditions with no apoptotic trigger. Hence if apo-LCN2 had any anti-apoptotic effect, it would not be significant.

Therefore, to examine if apo- and holo-LCN2 could potentiate or desensitise apoptotic effects, the cytotoxic agent used must induce apoptosis via activation of Bim. Since at 48 hours of holo-LCN2, Bim mRNA levels were elevated, primary neurons were pre-treated with 48 hours of apo-LCN2 or holo-LCN2, followed by post-treatment with tunicamycin or PBS for 24 hours. Tunicamycin is an antibiotic that

inhibits protein glycosylation and has been used in many studies to induce Bim-mediated ER stress-induced apoptosis (Chung et al., 2011; Han et al., 2008; Szegezdi et al., 2006). Upregulation of Bim expression was shown to be essential for ER stress-induced apoptosis (Morishima et al., 2004; Puthalakath et al., 2007). In the present study, preliminary studies on tunicamycin treatment on the primary hippocampal neurons showed upregulation of Bim mRNA and decrease in cell survival which were consistent with previous studies (Morishima et al., 2004; Puthalakath et al., 2007). However, even with tunicamycin post-treatment, no significant differences were observed between apo-LCN2 and vehicle treated primary neurons, regardless of the dosage of rLCN2. Apo-LCN2 did not desensitise the apoptotic effect of tunicamycin. Hence, apo-LCN2 is unlikely to have any anti-apoptotic/ protective effect on neurons, even though holo-LCN2 is pro-apoptotic.

When pre-treated with a lower dose of rLCN2, the cell survival of the primary neurons was similar after tunicamycin post-treatment regardless of apo- or holo-rLCN2 pre-treatment. This could be because the effect of tunicamycin on Bim-mediated apoptosis may have outweighed the effects of holo-LCN2 (Fig. 5.7). In contrast, a higher dose of holo-LCN2 (50 µg/ml) caused a further decrease in cell survival compared to apo-LCN2 (50 µg/ml) after tunicamycin treatment. This implies that a higher dose of holo-LCN2 may exert greater effects on Bim than tunicamycin (Fig. 5.7). It may be tempting to conclude that holo-LCN2 can potentiate the effect of tunicamycin-induced apoptosis, but since cell survival of holo-LCN2-treated neurons was not significantly different from vehicle-treated neurons, it would be premature. It is possible that with higher doses of holo-LCN2, the cell death potentiating effect may be more pronounced.

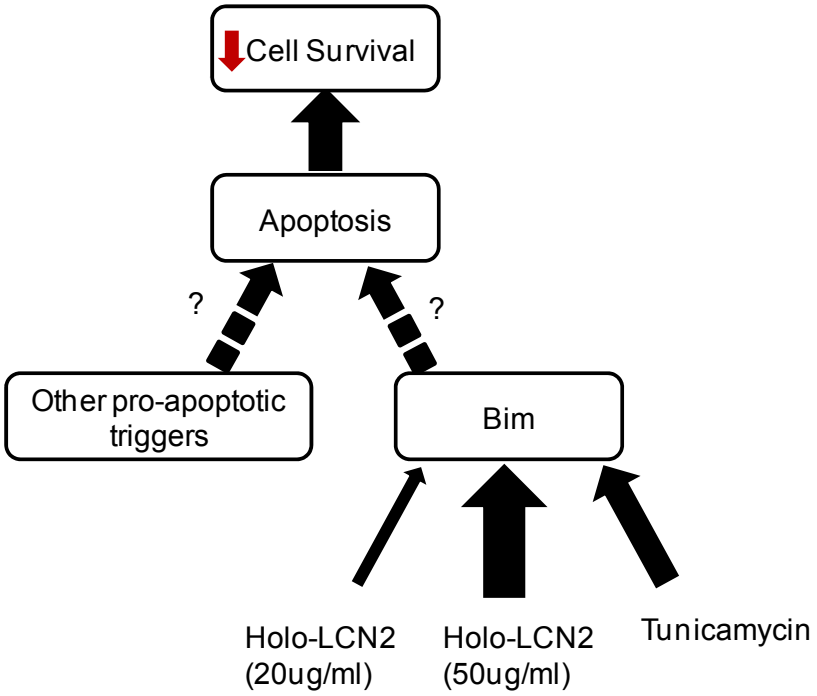

Fig. 5.7. Proposed effects of tunicamycin and different doses of holo-LCN2 on Bim mRNA expression. At lower dose of holo-LCN2, effect of tunicamycin on Bim expression outweighs its effect (as depicted by the thicker arrow). Higher dose of holo-LCN2 has a greater effect on Bim expression than tunicamycin (as depicted with the thickest arrow). Arrow indicates activation. Other pro-apoptotic triggers may exist other than Bim, but the amount of contribution to apoptosis is unknown (as represented by '?' in the figure) to decrease cell survival.

In the cell survival assay, neurons were treated 48 hours with apo- and holo-LCN2 and 24 hours with tunicamycin. Hence apo- and holo-LCN2 were present in the culture media for 72 hours in total. From the real-time RT-PCR analysis, neurons treated with 72 hours of holo-LCN2 had no significant difference in Bim mRNA levels compared to vehicle controls. However, in the cell survival assay, regardless of dose of holo-LCN2, decrease in cell survival was observed. This could be due to the delay in the onset of cell death. At 48 hours, Bim mRNA levels were increased, but time is required for protein translation, activation and localisation changes in other pro-apoptotic proteins, such as BAX/BAK, activation of caspases and caspase cascade, dysfunction of mitochondria and finally cell demise (Borner, 2003; Danial, 2007; Willis et al., 2003). Therefore, in consideration of the delay of onset of apoptosis, it could

explain the significant decrease in cell survival at 72 hours after holo-LCN2 treatment.

In summary, this chapter showed the interaction between LCN2R and LCN2 when applied in either apo- or holo-LCN2 treatment and the Bim-mediated apoptotic effect of holo-LCN2 on the primary neurons for the first time. Based on the present results, a mechanism for Bim-mediated apoptosis in neurons is proposed: Holo-LCN2 interacts with LCN2R (expressed on the hippocampal primary neuron) to be internalised with the import of iron into the cell. As a result of the iron influx, Bim is upregulated, stimulating apoptosis and causing a decrease in cell survival (Fig. 5.8). This phenomenon is parallel to the *in vivo* upregulation of Bim in apoptotic LCN2R-expressing neurons after KA-induced neurodegeneration. Thus, the *in vitro* results suggest that the import of iron assisted by an endogenous extracellular mammalian siderophore complex (holo-LCN2) into the neurons may be attributed to the apoptotic role of LCN2 after KA-induced neurodegeneration.

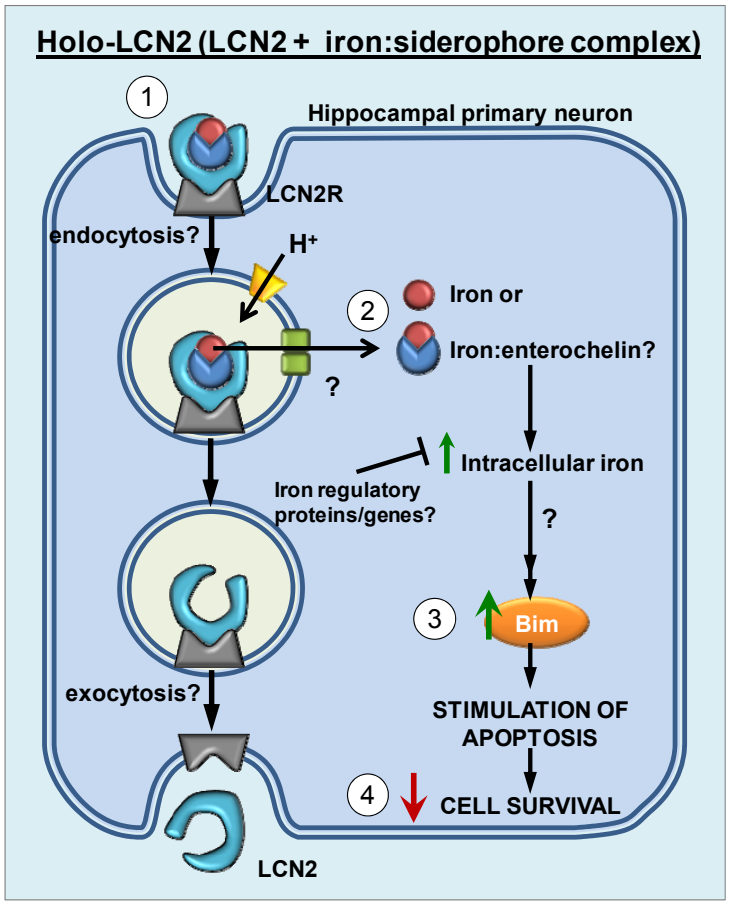

Fig. 5.8. Proposed mechanism of the pro-apoptotic effect of holo-LCN2 on primary hippocampal neurons. (1) Holo-LCN2 (LCN2:Fe:siderophore) interacts with LCN2R to be internalised into the neurons. (2) Due to the low pH, iron is dissociated from the tricomplex, increasing intracellular iron concentrations. Iron regulatory genes/proteins are activated to decrease the iron levels. (3) High iron levels induce upregulation of Bim. (4) Decrease in cell survival is observed as a result of holo-LCN2 treatment. Modified from Richardson (2005). Diagram not drawn to scale.

CHAPTER 6

GENERAL DISCUSSION AND CONCLUSION

6.1. GENERAL DICUSSION

Despite being well-studied in the periphery, little was known about LCN2 in the brain. Previously, LCN2 had only been detected in the CNS via microarray in several studies (Bonow et al., 2009; MacManus et al., 2004) and the most relevant studies related to the CNS were on the brain-derived cells, in the murine primary microglia, astrocytes, neurons and glioblastoma cells (Lee et al., 2007; 2009; 2011; Zheng et al., 2009), and at the choroid plexus *in vivo* (Marques et al., 2008). Therefore, this thesis started off by examining if those roles postulated in the periphery could be relevant in hypothesising LCN2's role in the CNS. In neurodegeneration, excess iron is often detected, along with generation of ROS, and neuronal loss via apoptosis. Hence, LCN2's ability to bind iron (via siderophore) and involvement in apoptosis led to the hypothesis that LCN2 may have a role in KA-induced neurodegeneration. This thesis have found an association between LCN2, LCN2R and Bim-mediated apoptosis; and postulated a likely mechanism for LCN2's role in Bim-mediated apoptosis in the neurons during KA-induced neurodegeneration.

In this thesis, the role of LCN2 in KA-induced neurodegeneration was covered in four chapters: (1) LCN2 expression physiologically and after KA injury, (2) LCN2R expression, (3) Bim expression after KA injury and (4) association of LCN2, LCN2R and Bim *in vitro*.

This study shows for the first time the localisation of LCN2 and its receptor LCN2R in the hippocampus. After KA injury, LCN2 was upregulated in the reactive astrocytes, while its receptor, LCN2R, was upregulated in the activated microglia, and expressed in the neurons physiologically. Upregulation of Bim in the LCN2R expressing-activated microglia did not lead to apoptosis, unlike in the LCN2R expressing-neurons at 1 day post-KA injection. The effect of LCN2 on apoptosis in

the neurons was studied with the treatment of apo-LCN2 and holo-LCN2 as iron was reported to confer LCN2 to have different effects on cells. Interaction between holo-LCN2 and LCN2R resulted in Bim-mediated apoptosis and decrease in cell survival in the primary neurons, while apo-LCN2 had no significant effect on the cells (Fig. 6.1).

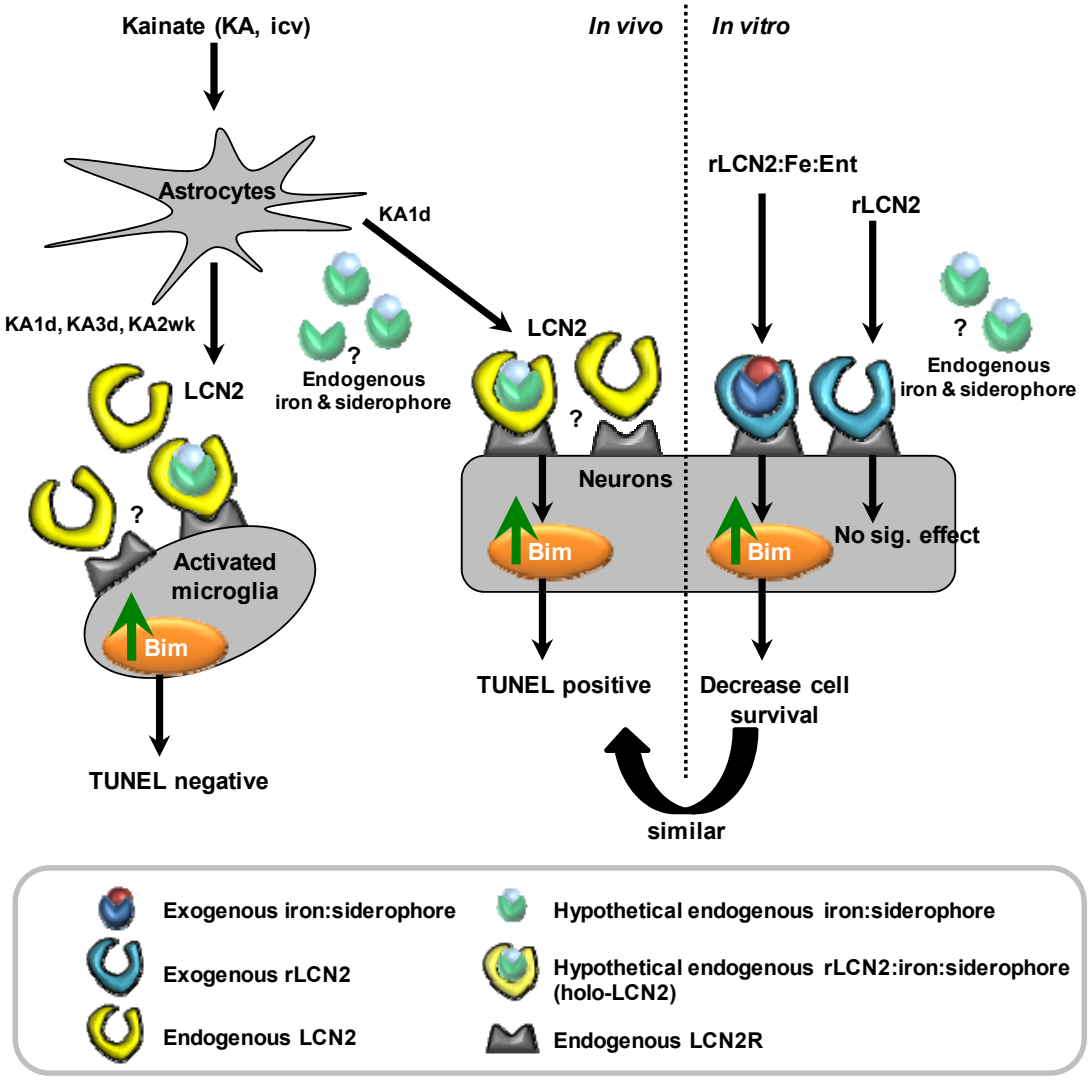

Fig. 6.1. Summary of the effects of LCN2 in KA-induced neurodegeneration.

In KA-induced neurodegeneration, LCN2 secreted by the reactive astrocytes could act on either the LCN2R–expressing neurons or activated microglia. At 1 day post-KA injection, LCN2 expression was upregulated, and upregulation of Bim was

detected in apoptotic neurons. This appears to support the proposed mechanism by Devireddy and colleagues (2005) that apo-LCN2 induces apoptosis. LCN2 released from astrocytes (apo-LCN2) could interact with LCN2R and induce upregulation of Bim in neurons, resulting in apoptosis.

However, the *in vitro* studies discussed in *Chapter 5* show otherwise as apo-LCN2 had no effect on the Bim mRNA expression or cell survival on primary hippocampal neurons. Also, apo-LCN2 neither sensitise nor desensitise neurons to tunicamycin-induced cell death further supports that apo-LCN2 has neither a pro-apoptotic nor an anti-apoptotic effect, even when apoptotic triggers are present. Instead, treatment of holo-LCN2 increased Bim mRNA expression and decreased cell survival, indicating holo-LCN2 is pro-apoptotic. This is different from the proposed mechanism by Devireddy et al. (2005) as apo-LCN2 was proposed to be pro-apoptotic and holo-LCN2 to be anti-apoptotic. Devireddy et al. (2005) used 24p3R-overexpressing HeLa cells, which could possibly give different effects from naturally occurring LCN2R-expressing neurons. Also in support of Devireddy and colleagues' mechanism, LCN2-induced cell death sensitisation was abolished with the addition of iron:siderophore complex in C6 glioma and BV-2 microglial cells (Lee et al., 2007; 2009), indicating that holo-LCN2 is anti-apoptotic, which is opposite from our analysis. This discrepancy could be due to difference in cell types, as neurons and glial cells have very different functions.

Although it was not investigated in this thesis how holo-LCN2 treatment leads to upregulation of Bim and decrease in cell survival, it is not far-fetched to postulate that holo-LCN2 delivers iron into the neurons to increase intracellular iron concentration. Increased intracellular iron, if not kept in check (sequestered by ferritin), will generate ROS, increasing vulnerability of neurons to oxidative stress (Sadrzadeh and Saffari, 2004; Zecca et al., 2004). Increased ROS was shown to

induce apoptosis, decreasing cell survival (Simon et al., 2000). This fits well into the paradigm in which increasing iron is thought to be detrimental to the CNS (Halliwell, 1992; Thomas and Jankovic, 2004). Iron accumulation in specific brain regions affected by AD and PD in aged brains and defects in iron homeostasis are often observed in many neurodegenerative diseases (Zecca et al., 2004). Therefore, to keep iron homeostasis in check, changes in intracellular iron concentration can lead to compensatory changes in the iron regulatory proteins/genes, such as ferritin, transferrin receptor 1 and other proteins of iron metabolism (Rouault, 2001; Zecca et al., 2004). Compensatory mechanisms, such as upregulation of ferritin, may be present in the neurons to sequester iron, but it may not be sufficient to cope with sudden import of iron. Each ferritin molecule can store up to 4,500 iron atoms, but it contains variable amounts of two types of polypeptide chains, heavy (H) and light (L) (Joshi et al., 1995). Neurons express mostly H-ferritin, which is associated with responses to stress unlike microglia which express mostly L-ferritin, which is associated with iron storage (Connor et al., 1994).

Therefore, based on the present results, a mechanism for Bim-mediated apoptosis in neurons is proposed: Holo-LCN2 interacts with LCN2R expressed on the hippocampal primary neuron to be internalised to import iron into the cell. Due to accumulation of iron, free radicals are generated, increasing oxidative stress in the cells. As a result, Bim is upregulated, stimulating apoptosis and causing decrease in cell survival (Fig. 6.2).

Unexpectedly, apo-LCN2 has no significant effect on primary neurons and also did not produce an opposite effect from holo-LCN2. Elucidated in recent studies (Bao et al., 2010; Devireddy et al., 2010), endogenous mammalian siderophores may be present in the primary hippocampal neurons. Together with availability of iron in the cells or from the culture media, and with the great affinity of siderophores to iron,

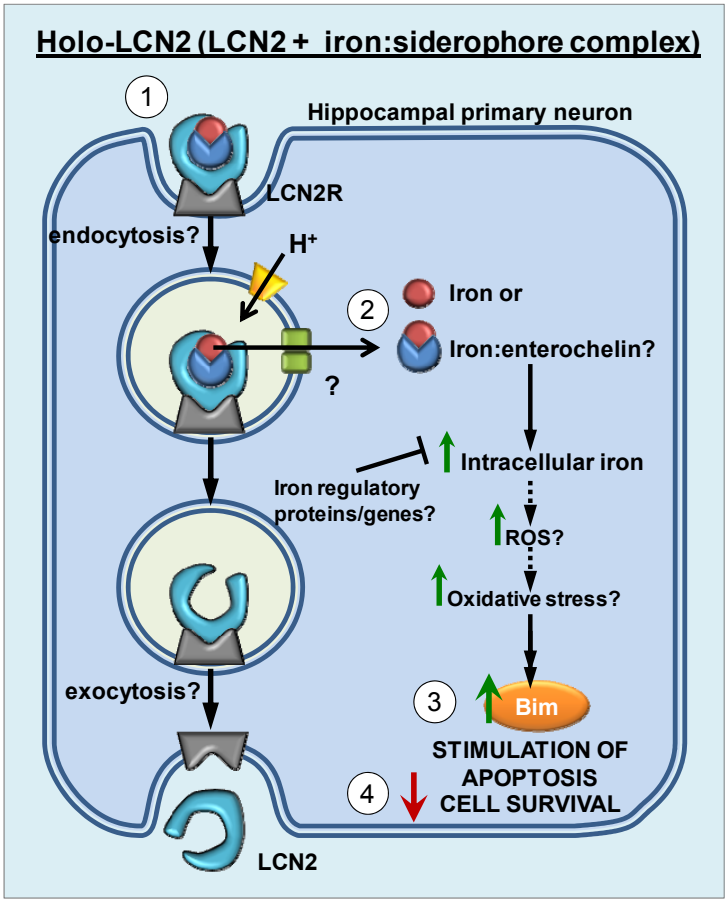

Fig. 6.2. Proposed mechanism of pro-apoptotic effect of holo-LCN2 on primary hippocampal neurons. (1) Holo-LCN2 (LCN2:Fe:siderophore) interacts with LCN2R to be internalised into the neurons. (2) Due to the low pH, iron is dissociated from the tricomplex, increasing intracellular iron concentrations. Iron regulatory genes/proteins are activated to decrease the iron levels. If free iron remains in excess, ROS are generated, increasing oxidative stress. (3) As a result, Bim is upregulated. (4) Decrease in cell survival is observed as a result of holo-LCN2 treatment. Modified from Richardson (2005). Diagram not drawn to scale.

apo-LCN2 treatment may well be converted to “holo-LCN2” treatment despite the addition of rLCN2 only. With the endogenous amount of iron and siderophore, the amount of tricomplex formed would be far lesser than the tricomplex present in the holo-LCN2 treatment, which has 5x molar excess of Fe:Ent than rLCN2 supplied. Therefore, apo-LCN2 could not produce a significant pro-apoptotic effect like holo-LCN2, or the opposite, i.e. anti-apoptotic effect. This is akin to the observations made by Mori and colleagues (2005) as they attempted to elucidate the effective

component of holo-NGAL (NGAL:enterochelin:Fe) that delivers iron into the kidney. They found NGAL:enterochelin was as effective as NGAL:enterochelin:Fe in delivering iron to the kidney because of the strong affinity of the enterochelin for iron strips iron from transferrin to form NGAL:enterochelin:Fe (Mori et al., 2005). Therefore, if mammalian siderophores were present in the primary neurons, they would have strong affinity to bind any existing iron to form holo-LCN2. Thus, the chances of having a real “apo-LCN2” condition would be slim. Further studies would have to be performed to identify whether the primary neurons have endogenous mammalian siderophore(s) present.

Having established that holo-LCN2 is pro-apoptotic, holo-LCN2-treated primary neurons have many points in common with the neurons at 1 day post-KA injection. In both *in vitro* and *in vivo* treatments, Bim was upregulated in the LCN2R-expressing neurons and cell survival was compromised with decreased cell survival *in vitro*, and apoptosis of neurons *in vivo (refer to Fig. 6.1)*. Increase in iron was also observed after KA injury (Ong et al., 1999), a phenomenon common to other types of neuronal injuries or neurodegenerative diseases (Thomas and Jankovic, 2004; Zecca et al., 2004). Thus, the accumulation of free iron and the rapid upregulation of LCN2 help to promote the formation of holo-LCN2. Therefore, this suggests the presence of an extracellular mammalian siderophore in the hippocampus. In many studies, bacterial enterochelin was used as the siderophore in many experimental setups as the presence of mammalian siderophore was still unclear despite many speculations.

Finally in 2010, the enzyme, BDH2, that synthesise the iron moiety (2,5-dihydroxybenzoic, 2,5-DHBA) of the mammalian siderophore was elucidated and required for 24p3-mediated iron transport and apoptosis (Devireddy et al., 2010). BDH2 mRNA expression was also detected in the brain from adult mice (Devireddy et al., 2010). In a preliminary attempt to examine the presence of mammalian siderophore, RT-PCR and western blot analysis show the presence of BDH2 mRNA

and protein expression in the rat hippocampus *(Appendix 1B and C)*. Although the detection of BDH2 does not equate to the detection of the mammalian siderophore, it gives a strong indication that the hippocampus has endogenous siderophore(s) because silencing of BDH2 resulted in siderophore depletion (Devireddy et al., 2010).

Also, another group found catechols to bind LCN2:iron complex in human and mouse urine and that the LCN2:Fe:catechol complex could deliver iron to the proximal tubule of the kidney (Bao et al., 2010). Interestingly, the CNS has high levels of catechols in the form of catecholamine neurotransmitters: dopamine, norepinephrine and epinephrine. These neurotransmitters could be potential candidates as mammalian siderophores, and their abundance in the CNS would possibly offer an alternative route of iron trafficking other than transferrin.

Bim-mediated apoptosis was only detected in neurons at 1 day post-KA injection, but not at later timepoints because the neurons with upregulated Bim would have undergone apoptosis by then. At 2 weeks post-KA injection, Bim and LCN2R were highly upregulated in the activated microglia. However, the activated microglia were not apoptotic even though 2 weeks post-KA injection samples had the highest Bim mRNA and protein expression. There could be a number of plausible reasons. Firstly, upregulation of Bim may have other unknown functions in activated microglia. Secondly, the absence of apoptosis may be due to the tolerance of microglia to the excess iron influx. Increase expression of ferritin was detected mostly in microglia and oligodendrocytes in KA-lesioned hippocampus (Huang and Ong, 2005). Since the microglia express mostly L-ferritin, which is associated with iron storage (Connor et al., 1994), the iron delivered into the activated microglia by holo-LCN2 may be effectively sequestered by the upregulated ferritin. Since iron homeostasis is not disrupted with free, labile iron to create havoc, apoptosis is not triggered. Alternatively, at 2 weeks post-KA injection, it might be too early to detect apoptosis of

activated microglia as they peak one month post-KA injection before declining (Jorgensen et al., 1993; Mitchell et al., 1993). Furthermore, Bim's gradual increase in expression from 1 day to 2 weeks post-KA injection indicates that it may increase further at later timepoints to signal clearing of activated microglia in the lesioned areas. The apoptotic status of the cells may be very dependent on the stage of neurodegeneration, as apoptotic neurons with upregulated Bim were only observed at 1 day post-KA injection in the present study. It is therefore possible that the appropriate timepoint for the activated microglia to apoptose has yet to be identified.

In summary, the data in this thesis shows that iron-loaded LCN2 is pro-apoptotic *in vitro*. Also, the great elevation of LCN2 together with accumulated iron in the lesioned area may promote the formation of holo-LCN2 (LCN2:Fe:siderophore) with unknown extracellular siderophore(s) to induce Bim-mediated apoptosis at the neurons after KA-induced neurodegeneration. Furthermore, LCN2-deficient mice showed no defects in apoptosis, iron metabolism, kidney development and reproduction (Berger et al., 2006; Flo et al., 2004), suggesting that LCN2 does not have an obligatory role in these biological processes. Thus it is important to keep in mind that LCN2-induced Bim-mediated apoptosis does not account for all cell demise during KA-induced neurodegeneration, and possibly only a population of cells undergo Bim-mediated apoptosis. There are also other pro-apoptotic factors other than Bim and other than apoptosis, necrosis and other forms of neuronal damage are also involved in neurodegeneration. Nevertheless, since Bim-mediated apoptosis is specific to LCN2R-expressing neurons, interventions can target the pathway to ameliorate the neuronal loss in neurodegeneration.

6. 2. Future studies

Having established that holo-LCN2 induces Bim-mediated apoptosis, more work has to be done to provide more evidence for this proposed mechanism. Firstly, siRNA-mediated silencing of LCN2R in the primary hippocampal neurons will help to verify if the effect of holo-LCN2 on neurons is mediated by LCN2R. More evidence is also required for the receptor-mediated endocytosis and exocytosis of LCN2 by using AlexaFluor-labelled LCN2 to treat the primary neurons, together with immunolabelling of late/recycling endosomes markers, such as DMT1 and Rab11. Since holo-LCN2 is suggested to induce Bim-mediated apoptosis due to influx of intracellular iron, intracellular iron levels could be measured using calcein assay (a cell permeable dye; its emission is quenched by iron binding) or deduced from the expression levels of iron-regulatory proteins, such as transferrin receptor 1, ferritin, and iron-regulatory protein 1 and 2. To examine if the increase of intracellular iron led to generation of ROS, ROS levels can be measured using fluorometric analysis by preloading cells with the non-fluorescent probe CDDHCF-DA, which is rapidly converted to the highly fluorescent compound CDCF-DA by ROS (Devireddy et al., 2010).

Furthermore, to validate the cellular localisation of Bim and LCN2R after KA injury, triple immunostaining of Bim, LCN2R and neuronal/microglial marker can be done. Although apo- and holo-LCN2 was detected to interact with LCN2R expressed on the primary neurons, it would be useful to demonstrate that LCN2 interacts with LCN2R *in vivo* using the Duolink assay on hippocampal sections as Duolink provides insights to the localisation of the interactions.

More importantly, further investigations have to be done to elucidate the presence of mammalian siderophore(s) in the hippocampus. Catechols have been elucidated as possible mammalian siderophores with the ability to deliver iron to the kidneys (Bao et al., 2010). Catechols are present in the CNS in the form of

catecholamines: dopamine, norepinephrine and epinephrine (for chemical structures see *Appendix 1D and E*). Tyrosine hydroxylase (TH) catalyses the first step in catecholamine synthesis from the conversion of tyrosine to dihydroxyphenylalanine (DOPA), which is the rate limiting step for catecholamine synthesis *(Appendix 1E).* TH has been shown to be expressed on hippocampal neurons *in vitro* (Aubert et al., 2001; Frotscher and Leranth, 1988). Thus, TH knockdown experiments can be done on the primary neurons, followed by treatment of rLCN2:Fe and rLCN2. Without the endogenous siderophore, both treatments should produce the same effect (no apoptosis). Although BDH2 has been identified as the enzyme responsible for the synthesis of the iron moiety (2,5 DHBA, for chemical structure see *Appendix IF*) of the *intracellular* mammalian siderophore, it would be interesting if it functions as an *extracellular* siderophore to import iron-loaded LCN2 into the neurons. Thus the same knockdown experiment can be performed for BDH2. With the elucidation of extracellular mammalian siderophore *in vitro*, more studies can be performed *in vivo*.

In the present study, the effect of LCN2 on the LCN2R-expressing microglia was not examined. At 2 weeks post-KA injection, LCN2R-expressing activated microglia had the highest Bim expression but were not apoptotic. Since activated microglia were suggested to peak at 1 month (Jorgensen et al., 1993; Mitchell et al., 1993), mRNA and protein expression of LCN2 and Bim could be investigated, followed by triple immunostaining of Bim, LCN2R and OX-42 at 1 month post-KA injection. TUNEL assay could be done to examine whether LCN2 has a Bim-mediated apoptotic effect on the activated microglia. If no apoptosis is observed, the upregulation of Bim may have other functions in the activated microglia.

6.3. Conclusion

In conclusion, this thesis has addressed the expression and localisation of LCN2 and its receptor, LCN2R, after KA injury, and associated the interaction of LCN2 and LCN2R with Bim-mediated apoptosis. Iron status of LCN2 was shown to affect its function as interaction between iron-loaded LCN2 and LCN2R led to Bim-mediated apoptosis in primary neurons, which was not observed for iron-lacking LCN2. The pro-apoptotic effect of iron-loaded LCN2 may account for a population of cell demise in KA-induced neurodegeneration. The present study also suggests the presence of extracellular mammalian siderophore(s) in the hippocampus to assist LCN2 to import iron into the neurons to induce apoptosis. The understanding of the role of LCN2 in the KA model could be a stepping stone to investigate the role of LCN2 in other neurodegenerative diseases as interventions can be targeted at the interaction between LCN2 and LCNR to retard neurodegeneration.

REFERENCES

Abergel, R.J., Clifton, M.C., Pizarro, J.C., Warner, J.A., Shuh, D.K., Strong, R.K., Raymond, K.N., 2008. The siderocalin/enterobactin interaction: a link between mammalian immunity and bacterial iron transport. J. Am. Chem. Soc. 130, 11524-11534.

Alpizar-Alpizar, W., Laerum, O.D., Illemann, M., Ramirez, J.A., Arias, A., Malespin-Bendana, W., Ramirez, V., Lund, L.R., Borregaard, N., Nielsen, B.S., 2009. Neutrophil gelatinase-associated lipocalin (NGAL/Lcn2) is upregulated in gastric mucosa infected with Helicobacter pylori. Virchows Arch. 455, 225-233.

Andras, I.E., Deli, M.A., Veszelka, S., Hayashi, K., Hennig, B., Toborek, M., 2007. The NMDA and AMPA/KA receptors are involved in glutamate-induced alterations of occludin expression and phosphorylation in brain endothelial cells. J. Cereb. Blood Flow Metab. 27, 1431-1443.

Aubert, M., Guiramand, J., Croce, A., Roch, G., Szafarczyk, A., Vignes, M., 2001. An endogenous adrenoceptor ligand potentiates excitatory synaptic transmission in cultured hippocampal neurons. Cereb. Cortex 11, 878-887.

Bao, G., Clifton, M., Hoette, T.M., Mori, K., Deng, S.X., Qiu, A., Viltard, M., Williams, D., Paragas, N., Leete, T., Kulkarni, R., Li, X., Lee, B., Kalandadze, A., Ratner, A.J., Pizarro, J.C., Schmidt-Ott, K.M., Landry, D.W., Raymond, K.N., Strong, R.K., Barasch, J., 2010. Iron traffics in circulation bound to a siderocalin (Ngal)-catechol complex. Nat Chem Biol 6, 602-609.

Barasch, J., Mori, K., 2004. Cell biology: iron thievery. Nature 432, 811-813.

Bauer, M., Eickhoff, J.C., Gould, M.N., Mundhenke, C., Maass, N., Friedl, A., 2008. Neutrophil gelatinase-associated lipocalin (NGAL) is a predictor of poor prognosis in human primary breast cancer. Breast Cancer Res. Treat. 108, 389-397.

Beal, M.F., 2001. Experimental models of Parkinson's disease. Nat Rev Neurosci 2, 325-334.

Ben-Ari, Y., Tremblay, E., Ottersen, O.P., 1980. Injections of kainic acid into the amygdaloid complex of the rat: an electrographic, clinical and histological study in relation to the pathology of epilepsy. Neuroscience 5, 515-528.

Ben-Ari, Y., Tremblay, E., Riche, D., Ghilini, G., Naquet, R., 1981. Electrographic, clinical and pathological alterations following systemic administration of kainic acid, bicuculline or pentetrazole: metabolic mapping using the deoxyglucose method with special reference to the pathology of epilepsy. Neuroscience 6, 1361-1391.

Ben-Ari, Y., Tremblay, E., Berger, M., Nitecka, L., 1984. Kainic acid seizure syndrome and binding sites in developing rats. Brain Res. 316, 284-288.

Ben-Ari, Y., 1985. Limbic seizure and brain damage produced by kainic acid: mechanisms and relevance to human temporal lobe epilepsy. Neuroscience 14, 375-403.

Benavides, J., Capdeville, C., Dauphin, F., Dubois, A., Duverger, D., Fage, D., Gotti, B., MacKenzie, E.T., Scatton, B., 1990. The quantification of brain lesions with an omega 3 site ligand: a critical analysis of animal models of cerebral ischaemia and neurodegeneration. Brain Res. 522, 275-289.

Bendotti, C., Guglielmetti, F., Tortarolo, M., Samanin, R., Hirst, W.D., 2000. Differential expression of S100beta and glial fibrillary acidic protein in the hippocampus after kainic acid-induced lesions and mossy fiber sprouting in adult rat. Exp. Neurol. 161, 317-329.

Bennett, K.M., Liu, J., Hoelting, C., Stoll, J., 2011. Expression and analysis of two novel rat organic cation transporter homologs, SLC22A17 and SLC22A23. Mol. Cell. Biochem. 352, 143-154.

Berger, M.L., Lefauconnier, J.M., Tremblay, E., Ben-Ari, Y., 1986. Limbic seizures induced by systemically applied kainic acid: how much kainic acid reaches the brain? Adv. Exp. Med. Biol. 203, 199-209.

Berger, T., Togawa, A., Duncan, G.S., Elia, A.J., You-Ten, A., Wakeham, A., Fong, H.E., Cheung, C.C., Mak, T.W., 2006. Lipocalin 2-deficient mice exhibit increased sensitivity to Escherichia coli infection but not to ischemia-reperfusion injury. Proc. Natl. Acad. Sci. U. S. A. 103, 1834-1839.

Birgens, H.S., Kristensen, L.O., Borregaard, N., Karle, H., Hansen, N.E., 1988. Lactoferrin-mediated transfer of iron to intracellular ferritin in human monocytes. Eur. J. Haematol. 41, 52-57.

Bleakman, D., Lodge, D., 1998. Neuropharmacology of AMPA and kainate receptors. Neuropharmacology 37, 1187-1204.

Block, M.L., Zecca, L., Hong, J.S., 2007. Microglia-mediated neurotoxicity: uncovering the molecular mechanisms. Nat Rev Neurosci 8, 57-69.

Bloss, E.B., Hunter, R.G., 2010. Hippocampal kainate receptors. Vitam. Horm. 82, 167-184.

Boje, K.M., Arora, P.K., 1992. Microglial-produced nitric oxide and reactive nitrogen oxides mediate neuronal cell death. Brain Res. 587, 250-256.

Bolignano, D., Donato, V., Coppolino, G., Campo, S., Buemi, A., Lacquaniti, A., Buemi, M., 2008. Neutrophil gelatinase-associated lipocalin (NGAL) as a marker of kidney damage. Am. J. Kidney Dis. 52, 595-605.

Bolignano, D., Coppolino, G., Donato, V., Lacquaniti, A., Bono, C., Buemi, M., 2010a. Neutrophil gelatinase-associated lipocalin (NGAL): a new piece of the anemia puzzle? Med Sci Monit 16, RA131-135.

Bolignano, D., Donato, V., Lacquaniti, A., Fazio, M.R., Bono, C., Coppolino, G., Buemi, M., 2010b. Neutrophil gelatinase-associated lipocalin (NGAL) in human neoplasias: a new protein enters the scene. Cancer Lett. 288, 10-16.

Bong, J.J., Seol, M.B., Kim, H.H., Han, O., Back, K., Baik, M., 2004. The 24p3 gene is induced during involution of the mammary gland and induces apoptosis of mammary epithelial cells. Mol. Cells 17, 29-34.

Bonow, R.H., Aid, S., Zhang, Y., Becker, K.G., Bosetti, F., 2009. The brain expression of genes involved in inflammatory response, the ribosome, and learning and memory is altered by centrally injected lipopolysaccharide in mice. Pharmacogenomics J 9, 116-126.

Borkham-Kamphorst, E., Drews, F., Weiskirchen, R., 2011. Induction of lipocalin-2 expression in acute and chronic experimental liver injury moderated by pro-inflammatory cytokines interleukin-1beta through nuclear factor-kappaB activation. Liver Int 31, 656-665.

Borner, C., 2003. The Bcl-2 protein family: sensors and checkpoints for life-or-death decisions. Mol. Immunol. 39, 615-647.

Braughler, J.M., Duncan, L.A., Chase, R.L., 1986. The involvement of iron in lipid peroxidation. Importance of ferric to ferrous ratios in initiation. J. Biol. Chem. 261, 10282-10289.

Braun, V., Killmann, H., 1999. Bacterial solutions to the iron-supply problem. Trends Biochem. Sci. 24, 104-109.

Bundgaard, J.R., Sengelov, H., Borregaard, N., Kjeldsen, L., 1994. Molecular cloning and expression of a cDNA encoding NGAL: a lipocalin expressed in human neutrophils. Biochem. Biophys. Res. Commun. 202, 1468-1475.

Calne, D.B., Hochberg, F.H., Snow, B.J., Nygaard, T., 1992. Theories of neurodegeneration. Ann. N. Y. Acad. Sci. 648, 1-5.

Candelario-Jalil, E., Al-Dalain, S.M., Castillo, R., Martinez, G., Fernandez, O.S., 2001. Selective vulnerability to kainate-induced oxidative damage in different rat brain regions. J. Appl. Toxicol. 21, 403-407.

Carro, E., Spuch, C., Trejo, J.L., Antequera, D., Torres-Aleman, I., 2005. Choroid plexus megalin is involved in neuroprotection by serum insulin-like growth factor I. J. Neurosci. 25, 10884-10893.

Ceciliani, F., Giordano, A., Spagnolo, V., 2002. The systemic reaction during inflammation: the acute-phase proteins. Protein Pept Lett 9, 211-223.

Chan, Y.L., Paz, V., Wool, I.G., 1988. The primary structure of rat alpha 2 mu globulin-related protein. Nucleic Acids Res 16, 11368.

Cheng, E.H., Wei, M.C., Weiler, S., Flavell, R.A., Mak, T.W., Lindsten, T., Korsmeyer, S.J., 2001. BCL-2, BCL-X(L) sequester BH3 domain-only molecules preventing BAX- and BAK-mediated mitochondrial apoptosis. Mol. Cell 8, 705-711.

Chia, W.J., Dawe, G.S., Ong, W.Y., 2011. Expression and localization of the iron-siderophore binding protein lipocalin 2 in the normal rat brain and after kainate-induced excitotoxicity. Neurochem. Int.

Cho, M., 2010. Focus on neurodegeneration. Nat. Neurosci. 13, 787.

Choi, S.H., Langenbach, R., Bosetti, F., 2008. Genetic deletion or pharmacological inhibition of cyclooxygenase-1 attenuate lipopolysaccharide-induced inflammatory response and brain injury. FASEB J. 22, 1491-1501.

Christensen, E.I., Birn, H., 2001. Megalin and cubilin: synergistic endocytic receptors in renal proximal tubule. Am J Physiol Renal Physiol 280, F562-573.

Christensen, E.I., Birn, H., 2002. Megalin and cubilin: multifunctional endocytic receptors. Nat Rev Mol Cell Biol 3, 256-266.

Chu, S.T., Lee, Y.C., Nein, K.M., Chen, Y.H., 2000. Expression, immunolocalization and sperm-association of a protein derived from 24p3 gene in mouse epididymis. Mol. Reprod. Dev. 57, 26-36.

Chung, H., Chung, H.Y., Bae, C.W., Kim, C.J., Park, S., 2011. Ghrelin suppresses tunicamycin- or thapsigargin-triggered endoplasmic reticulum stress-mediated apoptosis in primary cultured rat cortical neuronal cells. Endocr. J. 58, 409-420.

Clifton, M.C., Corrent, C., Strong, R.K., 2009. Siderocalins: siderophore-binding proteins of the innate immune system. Biometals 22, 557-564.

Coles, M., Diercks, T., Muehlenweg, B., Bartsch, S., Zolzer, V., Tschesche, H., Kessler, H., 1999. The solution structure and dynamics of human neutrophil gelatinase-associated lipocalin. J. Mol. Biol. 289, 139-157.

Connor, J.R., Boeshore, K.L., Benkovic, S.A., Menzies, S.L., 1994. Isoforms of ferritin have a specific cellular distribution in the brain. J. Neurosci. Res. 37, 461-465.

Conrotto, P., Roesli, C., Rybak, J., Kischel, P., Waltregny, D., Neri, D., Castronovo, V., 2008. Identification of new accessible tumor antigens in human colon cancer by ex vivo protein biotinylation and comparative mass spectrometry analysis. Int. J. Cancer 123, 2856-2864.

Coyle, J.T., 1987. Kainic acid: insights into excitatory mechanisms causing selective neuronal degeneration. Ciba Found. Symp. 126, 186-203.

Danial, N.N., 2007. BCL-2 family proteins: critical checkpoints of apoptotic cell death. Clin. Cancer Res. 13, 7254-7263.

Davis, E.J., Foster, T.D., Thomas, W.E., 1994. Cellular forms and functions of brain microglia. Brain Res. Bull. 34, 73-78.

Davis, T.R., Tabatabai, L., Bruns, K., Hamilton, R.T., Nilsen-Hamilton, M., 1991. Basic fibroblast growth factor induces 3T3 fibroblasts to synthesize and

secrete a cyclophilin-like protein and beta 2-microglobulin. Biochim. Biophys. Acta 1095, 145-152.

Deane, R., Wu, Z., Sagare, A., Davis, J., Du Yan, S., Hamm, K., Xu, F., Parisi, M., LaRue, B., Hu, H.W., Spijkers, P., Guo, H., Song, X., Lenting, P.J., Van Nostrand, W.E., Zlokovic, B.V., 2004. LRP/amyloid beta-peptide interaction mediates differential brain efflux of Abeta isoforms. Neuron 43, 333-344.

Devireddy, L.R., Teodoro, J.G., Richard, F.A., Green, M.R., 2001. Induction of apoptosis by a secreted lipocalin that is transcriptionally regulated by IL-3 deprivation. Science 293, 829-834.

Devireddy, L.R., Gazin, C., Zhu, X., Green, M.R., 2005. A cell-surface receptor for lipocalin 24p3 selectively mediates apoptosis and iron uptake. Cell 123, 1293-1305.

Devireddy, L.R., Hart, D.O., Goetz, D.H., Green, M.R., 2010. A mammalian siderophore synthesized by an enzyme with a bacterial homolog involved in enterobactin production. Cell 141, 1006-1017.

Dietrich, M.O., Spuch, C., Antequera, D., Rodal, I., de Yebenes, J.G., Molina, J.A., Bermejo, F., Carro, E., 2008. Megalin mediates the transport of leptin across the blood-CSF barrier. Neurobiol. Aging 29, 902-912.

Ding, M., Haglid, K.G., Hamberger, A., 2000. Quantitative immunochemistry on neuronal loss, reactive gliosis and BBB damage in cortex/striatum and hippocampus/amygdala after systemic kainic acid administration. Neurochem. Int. 36, 313-318.

Dittrich, A.M., Krokowski, M., Meyer, H.A., Quarcoo, D., Avagyan, A., Ahrens, B., Kube, S.M., Witzenrath, M., Loddenkemper, C., Cowland, J.B., Hamelmann, E., 2010. Lipocalin2 protects against airway inflammation and hyperresponsiveness in a murine model of allergic airway disease. Clin. Exp. Allergy 40, 1689-1700.

Doble, A., 1999. The role of excitotoxicity in neurodegenerative disease: implications for therapy. Pharmacol. Ther. 81, 163-221.

Dykens, J.A., Stern, A., Trenkner, E., 1987. Mechanism of kainate toxicity to cerebellar neurons in vitro is analogous to reperfusion tissue injury. J. Neurochem. 49, 1222-1228.

Elangovan, N., Lee, Y.C., Tzeng, W.F., Chu, S.T., 2004. Delivery of ferric ion to mouse spermatozoa is mediated by lipocalin internalization. Biochem. Biophys. Res. Commun. 319, 1096-1104.

Elder, G.A., Gama Sosa, M.A., De Gasperi, R., 2010. Transgenic mouse models of Alzheimer's disease. Mt. Sinai J. Med. 77, 69-81.

Ellison, R.T., 3rd, 1994. The effects of lactoferrin on gram-negative bacteria. Adv. Exp. Med. Biol. 357, 71-90.

Fernandez, C.A., Yan, L., Louis, G., Yang, J., Kutok, J.L., Moses, M.A., 2005. The matrix metalloproteinase-9/neutrophil gelatinase-associated lipocalin complex plays a role in breast tumor growth and is present in the urine of breast cancer patients. Clin. Cancer Res. 11, 5390-5395.

Filipkowski, R.K., Hetman, M., Kaminska, B., Kaczmarek, L., 1994. DNA fragmentation in rat brain after intraperitoneal administration of kainate. Neuroreport 5, 1538-1540.

Fischbach, M.A., Lin, H., Zhou, L., Yu, Y., Abergel, R.J., Liu, D.R., Raymond, K.N., Wanner, B.L., Strong, R.K., Walsh, C.T., Aderem, A., Smith, K.D., 2006. The pathogen-associated iroA gene cluster mediates bacterial evasion of lipocalin 2. Proc. Natl. Acad. Sci. U. S. A. 103, 16502-16507.

Flo, T.H., Smith, K.D., Sato, S., Rodriguez, D.J., Holmes, M.A., Strong, R.K., Akira, S., Aderem, A., 2004. Lipocalin 2 mediates an innate immune response to bacterial infection by sequestrating iron. Nature 432, 917-921.

Flower, D.R., North, A.C., Attwood, T.K., 1991. Mouse oncogene protein 24p3 is a member of the lipocalin protein family. Biochem. Biophys. Res. Commun. 180, 69-74.

Flower, D.R., North, A.C., Attwood, T.K., 1993. Structure and sequence relationships in the lipocalins and related proteins. Protein Sci. 2, 753-761.

Flower, D.R., 1994. The lipocalin protein family: a role in cell regulation. FEBS Lett. 354, 7-11.

Flower, D.R., 1996. The lipocalin protein family: structure and function. Biochem. J. 318 (Pt 1), 1-14.

Fluckinger, M., Haas, H., Merschak, P., Glasgow, B.J., Redl, B., 2004. Human tear lipocalin exhibits antimicrobial activity by scavenging microbial siderophores. Antimicrob. Agents Chemother. 48, 3367-3372.

Frotscher, M., Leranth, C., 1988. Catecholaminergic innervation of pyramidal and GABAergic nonpyramidal neurons in the rat hippocampus. Double label immunostaining with antibodies against tyrosine hydroxylase and glutamate decarboxylase. Histochemistry 88, 313-319.

Furutani, M., Arii, S., Mizumoto, M., Kato, M., Imamura, M., 1998. Identification of a neutrophil gelatinase-associated lipocalin mRNA in human pancreatic cancers using a modified signal sequence trap method. Cancer Lett. 122, 209-214.

Gabay, C., Kushner, I., 1999. Acute-phase proteins and other systemic responses to inflammation. N. Engl. J. Med. 340, 448-454.

Gajera, C.R., Emich, H., Lioubinski, O., Christ, A., Beckervordersandforth-Bonk, R., Yoshikawa, K., Bachmann, S., Christensen, E.I., Gotz, M., Kempermann, G., Peterson, A.S., Willnow, T.E., Hammes, A., 2010. LRP2 in ependymal cells regulates BMP signaling in the adult neurogenic niche. J. Cell Sci. 123, 1922-1930.

Gibbons, H.M., Dragunow, M., 2006. Microglia induce neural cell death via a proximity-dependent mechanism involving nitric oxide. Brain Res. 1084, 1-15.

Gliemann, J., 1998. Receptors of the low density lipoprotein (LDL) receptor family in man. Multiple functions of the large family members via interaction with complex ligands. Biol. Chem. 379, 951-964.

Gluck, M.R., Jayatilleke, E., Shaw, S., Rowan, A.J., Haroutunian, V., 2000. CNS oxidative stress associated with the kainic acid rodent model of experimental epilepsy. Epilepsy Res. 39, 63-71.

Godinez, I., Haneda, T., Raffatellu, M., George, M.D., Paixao, T.A., Rolan, H.G., Santos, R.L., Dandekar, S., Tsolis, R.M., Baumler, A.J., 2008. T cells help to amplify inflammatory responses induced by Salmonella enterica serotype Typhimurium in the intestinal mucosa. Infect. Immun. 76, 2008-2017.

Goetz, D.H., Willie, S.T., Armen, R.S., Bratt, T., Borregaard, N., Strong, R.K., 2000. Ligand preference inferred from the structure of neutrophil gelatinase associated lipocalin. Biochemistry (Mosc). 39, 1935-1941.

Goetz, D.H., Holmes, M.A., Borregaard, N., Bluhm, M.E., Raymond, K.N., Strong, R.K., 2002. The neutrophil lipocalin NGAL is a bacteriostatic agent that interferes with siderophore-mediated iron acquisition. Mol. Cell 10, 1033-1043.

Graham, T.E., Yang, Q., Bluher, M., Hammarstedt, A., Ciaraldi, T.P., Henry, R.R., Wason, C.J., Oberbach, A., Jansson, P.A., Smith, U., Kahn, B.B., 2006. Retinol-binding protein 4 and insulin resistance in lean, obese, and diabetic subjects. N. Engl. J. Med. 354, 2552-2563.

Greenamyre, J.T., Olson, J.M., Penney, J.B., Jr., Young, A.B., 1985. Autoradiographic characterization of N-methyl-D-aspartate-, quisqualate- and kainate-sensitive glutamate binding sites. J. Pharmacol. Exp. Ther. 233, 254-263.

Grigoryev, D.N., Liu, M., Hassoun, H.T., Cheadle, C., Barnes, K.C., Rabb, H., 2008. The local and systemic inflammatory transcriptome after acute kidney injury. J. Am. Soc. Nephrol. 19, 547-558.

Groticke, I., Hoffmann, K., Loscher, W., 2008. Behavioral alterations in a mouse model of temporal lobe epilepsy induced by intrahippocampal injection of kainate. Exp. Neurol. 213, 71-83.

Gruenthal, M., Armstrong, D.R., Ault, B., Nadler, J.V., 1986. Comparison of seizures and brain lesions produced by intracerebroventricular kainic acid and bicuculline methiodide. Exp. Neurol. 93, 621-630.

Gruzman, A., Wood, W.L., Alpert, E., Prasad, M.D., Miller, R.G., Rothstein, J.D., Bowser, R., Hamilton, R., Wood, T.D., Cleveland, D.W., Lingappa, V.R., Liu, J., 2007. Common molecular signature in SOD1 for both sporadic and familial amyotrophic lateral sclerosis. Proc. Natl. Acad. Sci. U. S. A. 104, 12524-12529.

Gullberg, M., Gustafsdottir, S.M., Schallmeiner, E., Jarvius, J., Bjarnegard, M., Betsholtz, C., Landegren, U., Fredriksson, S., 2004. Cytokine detection by antibody-based proximity ligation. Proc. Natl. Acad. Sci. U. S. A. 101, 8420-8424.

Guo, K., Lukacik, P., Papagrigoriou, E., Meier, M., Lee, W.H., Adamski, J., Oppermann, U., 2006. Characterization of human DHRS6, an orphan short chain dehydrogenase/reductase enzyme: a novel, cytosolic type 2 R-beta-hydroxybutyrate dehydrogenase. J. Biol. Chem. 281, 10291-10297.

Gupta, R.A., Brockman, J.A., Sarraf, P., Willson, T.M., DuBois, R.N., 2001. Target genes of peroxisome proliferator-activated receptor gamma in colorectal cancer cells. J. Biol. Chem. 276, 29681-29687.

Gustafsdottir, S.M., Schallmeiner, E., Fredriksson, S., Gullberg, M., Soderberg, O., Jarvius, M., Jarvius, J., Howell, M., Landegren, U., 2005. Proximity ligation assays for sensitive and specific protein analyses. Anal. Biochem. 345, 2-9.

Halaas, O., Steigedal, M., Haug, M., Awuh, J.A., Ryan, L., Brech, A., Sato, S., Husebye, H., Cangelosi, G.A., Akira, S., Strong, R.K., Espevik, T., Flo, T.H., 2010. Intracellular Mycobacterium avium intersect transferrin in the Rab11(+) recycling endocytic pathway and avoid lipocalin 2 trafficking to the lysosomal pathway. J. Infect. Dis. 201, 783-792.

Halliwell, B., Gutteridge, J.M., 1985. The importance of free radicals and catalytic metal ions in human diseases. Mol. Aspects Med. 8, 89-193.

Halliwell, B., 1992. Reactive oxygen species and the central nervous system. J. Neurochem. 59, 1609-1623.

Hamilton, R.T., Nilsen-Hamilton, M., Adams, G., 1985. Superinduction by cycloheximide of mitogen-induced secreted proteins produced by Balb/c 3T3 cells. J. Cell. Physiol. 123, 201-208.

Hammad, S.M., Ranganathan, S., Loukinova, E., Twal, W.O., Argraves, W.S., 1997. Interaction of apolipoprotein J-amyloid beta-peptide complex with low density lipoprotein receptor-related protein-2/megalin. A mechanism to prevent pathological accumulation of amyloid beta-peptide. J. Biol. Chem. 272, 18644-18649.

Han, C., Nam, M.K., Park, H.J., Seong, Y.M., Kang, S., Rhim, H., 2008. Tunicamycin-induced ER stress upregulates the expression of mitochondrial HtrA2 and promotes apoptosis through the cytosolic release of HtrA2. J Microbiol Biotechnol 18, 1197-1202.

Han, H., Bearss, D.J., Browne, L.W., Calaluce, R., Nagle, R.B., Von Hoff, D.D., 2002. Identification of differentially expressed genes in pancreatic cancer cells using cDNA microarray. Cancer Res. 62, 2890-2896.

Hanai, J., Mammoto, T., Seth, P., Mori, K., Karumanchi, S.A., Barasch, J., Sukhatme, V.P., 2005. Lipocalin 2 diminishes invasiveness and metastasis of Ras-transformed cells. J. Biol. Chem. 280, 13641-13647.

Harrison, P.M., Arosio, P., 1996. The ferritins: molecular properties, iron storage function and cellular regulation. Biochim. Biophys. Acta 1275, 161-203.

Herb, A., Burnashev, N., Werner, P., Sakmann, B., Wisden, W., Seeburg, P.H., 1992. The KA-2 subunit of excitatory amino acid receptors shows widespread expression in brain and forms ion channels with distantly related subunits. Neuron 8, 775-785.

Hider, R.C., Kong, X., 2010. Chemistry and biology of siderophores. Nat. Prod. Rep. 27, 637-657.

Hraba-Renevey, S., Turler, H., Kress, M., Salomon, C., Weil, R., 1989. SV40-induced expression of mouse gene 24p3 involves a post-transcriptional mechanism. Oncogene 4, 601-608.

Huang, E., Ong, W.Y., 2005. Distribution of ferritin in the rat hippocampus after kainate-induced neuronal injury. Exp. Brain Res. 161, 502-511.

Hvidberg, V., Jacobsen, C., Strong, R.K., Cowland, J.B., Moestrup, S.K., Borregaard, N., 2005. The endocytic receptor megalin binds the iron transporting neutrophil-gelatinase-associated lipocalin with high affinity and mediates its cellular uptake. FEBS Lett. 579, 773-777.

Iannetti, A., Pacifico, F., Acquaviva, R., Lavorgna, A., Crescenzi, E., Vascotto, C., Tell, G., Salzano, A.M., Scaloni, A., Vuttariello, E., Chiappetta, G., Formisano, S., Leonardi, A., 2008. The neutrophil gelatinase-associated lipocalin (NGAL), a NF-kappaB-regulated gene, is a survival factor for thyroid neoplastic cells. Proc. Natl. Acad. Sci. U. S. A. 105, 14058-14063.

Ip, J.P., Nocon, A.L., Hofer, M.J., Lim, S.L., Muller, M., Campbell, I.L., 2011. Lipocalin 2 in the central nervous system host response to systemic lipopolysaccharide administration. J Neuroinflammation 8, 124.

Jarrard, L.E., 2002. Use of excitotoxins to lesion the hippocampus: update. Hippocampus 12, 405-414.

Jellinger, K.A., 2003. General aspects of neurodegeneration. J. Neural Transm. Suppl., 101-144.

Jellinger, K.A., 2009. Recent advances in our understanding of neurodegeneration. J. Neural Transm. 116, 1111-1162.

Jellinger, K.A., 2010. Basic mechanisms of neurodegeneration: a critical update. J Cell Mol Med 14, 457-487.

Jeohn, G.H., Kong, L.Y., Wilson, B., Hudson, P., Hong, J.S., 1998. Synergistic neurotoxic effects of combined treatments with cytokines in murine primary mixed neuron/glia cultures. J. Neuroimmunol. 85, 1-10.

Jorgensen, M.B., Finsen, B.R., Jensen, M.B., Castellano, B., Diemer, N.H., Zimmer, J., 1993. Microglial and astroglial reactions to ischemic and kainic acid-induced lesions of the adult rat hippocampus. Exp. Neurol. 120, 70-88.

Joshi, J.G., Fleming, J.T., Dhar, M., Chauthaiwale, V., 1995. A novel ferritin heavy chain messenger ribonucleic acid in the human brain. J. Neurol. Sci. 134 Suppl, 52-56.

Jurado, R.L., 1997. Iron, infections, and anemia of inflammation. Clin. Infect. Dis. 25, 888-895.

Kaminska, B., Filipkowski, R.K., Zurkowska, G., Lason, W., Przewlocki, R., Kaczmarek, L., 1994. Dynamic changes in the composition of the AP-1 transcription factor DNA-binding activity in rat brain following kainate-induced seizures and cell death. Eur. J. Neurosci. 6, 1558-1566.

Kaneta, Y., Kagami, Y., Tsunoda, T., Ohno, R., Nakamura, Y., Katagiri, T., 2003. Genome-wide analysis of gene-expression profiles in chronic myeloid leukemia cells using a cDNA microarray. Int. J. Oncol. 23, 681-691.

Kehrer, J.P., 2010. Lipocalin-2: pro- or anti-apoptotic? Cell Biol. Toxicol. 26, 83-89.

Kerjaschki, D., Farquhar, M.G., 1982. The pathogenic antigen of Heymann nephritis is a membrane glycoprotein of the renal proximal tubule brush border. Proc. Natl. Acad. Sci. U. S. A. 79, 5557-5561.

Kerjaschki, D., Farquhar, M.G., 1983. Immunocytochemical localization of the Heymann nephritis antigen (GP330) in glomerular epithelial cells of normal Lewis rats. J. Exp. Med. 157, 667-686.

Kerjaschki, D., Noronha-Blob, L., Sacktor, B., Farquhar, M.G., 1984. Microdomains of distinctive glycoprotein composition in the kidney proximal tubule brush border. J. Cell Biol. 98, 1505-1513.

Kjeldsen, L., Johnsen, A.H., Sengelov, H., Borregaard, N., 1993. Isolation and primary structure of NGAL, a novel protein associated with human neutrophil gelatinase. J. Biol. Chem. 268, 10425-10432.

Kjeldsen, L., Bainton, D.F., Sengelov, H., Borregaard, N., 1994. Identification of neutrophil gelatinase-associated lipocalin as a novel matrix protein of specific granules in human neutrophils. Blood 83, 799-807.

Kjeldsen, L., Cowland, J.B., Borregaard, N., 2000. Human neutrophil gelatinase-associated lipocalin and homologous proteins in rat and mouse. Biochim. Biophys. Acta 1482, 272-283.

Klausen, P., Niemann, C.U., Cowland, J.B., Krabbe, K., Borregaard, N., 2005. On mouse and man: neutrophil gelatinase associated lipocalin is not involved in apoptosis or acute response. Eur. J. Haematol. 75, 332-340.

Kneussel, M., Brandstatter, J.H., Laube, B., Stahl, S., Muller, U., Betz, H., 1999. Loss of postsynaptic GABA(A) receptor clustering in gephyrin-deficient mice. J. Neurosci. 19, 9289-9297.

Koepsell, H., Busch, A., Gorboulev, V., Arndt, P., 1998. Structure and Function of Renal Organic Cation Transporters. News Physiol Sci 13, 11-16.

Kohler, C., Schwarcz, R., Fuxe, K., 1979. Intrahippocampal injections of ibotenic acid provide histological evidence for a neurotoxic mechanism different from kainic acid. Neurosci. Lett. 15, 223-228.

Korhonen, L., Belluardo, N., Mudo, G., Lindholm, D., 2003. Increase in Bcl-2 phosphorylation and reduced levels of BH3-only Bcl-2 family proteins in kainic acid-mediated neuronal death in the rat brain. Eur. J. Neurosci. 18, 1121-1134.

Kounnas, M.Z., Haudenschild, C.C., Strickland, D.K., Argraves, W.S., 1994. Immunological localization of glycoprotein 330, low density lipoprotein receptor related protein and 39 kDa receptor associated protein in embryonic mouse tissues. In Vivo 8, 343-351.

Kubben, F.J., Sier, C.F., Hawinkels, L.J., Tschesche, H., van Duijn, W., Zuidwijk, K., van der Reijden, J.J., Hanemaaijer, R., Griffioen, G., Lamers, C.B., Verspaget, H.W., 2007. Clinical evidence for a protective role of lipocalin-2 against MMP-9 autodegradation and the impact for gastric cancer. Eur. J. Cancer 43, 1869-1876.

Lee, S., Lee, J., Kim, S., Park, J.Y., Lee, W.H., Mori, K., Kim, S.H., Kim, I.K., Suk, K., 2007. A dual role of lipocalin 2 in the apoptosis and deramification of activated microglia. J. Immunol. 179, 3231-3241.

Lee, S., Park, J.Y., Lee, W.H., Kim, H., Park, H.C., Mori, K., Suk, K., 2009. Lipocalin-2 is an autocrine mediator of reactive astrocytosis. J. Neurosci. 29, 234-249.

Lee, S., Lee, W.H., Lee, M.S., Mori, K., Suk, K., 2011. Regulation by lipocalin-2 of neuronal cell death, migration, and morphology. J. Neurosci. Res.

Lee, Y.C., Liao, C., Jr., Li, P.T., Tzeng, W.F., Chu, S.T., 2003. Mouse lipocalin as an enhancer of spermatozoa motility. Mol. Biol. Rep. 30, 165-172.

Lee, Y.C., Elangovan, N., Tzeng, W.F., Chu, S.T., 2005. Mouse uterine 24p3 protein as a suppressor of sperm acrosome reaction. Mol. Biol. Rep. 32, 237-245.

Leheste, J.R., Rolinski, B., Vorum, H., Hilpert, J., Nykjaer, A., Jacobsen, C., Aucouturier, P., Moskaug, J.O., Otto, A., Christensen, E.I., Willnow, T.E., 1999. Megalin knockout mice as an animal model of low molecular weight proteinuria. Am. J. Pathol. 155, 1361-1370.

Li, C., Chan, Y.R., 2011. Lipocalin 2 regulation and its complex role in inflammation and cancer. Cytokine.

Li, J.Y., Ram, G., Gast, K., Chen, X., Barasch, K., Mori, K., Schmidt-Ott, K., Wang, J., Kuo, H.C., Savage-Dunn, C., Garrick, M.D., Barasch, J., 2004. Detection of intracellular iron by its regulatory effect. Am J Physiol Cell Physiol 287, C1547-1559.

Lim, R., Ahmed, N., Borregaard, N., Riley, C., Wafai, R., Thompson, E.W., Quinn, M.A., Rice, G.E., 2007. Neutrophil gelatinase-associated lipocalin (NGAL) an early-screening biomarker for ovarian cancer: NGAL is associated with

epidermal growth factor-induced epithelio-mesenchymal transition. Int. J. Cancer 120, 2426-2434.

Liu, J., Duncan, K., Walsh, C.T., 1989. Nucleotide sequence of a cluster of Escherichia coli enterobactin biosynthesis genes: identification of entA and purification of its product 2,3-dihydro-2,3-dihydroxybenzoate dehydrogenase. J. Bacteriol. 171, 791-798.

Liu, Q., Nilsen-Hamilton, M., 1995. Identification of a new acute phase protein. J. Biol. Chem. 270, 22565-22570.

Livak, K.J., Schmittgen, T.D., 2001. Analysis of relative gene expression data using real-time quantitative PCR and the 2(-Delta Delta C(T)) Method. Methods 25, 402-408.

MacManus, J.P., Graber, T., Luebbert, C., Preston, E., Rasquinha, I., Smith, B., Webster, J., 2004. Translation-state analysis of gene expression in mouse brain after focal ischemia. J. Cereb. Blood Flow Metab. 24, 657-667.

Madoz-Gurpide, J., Lopez-Serra, P., Martinez-Torrecuadrada, J.L., Sanchez, L., Lombardia, L., Casal, J.I., 2006. Proteomics-based validation of genomic data: applications in colorectal cancer diagnosis. Mol Cell Proteomics 5, 1471-1483.

Malva, J.O., Carvalho, A.P., Carvalho, C.M., 1998. Kainate receptors in hippocampal CA3 subregion: evidence for a role in regulating neurotransmitter release. Neurochem. Int. 32, 1-6.

Marques, F., Rodrigues, A.J., Sousa, J.C., Coppola, G., Geschwind, D.H., Sousa, N., Correia-Neves, M., Palha, J.A., 2008. Lipocalin 2 is a choroid plexus acute-phase protein. J. Cereb. Blood Flow Metab. 28, 450-455.

Martineau, A.R., Newton, S.M., Wilkinson, K.A., Kampmann, B., Hall, B.M., Nawroly, N., Packe, G.E., Davidson, R.N., Griffiths, C.J., Wilkinson, R.J., 2007. Neutrophil-mediated innate immune resistance to mycobacteria. J. Clin. Invest. 117, 1988-1994.

Marzolo, M.P., Farfan, P., 2011. New insights into the roles of megalin/LRP2 and the regulation of its functional expression. Biol. Res. 44, 89-105.

McCarthy, R.A., Barth, J.L., Chintalapudi, M.R., Knaak, C., Argraves, W.S., 2002. Megalin functions as an endocytic sonic hedgehog receptor. J. Biol. Chem. 277, 25660-25667.

McGeer, P.L., McGeer, E.G., 1982. Kainic acid: The neurotoxic breakthrough. Crit. Rev. Toxicol. 10, 1-26.

McNeill, A., Chinnery, P.F., 2011. Neurodegeneration with brain iron accumulation. Handb Clin Neurol 100, 161-172.

Meldrum, B.S., 2000. Glutamate as a neurotransmitter in the brain: review of physiology and pathology. J. Nutr. 130, 1007S-1015S.

Miharada, K., Hiroyama, T., Sudo, K., Nagasawa, T., Nakamura, Y., 2005. Lipocalin 2 functions as a negative regulator of red blood cell production in an autocrine fashion. FASEB J. 19, 1881-1883.

Miharada, K., Hiroyama, T., Sudo, K., Danjo, I., Nagasawa, T., Nakamura, Y., 2008. Lipocalin 2-mediated growth suppression is evident in human erythroid and monocyte/macrophage lineage cells. J. Cell. Physiol. 215, 526-537.

Mishra, J., Mori, K., Ma, Q., Kelly, C., Yang, J., Mitsnefes, M., Barasch, J., Devarajan, P., 2004. Amelioration of ischemic acute renal injury by neutrophil gelatinase-associated lipocalin. J. Am. Soc. Nephrol. 15, 3073-3082.

Mitchell, J., Sundstrom, L.E., Wheal, H.V., 1993. Microglial and astrocytic cell responses in the rat hippocampus after an intracerebroventricular kainic acid injection. Exp. Neurol. 121, 224-230.

Mokin, M., Keifer, J., 2006. Quantitative analysis of immunofluorescent punctate staining of synaptically localized proteins using confocal microscopy and stereology. J. Neurosci. Methods 157, 218-224.

Morais Cabral, J.H., Atkins, G.L., Sanchez, L.M., Lopez-Boado, Y.S., Lopez-Otin, C., Sawyer, L., 1995. Arachidonic acid binds to apolipoprotein D: implications for the protein's function. FEBS Lett 366, 53-56.

Mori, K., Lee, H.T., Rapoport, D., Drexler, I.R., Foster, K., Yang, J., Schmidt-Ott, K.M., Chen, X., Li, J.Y., Weiss, S., Mishra, J., Cheema, F.H., Markowitz, G., Suganami, T., Sawai, K., Mukoyama, M., Kunis, C., D'Agati, V., Devarajan, P., Barasch, J., 2005. Endocytic delivery of lipocalin-siderophore-iron complex rescues the kidney from ischemia-reperfusion injury. J. Clin. Invest. 115, 610-621.

Morishima, N., Nakanishi, K., Tsuchiya, K., Shibata, T., Seiwa, E., 2004. Translocation of Bim to the endoplasmic reticulum (ER) mediates ER stress signaling for activation of caspase-12 during ER stress-induced apoptosis. J. Biol. Chem. 279, 50375-50381.

Morley, J.J., Kushner, I., 1982. Serum C-reactive protein levels in disease. Ann. N. Y. Acad. Sci. 389, 406-418.

Murphy, B.M., Engel, T., Paucard, A., Hatazaki, S., Mouri, G., Tanaka, K., Tuffy, L.P., Jimenez-Mateos, E.M., Woods, I., Dunleavy, M., Bonner, H.P., Meller, R., Simon, R.P., Strasser, A., Prehn, J.H., Henshall, D.C., 2010. Contrasting patterns of Bim induction and neuroprotection in Bim-deficient mice between hippocampus and neocortex after status epilepticus. Cell Death Differ. 17, 459-468.

Nadler, J.V., Perry, B.W., Cotman, C.W., 1978. Intraventricular kainic acid preferentially destroys hippocampal pyramidal cells. Nature 271, 676-677.

Nadler, J.V., Perry, B.W., Gentry, C., Cotman, C.W., 1980a. Degeneration of hippocampal CA3 pyramidal cells induced by intraventricular kainic acid. J. Comp. Neurol. 192, 333-359.

Nadler, J.V., Shelton, D.L., Perry, B.W., Cotman, C.W., 1980b. Regional distribution of [3H]kainic acid after intraventricular injection. Life Sci. 26, 133-138.

Nagy, G.G., Al-Ayyan, M., Andrew, D., Fukaya, M., Watanabe, M., Todd, A.J., 2004. Widespread expression of the AMPA receptor GluR2 subunit at glutamatergic synapses in the rat spinal cord and phosphorylation of GluR1 in response to noxious stimulation revealed with an antigen-unmasking method. J. Neurosci. 24, 5766-5777.

Nairz, M., Theurl, I., Ludwiczek, S., Theurl, M., Mair, S.M., Fritsche, G., Weiss, G., 2007. The co-ordinated regulation of iron homeostasis in murine macrophages limits the availability of iron for intracellular Salmonella typhimurium. Cell Microbiol 9, 2126-2140.

Nelson, A.M., Zhao, W., Gilliland, K.L., Zaenglein, A.L., Liu, W., Thiboutot, D.M., 2008. Neutrophil gelatinase-associated lipocalin mediates 13-cis retinoic acid-induced apoptosis of human sebaceous gland cells. J. Clin. Invest. 118, 1468-1478.

Nicholson, H., Anderson, B.F., Bland, T., Shewry, S.C., Tweedie, J.W., Baker, E.N., 1997. Mutagenesis of the histidine ligand in human lactoferrin: iron binding properties and crystal structure of the histidine-253-->methionine mutant. Biochemistry (Mosc). 36, 341-346.

Nilsen-Hamilton, M., Hamilton, R.T., Adams, G.A., 1982. Rapid selective stimulation by growth factors of the incorporation by BALB/C 3T3 cells of [35S]methionine into a glycoprotein and five superinducible proteins. Biochem. Biophys. Res. Commun. 108, 158-166.

Nishiyama, K., Kwak, S., Takekoshi, S., Watanabe, K., Kanazawa, I., 1996. In situ nick end-labeling detects necrosis of hippocampal pyramidal cells induced by kainic acid. Neurosci. Lett. 212, 139-142.

Nykjaer, A., Dragun, D., Walther, D., Vorum, H., Jacobsen, C., Herz, J., Melsen, F., Christensen, E.I., Willnow, T.E., 1999. An endocytic pathway essential for renal uptake and activation of the steroid 25-(OH) vitamin D3. Cell 96, 507-515.

O'Connor, L., Strasser, A., O'Reilly, L.A., Hausmann, G., Adams, J.M., Cory, S., Huang, D.C., 1998. Bim: a novel member of the Bcl-2 family that promotes apoptosis. EMBO J. 17, 384-395.

O'Reilly, L.A., Cullen, L., Visvader, J., Lindeman, G.J., Print, C., Bath, M.L., Huang, D.C., Strasser, A., 2000. The proapoptotic BH3-only protein bim is expressed in hematopoietic, epithelial, neuronal, and germ cells. Am. J. Pathol. 157, 449-461.

Ong, D.E., Newcomer, M.E., Lareyre, J.J., Orgebin-Crist, M.C., 2000. Epididymal retinoic acid-binding protein. Biochim. Biophys. Acta 1482, 209-217.

Ong, W.Y., Leong, S.K., Garey, L.J., Reynolds, R., Liang, A.W., 1996. An immunocytochemical study of glutamate receptors and glutamine synthetase

in the hippocampus of rats injected with kainate. Exp. Brain Res. 109, 251-267.

Ong, W.Y., He, Y., Suresh, S., Patel, S.C., 1997. Differential expression of apolipoprotein D and apolipoprotein E in the kainic acid-lesioned rat hippocampus. Neuroscience 79, 359-367.

Ong, W.Y., Ren, M.Q., Makjanic, J., Lim, T.M., Watt, F., 1999. A nuclear microscopic study of elemental changes in the rat hippocampus after kainate-induced neuronal injury. J. Neurochem. 72, 1574-1579.

Patel, R.C., Lange, D., McConathy, W.J., Patel, Y.C., Patel, S.C., 1997. Probing the structure of the ligand binding cavity of lipocalins by fluorescence spectroscopy. Protein Eng. 10, 621-625.

Patel, S., Meldrum, B.S., Collins, J.F., 1986. Distribution of [3H]kainic acid and binding sites in the rat brain: in vivo and in vitro receptor autoradiography. Neurosci. Lett. 70, 301-307.

Pollard, H., Cantagrel, S., Charriaut-Marlangue, C., Moreau, J., Ben Ari, Y., 1994a. Apoptosis associated DNA fragmentation in epileptic brain damage. Neuroreport 5, 1053-1055.

Pollard, H., Charriaut-Marlangue, C., Cantagrel, S., Represa, A., Robain, O., Moreau, J., Ben-Ari, Y., 1994b. Kainate-induced apoptotic cell death in hippocampal neurons. Neuroscience 63, 7-18.

Ponka, P., Beaumont, C., Richardson, D.R., 1998. Function and regulation of transferrin and ferritin. Semin. Hematol. 35, 35-54.

Portera-Cailliau, C., Price, D.L., Martin, L.J., 1997. Non-NMDA and NMDA receptor-mediated excitotoxic neuronal deaths in adult brain are morphologically distinct: further evidence for an apoptosis-necrosis continuum. J. Comp. Neurol. 378, 88-104.

Price, D.L., 1986. New perspectives on Alzheimer's disease. Annu. Rev. Neurosci. 9, 489-512.

Przedborski, S., Vila, M., Jackson-Lewis, V., 2003. Neurodegeneration: what is it and where are we? J. Clin. Invest. 111, 3-10.

Putcha, G.V., Moulder, K.L., Golden, J.P., Bouillet, P., Adams, J.A., Strasser, A., Johnson, E.M., 2001. Induction of BIM, a proapoptotic BH3-only BCL-2 family member, is critical for neuronal apoptosis. Neuron 29, 615-628.

Putcha, G.V., Le, S., Frank, S., Besirli, C.G., Clark, K., Chu, B., Alix, S., Youle, R.J., LaMarche, A., Maroney, A.C., Johnson, E.M., Jr., 2003. JNK-mediated BIM phosphorylation potentiates BAX-dependent apoptosis. Neuron 38, 899-914.

Puthalakath, H., Huang, D.C., O'Reilly, L.A., King, S.M., Strasser, A., 1999. The proapoptotic activity of the Bcl-2 family member Bim is regulated by interaction with the dynein motor complex. Mol. Cell 3, 287-296.

Puthalakath, H., O'Reilly, L.A., Gunn, P., Lee, L., Kelly, P.N., Huntington, N.D., Hughes, P.D., Michalak, E.M., McKimm-Breschkin, J., Motoyama, N., Gotoh, T., Akira, S., Bouillet, P., Strasser, A., 2007. ER stress triggers apoptosis by activating BH3-only protein Bim. Cell 129, 1337-1349.

Raffatellu, M., George, M.D., Akiyama, Y., Hornsby, M.J., Nuccio, S.P., Paixao, T.A., Butler, B.P., Chu, H., Santos, R.L., Berger, T., Mak, T.W., Tsolis, R.M., Bevins, C.L., Solnick, J.V., Dandekar, S., Baumler, A.J., 2009. Lipocalin-2 resistance confers an advantage to Salmonella enterica serotype Typhimurium for growth and survival in the inflamed intestine. Cell Host Microbe 5, 476-486.

Ratte, S., Lacaille, J.C., 2006. Selective degeneration and synaptic reorganization of hippocampal interneurons in a chronic model of temporal lobe epilepsy. Adv. Neurol. 97, 69-76.

Ravizza, T., Rizzi, M., Perego, C., Richichi, C., Veliskova, J., Moshe, S.L., De Simoni, M.G., Vezzani, A., 2005. Inflammatory response and glia activation in developing rat hippocampus after status epilepticus. Epilepsia 46 Suppl 5, 113-117.

Raymond, K.N., Dertz, E.A., Kim, S.S., 2003. Enterobactin: an archetype for microbial iron transport. Proc. Natl. Acad. Sci. U. S. A. 100, 3584-3588.

Reed, T.T., Pierce, W.M., Jr., Turner, D.M., Markesbery, W.R., Butterfield, D.A., 2009. Proteomic identification of nitrated brain proteins in early Alzheimer's disease inferior parietal lobule. J Cell Mol Med 13, 2019-2029.

Richardson, D.R., 2005. 24p3 and its receptor: dawn of a new iron age? Cell 123, 1175-1177.

Rizzi, M., Perego, C., Aliprandi, M., Richichi, C., Ravizza, T., Colella, D., Veliskova, J., Moshe, S.L., De Simoni, M.G., Vezzani, A., 2003. Glia activation and cytokine increase in rat hippocampus by kainic acid-induced status epilepticus during postnatal development. Neurobiol. Dis. 14, 494-503.

Rodriguez, N., Mages, J., Dietrich, H., Wantia, N., Wagner, H., Lang, R., Miethke, T., 2007. MyD88-dependent changes in the pulmonary transcriptome after infection with Chlamydia pneumoniae. Physiol Genomics 30, 134-145.

Rouault, T.A., 2001. Systemic iron metabolism: a review and implications for brain iron metabolism. Pediatr. Neurol. 25, 130-137.

Roudkenar, M.H., Halabian, R., Roushandeh, A.M., Nourani, M.R., Masroori, N., Ebrahimi, M., Nikogoftar, M., Rouhbakhsh, M., Bahmani, P., Najafabadi, A.J., Shokrgozar, M.A., 2009. Lipocalin 2 regulation by thermal stresses: protective role of Lcn2/NGAL against cold and heat stresses. Exp. Cell Res. 315, 3140-3151.

Sadrzadeh, S.M., Saffari, Y., 2004. Iron and brain disorders. Am. J. Clin. Pathol. 121 Suppl, S64-70.

Saiga, H., Nishimura, J., Kuwata, H., Okuyama, M., Matsumoto, S., Sato, S., Matsumoto, M., Akira, S., Yoshikai, Y., Honda, K., Yamamoto, M., Takeda, K., 2008. Lipocalin 2-dependent inhibition of mycobacterial growth in alveolar epithelium. J. Immunol. 181, 8521-8527.

Saito, A., Pietromonaco, S., Loo, A.K., Farquhar, M.G., 1994. Complete cloning and sequencing of rat gp330/"megalin," a distinctive member of the low density lipoprotein receptor gene family. Proc. Natl. Acad. Sci. U. S. A. 91, 9725-9729.

Santin, A.D., Zhan, F., Bellone, S., Palmieri, M., Cane, S., Bignotti, E., Anfossi, S., Gokden, M., Dunn, D., Roman, J.J., O'Brien, T.J., Tian, E., Cannon, M.J., Shaughnessy, J., Jr., Pecorelli, S., 2004. Gene expression profiles in primary ovarian serous papillary tumors and normal ovarian epithelium: identification of candidate molecular markers for ovarian cancer diagnosis and therapy. Int. J. Cancer 112, 14-25.

Sater, R.A., Nadler, J.V., 1988. On the relation between seizures and brain lesions after intracerebroventricular kainic acid. Neurosci. Lett. 84, 73-78.

Schaeffer, E.L., Figueiro, M., Gattaz, W.F., 2011. Insights into Alzheimer disease pathogenesis from studies in transgenic animal models. Clinics (Sao Paulo) 66 Suppl 1, 45-54.

Schmidt-Ott, K.M., Mori, K., Kalandadze, A., Li, J.Y., Paragas, N., Nicholas, T., Devarajan, P., Barasch, J., 2006. Neutrophil gelatinase-associated lipocalin-mediated iron traffic in kidney epithelia. Curr. Opin. Nephrol. Hypertens. 15, 442-449.

Schmidt-Ott, K.M., Mori, K., Li, J.Y., Kalandadze, A., Cohen, D.J., Devarajan, P., Barasch, J., 2007. Dual action of neutrophil gelatinase-associated lipocalin. J. Am. Soc. Nephrol. 18, 407-413.

Schwob, J.E., Fuller, T., Price, J.L., Olney, J.W., 1980. Widespread patterns of neuronal damage following systemic or intracerebral injections of kainic acid: a histological study. Neuroscience 5, 991-1014.

Shibata, M., Hattori, H., Sasaki, T., Gotoh, J., Hamada, J., Fukuuchi, Y., 2002. Temporal profiles of the subcellular localization of Bim, a BH3-only protein, during middle cerebral artery occlusion in mice. J. Cereb. Blood Flow Metab. 22, 810-820.

Shimohama, S., Sawada, H., Kitamura, Y., Taniguchi, T., 2003. Disease model: Parkinson's disease. Trends Mol Med 9, 360-365.

Shinoda, S., Schindler, C.K., Meller, R., So, N.K., Araki, T., Yamamoto, A., Lan, J.Q., Taki, W., Simon, R.P., Henshall, D.C., 2004. Bim regulation may determine hippocampal vulnerability after injurious seizures and in temporal lobe epilepsy. J. Clin. Invest. 113, 1059-1068.

Siegel, G.J., Agranoff, B.W., Albers, R.W., Fisher, S.K., Uhler, M.D., 1999. Basic Neurochemistry: Molecular, Cellular and Medical Aspects. Lippincott-Raven, Philadelphia.

Simon, H.U., Haj-Yehia, A., Levi-Schaffer, F., 2000. Role of reactive oxygen species (ROS) in apoptosis induction. Apoptosis 5, 415-418.

Smith, E.R., Zurakowski, D., Saad, A., Scott, R.M., Moses, M.A., 2008. Urinary biomarkers predict brain tumor presence and response to therapy. Clin. Cancer Res. 14, 2378-2386.

Sperk, G., Lassmann, H., Baran, H., Kish, S.J., Seitelberger, F., Hornykiewicz, O., 1983. Kainic acid induced seizures: neurochemical and histopathological changes. Neuroscience 10, 1301-1315.

Sperk, G., 1994. Kainic acid seizures in the rat. Prog. Neurobiol. 42, 1-32.

Spoelgen, R., Hammes, A., Anzenberger, U., Zechner, D., Andersen, O.M., Jerchow, B., Willnow, T.E., 2005. LRP2/megalin is required for patterning of the ventral telencephalon. Development 132, 405-414.

Stoll, G., Jander, S., 1999. The role of microglia and macrophages in the pathophysiology of the CNS. Prog. Neurobiol. 58, 233-247.

Streit, W.J., Walter, S.A., Pennell, N.A., 1999. Reactive microgliosis. Prog. Neurobiol. 57, 563-581.

Streit, W.J., 2000. Microglial response to brain injury: a brief synopsis. Toxicol. Pathol. 28, 28-30.

Suzuki, F., Junier, M.P., Guilhem, D., Sorensen, J.C., Onteniente, B., 1995. Morphogenetic effect of kainate on adult hippocampal neurons associated with a prolonged expression of brain-derived neurotrophic factor. Neuroscience 64, 665-674.

Szegezdi, E., Logue, S.E., Gorman, A.M., Samali, A., 2006. Mediators of endoplasmic reticulum stress-induced apoptosis. EMBO Rep 7, 880-885.

Tabuchi, M., Yoshimori, T., Yamaguchi, K., Yoshida, T., Kishi, F., 2000. Human NRAMP2/DMT1, which mediates iron transport across endosomal membranes, is localized to late endosomes and lysosomes in HEp-2 cells. J. Biol. Chem. 275, 22220-22228.

Theofilas, P., Bedner, P., Huttmann, K., Theis, M., Steinhauser, C., Frank, S., 2009. The proapoptotic BCL-2 homology domain 3-only protein Bim is not critical for acute excitotoxic cell death. J. Neuropathol. Exp. Neurol. 68, 102-110.

Thomas, M., Jankovic, J., 2004. Neurodegenerative disease and iron storage in the brain. Curr. Opin. Neurol. 17, 437-442.

Thorne, R.G., Pronk, G.J., Padmanabhan, V., Frey, W.H., 2nd, 2004. Delivery of insulin-like growth factor-I to the rat brain and spinal cord along olfactory and trigeminal pathways following intranasal administration. Neuroscience 127, 481-496.

Tillett, W.S., Francis, T., 1930. Serological reactions in pneumonia with a non-protein somatic fraction of Pneumococcus. J. Exp. Med. 52, 561-571.

Tokuhara, D., Sakuma, S., Hattori, H., Matsuoka, O., Yamano, T., 2007. Kainic acid dose affects delayed cell death mechanism after status epilepticus. Brain Dev. 29, 2-8.

Tong, Z., Wu, X., Kehrer, J.P., 2003. Increased expression of the lipocalin 24p3 as an apoptotic mechanism for MK886. Biochem. J. 372, 203-210.

Tong, Z., Wu, X., Ovcharenko, D., Zhu, J., Chen, C.S., Kehrer, J.P., 2005. Neutrophil gelatinase-associated lipocalin as a survival factor. Biochem. J. 391, 441-448.

Tong, Z., Kunnumakkara, A.B., Wang, H., Matsuo, Y., Diagaradjane, P., Harikumar, K.B., Ramachandran, V., Sung, B., Chakraborty, A., Bresalier, R.S., Logsdon, C., Aggarwal, B.B., Krishnan, S., Guha, S., 2008. Neutrophil gelatinase-associated lipocalin: a novel suppressor of invasion and angiogenesis in pancreatic cancer. Cancer Res. 68, 6100-6108.

Urade, Y., Hayaishi, O., 2000. Biochemical, structural, genetic, physiological, and pathophysiological features of lipocalin-type prostaglandin D synthase. Biochim. Biophys. Acta 1482, 259-271.

Villalva, C., Sorel, N., Bonnet, M.L., Guilhot, J., Mayeur-Rousse, C., Guilhot, F., Chomel, J.C., Turhan, A.G., 2008. Neutrophil gelatinase-associated lipocalin expression in chronic myeloid leukemia. Leuk. Lymphoma 49, 984-988.

Vogt, M., Skerra, A., 2001. Bacterially produced apolipoprotein D binds progesterone and arachidonic acid, but not bilirubin or E-3M2H. J. Mol. Recognit. 14, 79-86.

Wang, Q., Yu, S., Simonyi, A., Sun, G.Y., Sun, A.Y., 2005. Kainic acid-mediated excitotoxicity as a model for neurodegeneration. Mol. Neurobiol. 31, 3-16.

Wang, Y., Lam, K.S., Kraegen, E.W., Sweeney, G., Zhang, J., Tso, A.W., Chow, W.S., Wat, N.M., Xu, J.Y., Hoo, R.L., Xu, A., 2007. Lipocalin-2 is an inflammatory marker closely associated with obesity, insulin resistance, and hyperglycemia in humans. Clin. Chem. 53, 34-41.

Ward, T.R., Lutz, A., Parel, S.P., Ensling, J., Gutlich, P., Buglyo, P., Orvig, C., 1999. An Iron-Based Molecular Redox Switch as a Model for Iron Release from Enterobactin via the Salicylate Binding Mode. Inorg Chem 38, 5007-5017.

Wei, M.C., Zong, W.X., Cheng, E.H., Lindsten, T., Panoutsakopoulou, V., Ross, A.J., Roth, K.A., MacGregor, G.R., Thompson, C.B., Korsmeyer, S.J., 2001. Proapoptotic BAX and BAK: a requisite gateway to mitochondrial dysfunction and death. Science 292, 727-730.

Weibrecht, I., Leuchowius, K.J., Clausson, C.M., Conze, T., Jarvius, M., Howell, W.M., Kamali-Moghaddam, M., Soderberg, O., 2010. Proximity ligation assays: a recent addition to the proteomics toolbox. Expert Rev Proteomics 7, 401-409.

Whitfield, J., Neame, S.J., Paquet, L., Bernard, O., Ham, J., 2001. Dominant-negative c-Jun promotes neuronal survival by reducing BIM expression and inhibiting mitochondrial cytochrome c release. Neuron 29, 629-643.

Wicher, G., Larsson, M., Fex Svenningsen, A., Gyllencreutz, E., Rask, L., Aldskogius, H., 2006. Low density lipoprotein receptor-related protein-2/megalin is expressed in oligodendrocytes in the mouse spinal cord white matter. J. Neurosci. Res. 83, 864-873.

Willis, S., Day, C.L., Hinds, M.G., Huang, D.C., 2003. The Bcl-2-regulated apoptotic pathway. J. Cell Sci. 116, 4053-4056.

Willnow, T.E., Goldstein, J.L., Orth, K., Brown, M.S., Herz, J., 1992. Low density lipoprotein receptor-related protein and gp330 bind similar ligands, including plasminogen activator-inhibitor complexes and lactoferrin, an inhibitor of chylomicron remnant clearance. J. Biol. Chem. 267, 26172-26180.

Willnow, T.E., Hilpert, J., Armstrong, S.A., Rohlmann, A., Hammer, R.E., Burns, D.K., Herz, J., 1996. Defective forebrain development in mice lacking gp330/megalin. Proc. Natl. Acad. Sci. U. S. A. 93, 8460-8464.

Woo, J.S., Kim, K.M., Kang, J.S., Zodpe, P., Chae, S.W., Hwang, S.J., Lee, H.M., 2007. Expression of neutrophil gelatinase-associated lipocalin in human salivary glands. Ann. Otol. Rhinol. Laryngol. 116, 599-603.

Wu, H., Santoni-Rugiu, E., Ralfkiaer, E., Porse, B.T., Moser, C., Hoiby, N., Borregaard, N., Cowland, J.B., 2010. Lipocalin 2 is protective against E. coli pneumonia. Respir Res 11, 96.

Yan, Q.W., Yang, Q., Mody, N., Graham, T.E., Hsu, C.H., Xu, Z., Houstis, N.E., Kahn, B.B., Rosen, E.D., 2007. The adipokine lipocalin 2 is regulated by obesity and promotes insulin resistance. Diabetes 56, 2533-2540.

Yang, J., Blum, A., Novak, T., Levinson, R., Lai, E., Barasch, J., 2002a. An epithelial precursor is regulated by the ureteric bud and by the renal stroma. Dev. Biol. 246, 296-310.

Yang, J., Goetz, D., Li, J.Y., Wang, W., Mori, K., Setlik, D., Du, T., Erdjument-Bromage, H., Tempst, P., Strong, R., Barasch, J., 2002b. An iron delivery pathway mediated by a lipocalin. Mol. Cell 10, 1045-1056.

Yang, J., Mori, K., Li, J.Y., Barasch, J., 2003. Iron, lipocalin, and kidney epithelia. Am J Physiol Renal Physiol 285, F9-18.

Yang, J., Bielenberg, D.R., Rodig, S.J., Doiron, R., Clifton, M.C., Kung, A.L., Strong, R.K., Zurakowski, D., Moses, M.A., 2009. Lipocalin 2 promotes breast cancer progression. Proc. Natl. Acad. Sci. U. S. A. 106, 3913-3918.

Youle, R.J., Strasser, A., 2008. The BCL-2 protein family: opposing activities that mediate cell death. Nat Rev Mol Cell Biol 9, 47-59.

Zagulska-Szymczak, S., Filipkowski, R.K., Kaczmarek, L., 2001. Kainate-induced genes in the hippocampus: lessons from expression patterns. Neurochem. Int. 38, 485-501.

Zecca, L., Youdim, M.B., Riederer, P., Connor, J.R., Crichton, R.R., 2004. Iron, brain ageing and neurodegenerative disorders. Nat Rev Neurosci 5, 863-873.

Zhang, H., Xu, L., Xiao, D., Xie, J., Zeng, H., Wang, Z., Zhang, X., Niu, Y., Shen, Z., Shen, J., Wu, X., Li, E., 2007. Upregulation of neutrophil gelatinase-associated lipocalin in oesophageal squamous cell carcinoma: significant correlation with cell differentiation and tumour invasion. J. Clin. Pathol. 60, 555-561.

Zhang, J., Wu, Y., Zhang, Y., Leroith, D., Bernlohr, D.A., Chen, X., 2008. The role of lipocalin 2 in the regulation of inflammation in adipocytes and macrophages. Mol. Endocrinol. 22, 1416-1426.

Zheng, G., Bachinsky, D.R., Stamenkovic, I., Strickland, D.K., Brown, D., Andres, G., McCluskey, R.T., 1994. Organ distribution in rats of two members of the low-density lipoprotein receptor gene family, gp330 and LRP/alpha 2MR, and the receptor-associated protein (RAP). J. Histochem. Cytochem. 42, 531-542.

Zheng, L.T., Lee, S., Yin, G.N., Mori, K., Suk, K., 2009. Down-regulation of lipocalin 2 contributes to chemoresistance in glioblastoma cells. J. Neurochem. 111, 1238-1251.

Zheng, X.Y., Zhang, H.L., Luo, Q., Zhu, J., 2011. Kainic acid-induced neurodegenerative model: potentials and limitations. J Biomed Biotechnol 2011, 457079.

Zlokovic, B.V., 1996. Cerebrovascular transport of Alzheimer's amyloid beta and apolipoproteins J and E: possible anti-amyloidogenic role of the blood-brain barrier. Life Sci. 59, 1483-1497.

ADDITIONAL FIGURES

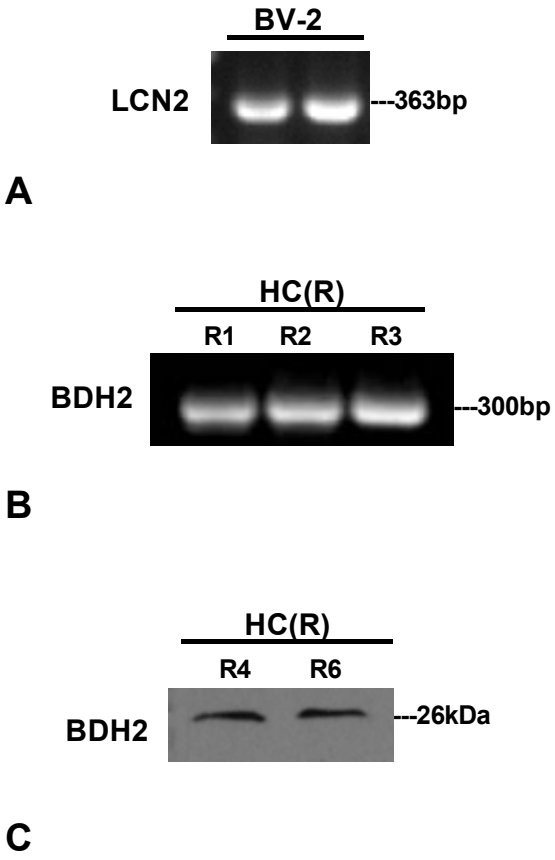

(A) RT-PCR analysis shows that LCN2 mRNA expression is present in BV-2 microglial cell line. Reverse transcribed BV-2 cDNA was used as a template for PCR using Go Taq Master Mix (Promega). RT-PCR was conducted with specific primers for the LCN2 mouse transcript (forward: 5'-ATG TCA CCT CCA TCC TGG TC-3', reverse: 5'-CAC ACT CAC CAC CCA TTC AG-3').

(B) RT-PCR analysis shows that BDH2 mRNA expression is present in the right hippocampus of 3 individual normal animals. Rat hippocampal cDNA was used as a template for PCR using Go Taq Master Mix (Promega). RT-PCR was conducted with specific primers for the BDH2 rat transcript (forward: 5'-GAG AAC AGA TGT GTG TAC AGT GCA ACC-3', reverse: 5'-CT AGG GAG GGC CTG TCT TCC AGC-3').

(C) Western blot analysis indicates that BDH2 protein is present in 2 weeks post-KA injection hippocampal samples (R4 and R6). Membrane was probed with goat anti-BDH2 antibody at 1 µg/ml (Everest Biotech Ltd, OX, UK).

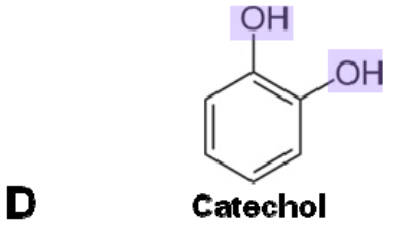

D **Catechol**

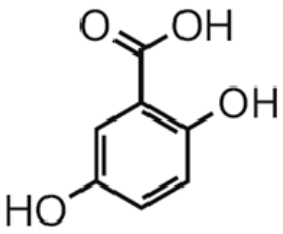

F **2,5-DHBA**

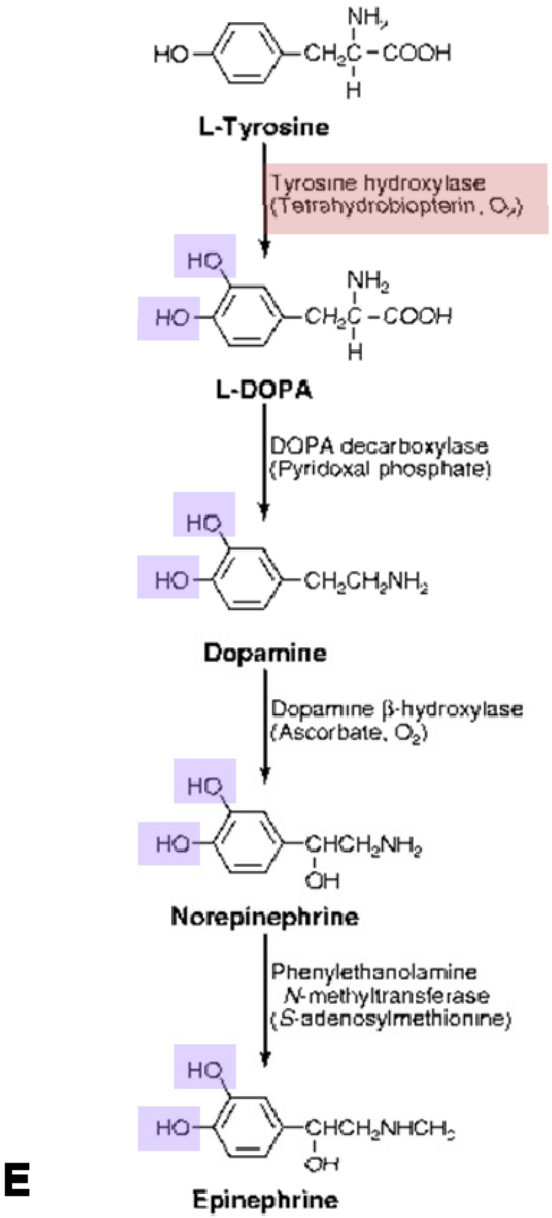

E

(D) Chemical structure of catechol.

(E) Catechols in the CNS in the form of catecholamines. Tyrosine hydroxylase (TH) catalyses the rate limiting step of catecholamines in their biosynthesis. Modified from (Siegel, 1999).

(F) Chemical structure of 2,5-dihydroxybenzoic acid (2,5-DHBA), the iron-binding moiety of the mammalian siderophore identified. BDH2 catalyses the production of 2,5-DHBA (Devireddy et al., 2010).

PUBLICATIONS

Various portions of the study have been published or in preparation for publication in international refereed journals

1. **Chia, W.J**., Dawe, G.S., Ong, W.Y., 2011. Expression and localization of the iron-siderophore binding protein lipocalin 2 in the normal rat brain and after kainate-induced excitotoxicity. Neurochemistry International (published).
2. **Chia, W.J**., Ong, W.Y., Dawe, G.S., 2011. Lipocalin 2 mediates apoptosis in neurons through LCN2R (in preparation).